12-2009

Synthesis, modification of mesoporous carbons and their application in polymer electrolyte membrane fuel cells

Bing Liu
Clemson University, bingl1224@yahoo.com

SYNTHESIS AND MODIFICATION OF MESOPOROUS CARBONS AND THEIR APPLICATION IN POLYMER ELECTROLYTE MEMBRANE FUEL CELLS

A Dissertation
Presented to
the Graduate School of
Clemson University

In Partial Fulfillment
of the Requirements for the Degree
Doctor of Philosophy
Chemistry

by
Bing Liu
December 2009

Accepted by:
Dr. Stephen Creager, Committee Chair
Dr. Darryl DesMarteau
Dr. Dennis Smith
Dr. George Chumanov

ABSTRACT

Mesoporous carbon materials of carbon xerogel (CX) and silica-templated carbon (MC) were synthesized and explored as catalyst supports alternative to the most commonly used carbon black (CB) support, for polymer-electrolyte-membrane fuel cell (PEMFC) application. Pt catalyst was loaded on these carbons and electrodes were fabricated from them. These Pt-loaded carbon supports were characterized with XRD, TEM, *ex-situ* and *in-situ* cyclic voltammetry, etc. The fabricated electrodes were evaluated in single-cell testing in comparison with commercial CB-supported Pt catalyst fabricated electrodes. The experimental results showed that CX-supported Pt catalyst had close or better performance than that of CB-supported Pt, possibly due to CX's 3-D porous structure, but MC had inferior performance to that of CB. MC's high specific surface area, large pore size, high pore volume structure advantages did not transfer to a higher cell performance as expected. The reasons for MC support's poor performance were discussed.

Monofunctional fluorosulfonimide electrolyte ($-C_6H_4SO_2N(H)SO_2CF_3$) was electrochemically grafted via its parent diazonium zwitterion onto planar glassy carbon electrode and the properties of the grafted layer on the electrode were investigated with electrochemical probes, XPS and chemical methods. The same monofunctional fluorosulfonimide electrolyte was also chemically grafted onto mesoporous CX and CB supports, a polymer electrolyte of sulfonated poly(arylene ether sulfone) was grafted onto CB support via the step-growth polymerization method. These monofunctional or polymeric electrolyte grafted mesoporous carbons were applied in PEMFC electrodes in

the hope to increase three-phase zone and stability of the electrodes via covalently bonding of electrolyte onto electrodes. Single-cell testing results of MEAs made from these Pt-loaded, the sulfonimide-grafted CX or the polysulfone-electrolyte-grafted CB supports showed unexpectedly lower performance than that of un-graft commercial Pt-loaded CB support. The reasons for the poor performance were explored.

In addition, sulfonimide polymers prepared by blending two different equivalent weight (EW, 1600 and 1300) plain sulfonimide polymers or crosslinking a low EW (1000) polymer were evaluated as membrane materials for PEMFCs in comparison with Nafion membranes. The results showed even blending the same sulfonimide polymer with different EWs might improve membrane performance, and cross-linking of low EW sulfonimide also improved the membrane.

From current work, it is worth to mention, PEMFC is a complicated and delicate system, whose performance is a combination of many different, even conflicting parameters of the Pt catalyst, the catalyst support, the electrolyte in the electrode, the membrane, the gas diffusion layer, and others. For fair comparison of cell performance in PEMFCs, well-designed, well-controlled experiments and methods are needed.

DEDICATION

I dedicate this work to my wife and son, who have given me consistent love, support and encouragement during my academic study.

ACKNOWLEDGMENTS

TABLE OF CONTENTS

Page

LIST OF FIGURES

xvi

LIST OF TABLES

CHAPTER 1

INTRODUCTION

1.1 Polymer electrode membrane fuel cells and electrodes

Fuel cells are electrochemical devices which directly convert chemical energy in fuels and oxidants into electrical energy and waste products (e.g. H_2O and/or CO_2) without limitation of Carnot efficiency. They consist of two electrodes with an electrolyte sandwiched between them, with the fuel and oxidant fed into anode and cathode respectively. In the anode, fuel is oxidized electrochemically, and in the cathode oxidant is reduced electrochemically. In operation of fuel cells, the ions produced at anode or cathode transport from one electrode to the other through the ionically conducting while electronically insulating electrolyte; electrons generated at the anode pass through the external circuit (hence generating electricity) to the cathode, where they complete the reduction reaction. According to the electrolyte materials used in the fuel cells, they are mainly classified into (1) phosphoric acid fuel cell (PAFC), (2) polymer electrolyte membrane (or proton exchange membrane) fuel cell (PEMFC) including direct methanol fuel cell (DMFC) (3) alkaline fuel cell (AFC), (4) molten carbonate fuel cell (MCFC) and (5) solid-oxide fuel cell (SOFC). Among these fuel cells, PEMFCs possess quite a few advantages over others such as low-operating temperature, high power density, low weight, compactness, fast start-ups, suitability for discontinuous operation, potential for low cost and volume, and long stack life. Therefore, PEMFCs have been intensively investigated worldwide in academia and industry as promising and attractive power

sources in transportation, stationary and portable applications. However for PEMFCs to be commercially viable, several technical barriers need to be overcome. Most significant among them are the production cost, performance, and the durability. The product cost, performance and durability of a fuel cell are all related to the electrodes employed in the fuel cell. So, improving the catalyst activity, lowering the catalyst loading, optimizing of electrode structure and increasing the electrode stability and durability are all important research areas in fuel cell research and development.
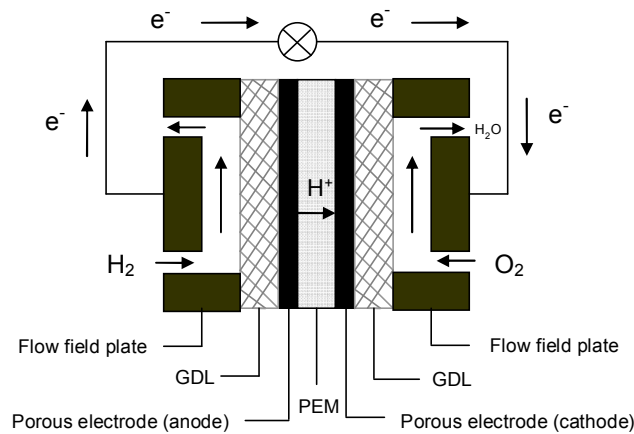
Figure 1.1 Schematic drawing of operation of PEMFC (direct H_2)

At the heart of a PEM fuel cell is the membrane electrode assembly (MEA). The MEA typically consists of a proton exchange membrane, two catalyst layers and two gas diffusion layers (GDL), one on each side of the membrane (as shown in Figure 1.1). In a broad sense, the electrode is regarded as the components that start from the surface of the membrane to the gas channel and current collector including catalyst layer and GDL. In a narrow sense, the electrode is taken as the catalyst layer on each side of the membrane

(shown in Figure 1.2). The latter meaning of electrode is usually used this work unless otherwise specified.
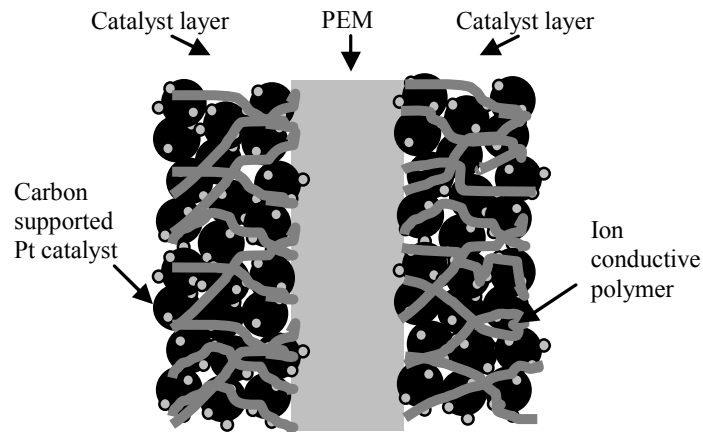
Figure 1.2 Schematic of 3-layer MEA (two catalyst layers plus a membrane) of PEM fuel cells

The first generation electrode for PEMFC was fabricated using polytetrafluoroethylene (PTFE) bound, Pt-black electrocatalyst with very high Pt loading (4-10 and up to 28 mg_{Pt} cm^{-2}), which exhibited excellent long-term performance, but prohibitive cost. The second generation PEMFC electrode was fabricated using PTFE bound, carbon-supported Pt catalyst. Without proton conduction media in the catalyst layer for the PTFE-bound electrode, the formed electrode was usually impregnated with Nafion solution by brushing or spraying, to increase the proton conduction. The Pt loading in the second generation electrode could be lowered to 0.4 mg cm^{-2}. The third generation (also the state-of-the-art) PEMFC electrode was the thin-film electrode fabricated using the Nafion bound, carbon-supported Pt catalyst. The thin-film electrode has significant improvement than its predecessor and its Pt loading was decrease to as low as about 0.1 mg cm^{-2}. The Pt utilization was increased from 20% to 40-50%. Excellent reviews on PEMFC

electrodes made by above-mentioned methods and alternative methods were given by Litster et al,[1] and Wee et al.[2]

Although electrode fabrication method has much advanced in recent years, to meet commercialization requirements, there is much work to do, such as increasing the electrode performance while decreasing the catalyst loading and also keeping its durability. The electrode in PEM fuel cell is a porous composite electrode containing both electronically conducting (e.g. Pt/C) and ionically conducting materials (e.g. Nafion[®] from DuPont). The optimization of the electrode is to carefully balance the different transport processes in the electrode such electron, proton, and reactant and product transports.[3]

Pt (or Pt alloy) catalyst directly affect the electrode activity, stability and durability. The catalyst support material (usually carbon) also has important influence on the electrode. Higher surface area porous carbon can provide high dispersion and narrow size distribution of the nanocatalyst particles. The support material can interact with catalyst particles, which also affects the catalysts activity. The corrosion resistance of support material also can affect the catalyst (electrode) durability.

1.2   Mesoporous carbons as catalyst supports

Carbon has four crystalline allotropes: diamond (sp^3 bonding), graphite (sp^2) carbye (sp^1) and fullerene ('distorted' sp^2). Graphite and diamond can be found on earth; the other forms of carbon are synthetic. Currently, a wide range of carbon materials are available. Different forms of carbon have different properties; therefore carbon materials have a wide range of applications.[4, 5]

Due to its properties such as high electrical conduc[5]tivity, reasonable thermal and chemical stability, high surface area, and favorable pore structure, porous carbon materials are usually used as catalyst supports for PEM fuel cells and industry catalyst supports.[6]

According to International Union of Pure and Applied Chemistry (IUPAC), porous materials (including porous carbon) can be classified as (1) microporous (< 2 nm), (2) mesoporous (2-50 nm) and (3) macroporous (>50 nm).[7] Again, according to the order of their structure and pores, porous materials can generally be divided into (1) ordered, with periodical uniform pore structure and (2) disordered, with irregular pores.[8]

When used as catalyst supports in fuel cells, it is difficult for microporous carbon materials to form good three-phase contacts because it is difficult for the reactants and large size proton conductor (e.g., Nafion) to access the micropores when Pt nanoparticles are deposited inside the micropores. While macroporous carbon materials with pore size larger than 50 nm usually have a lower surface area and a higher electrical resistance. It is also not a good candidate for catalyst support in fuel cells. Mesoporous carbon materials with pore size between 2 and 50 nm exhibit an attractive structure property as a catalyst support, i.e., a large surface area with larger size mesopores and is expected to bring about better three-phase contacts and therefore better electrode performance.

Due to its easy availability and lost cost, mesoporous carbon of carbon black (e.g. Vulcan XC-72/72R, BP 2000, Ketjen black) is commonly used in PEMFC as catalyst supports. As research and development in PEMFC focuses shift to cell (system) durability issue, more attention is put on alternative supports other than carbon black,

such as carbon aerogel/xerogel, templated mesoporous carbon, carbon nanotube, carbon nanofiber, etc.[9] In the following sections, alternative carbon supports of carbon xerogel and silica-templated carbon are briefly reviewed in comparison with conventional support of carbon black.

1.2.1　Carbon black

Carbon black is a particulate form of elemental carbon and can be regarded as a disordered mesoporous carbon (MC). Carbon blacks are mainly manufactured by either incomplete combustion of hydrocarbons, or the thermal decomposition of hydrocarbons. According to the manufacture processes, carbon blacks can be classified into furnace black, thermal black, lampblack, channel black, and acetylene black, etc. Among them, furnace black are the most commercially available product. Furnace black such as Vulcan XC-72/72R is most commonly used catalyst support in low temperature fuel cells (e.g. PEMFC, PAFC, and AFC); sometimes acetylene black is used in gas diffusion layer.

Carbon black usually consists of primary particles that are generally spherical with diameters varying from ten to hundreds of nanometers. These particles are collected in secondary structures called aggregates, which form agglomerates. The first two structural levels exhibit strong covalent bonds, whereas the agglomerate is bonded of weak van der Waals force. The schematic description of this different level structure of carbon black is shown in Figure 1.3. Aggregate is the basic unit of carbon black, and agglomerates can be broken up, when carbon black is dispersed well in solution. The most important properties of carbon black include the surface area, primary particle size, structure

6

(complexity of composition), surface chemistry, and electrical conductivity. The basic textural properties[10] of carbon black including Vulcan XC-72R, are given in Table 1.1.
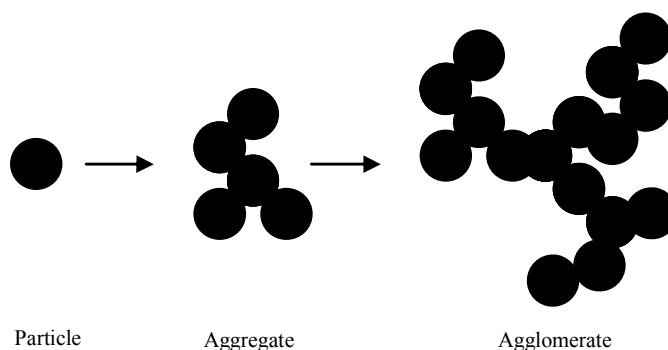
Figure 1.3 Schematic description of structure of carbon back (particle, aggregate and agglomerate)

Table 1.1 Textural properties of carbon blacks

Property	Vulcan XC-72R	Ketjenblack DJ-600	Black Pearls BP-2000	Acetylene Black
S_{BET} / $m^2 g^{-1}$ [a]	252	1300	1500	64
S_{meso} / $m^2 g^{-1}$ [b]	177	1230	1020	64
V_T / $cm^3 g^{-1}$ [c]	0.63	2.68	2.56	0.20
V_{micro} /$cm^3 g^{-1}$ [d]	0.037	0.029	0.208	0.00
d_{aver} / nm [e]	15.9	9.45	20.6	14.4

[a] S_{BET}, BET surface area; [b] S_{meso}, mesopore surface area; [c] V_T, total pore volume; [d] V_{micro}, micropore volume; [e] d_{aver}, average pore diameter

Although carbon black is extensively used as catalyst support in PEMFCs, it is generally thought to have many micropores. This is not good for Nafion (electrolyte) penetration, and mass transport of reactants and products in the electrodes of PEMFC.

Therefore, alternative supports other than carbon black get more attention for PEMFC application.

1.2.2 Carbon aerogel/xerogel

Carbon aerogel is highly porous carbon material with random three-dimensional structure of interconnected nanoparticles and interconnected open pore network. Since it was first synthesized by Pekala in 1989[11-14], carbon aerogel has received much attention [15-17] and has been applied in many fields including fuel cells. Carbon aerogels are usually prepared from pyrolysis of its precursor organic gels synthesized by sol-gel method of polycondensation of resorcinol (R) with formaldehyde (F) at slightly basic solution using supercritical CO_2 drying. Schematic presentation of the carbon xerogel synthesis processes is shown in Figure 1.4. Because supercritical drying is complex, costly, and high pressure in nature (possibly dangerous), other drying techniques such as freeze drying, vacuum drying [15] and even ambient pressure drying[16-18] were also employed. The aerogel obtained from freeze drying is called cryogel, and the aerogel made from ambient pressure drying is called xerogel. Among these drying methods, the ambient pressure drying is simple, quick and less expensive, but usually ambient pressure drying causes the gels to shrink and crack due to the capillary forces from the liquid-vapor interface formed inside the pores o the gels. However, after the synthesis conditions were carefully chosen, organic xerogels which almost retain their original wet gels structure could be obtained.[9-11]
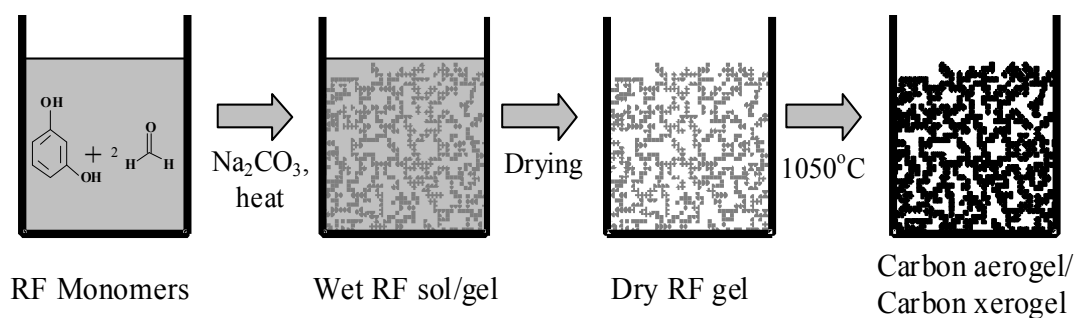
Figure 1.4 Schematic presentation of processes of carbon aerogel/xerogel synthesis

Due to their unique porous structures, carbon aerogel, xerogel and cryogel materials have all been applied in PEMFC electrodes.[18-28] However, most of these applications are characterized only with *ex-situ* methods and *ex-situ* performance of the relevant electrodes fabricated from these aerogels (xerogels, crygels) is not easily to completely transferred to full-cell performance. Even for full-cell (single cell) characterizations of these electrodes, comparison with electrodes made from most commonly used carbon black supported Pt catalyst is not always performed. So, in order to fully take advantage of carbon aerogel/xerogel properties, further exploration of carbon aerogels/xerogels as electrodes materials (e.g. catalyst supports) is worth investigating.

1.2.3 Silica-templated mesoporous carbon

Mesoporous carbon can be classified into two categories according to their structures and morphologies: (1) ordered mesoporous carbon (OMC), which is constructed of regular arrays of uniform mesopores and usually synthesized by nanocasting ordered mesoporous silica templates or by directly templating triblock copolymer structure-directing species and (2) disordered mesoporous carbon (DOMC) with irregular pore structures. In regard to pore structure, OMC is generally regarded as preferred catalyst

9

support in terms of specific surface area, electrical conductivity, and mass transport and has been extensively studied as catalyst supports for PEM fuel cells. But Rolison[29] has argued the need of periodicity of support for catalyst. OMCs are generally prepared using ordered mesoporous silicas as hard templates; the long, complex, expensive synthesis of ordered mesoporous silicas makes their widespread applications limited. Also, the control of pore diameter in the synthesis of OMC is not easy because the control of the pore diameter in the carbon results from controlling the pore-wall thickness of the template. This is not easy to execute in synthesis.
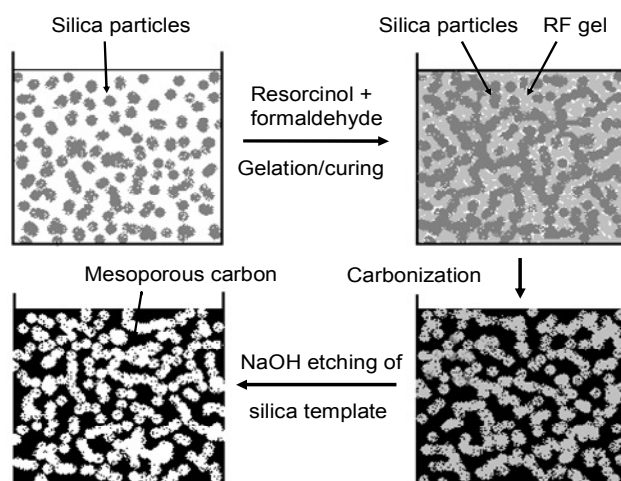
Figure 1.5 Schematic presentation for the synthesis of mesoporous carbons: (1) gelation/curing of resorcinol and formaldehyde (RF) in the presence of silica nanoparticles; (2) carbonization of RF gel-silica composite at 850 °C to get a carbon-silica composite; (3) NaOH etching of silica template to obtain mesoporous carbon

However, the synthesis of DOMC is usually simple, easy and the resulting carbon with high surface area, high pore volume, large pore size and pore size distribution can be obtained. An example of the synthesis of silica-templated (disordered template)

mesoporous with RF sol-gel method is given in Figure 1.5. The general synthesis process for OMC with template method is similar to that of DOMC, but ordered templates are used in OMC synthesis. Disordered silica-templated carbons were synthesized and explored as catalyst support for PEMFC and DMFC by Joo and co-workers. But its comparison with the most commonly used support of carbon black Vulcan XC-72R has not been done [30-32]. It's worthwhile to do more study on these DOMCs compared with XC-72R and investigate how the support affects mass transfer in the electrodes in these carbons perhaps compared with OMC as support.

1.3   Grafting electrolyte onto mesoporous carbons

The most popular thin-film PEMC electrode fabrication method, mentioned in Section 1.1 was realized from an ink formed by simply mixing of carbon-supported Pt catalyst with solubilized Nafion solution. The three-phase zone in the electrodes made this way may not be maximized and may not be stable during the operation of fuel cells. One way to increase the three-phase zone in the electrode and improve the electrode stability is to bind the electrolyte onto the carbon support (or catalyst-loaded carbon support) by covalent bonding. Figure 1.5 schematically represents the three-phase zone improvement in electrode for the proposed electrolyte covalent bonding strategy relative to the usual simple mixing method.
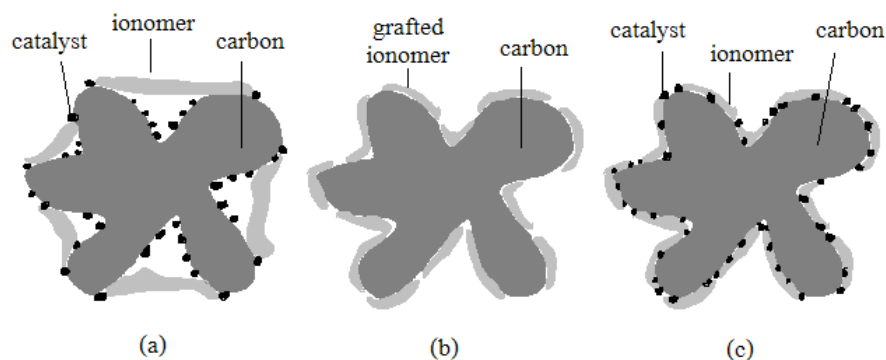
Figure 6 Schematics of the three-phase zone in MEA made conventionally, contrasted with that made by the proposed modified material (a) the catalyst particles not intimately contacted with polymer electrolyte are not utilized in fuel cell (conventionally made electrode) (b) chemically bonded polymer electrolyte onto the carbon surface (c) the catalyst particles both intimately contacted with carbon and polymer electrolyte grafted on the carbon surface are expected to be fully utilized in fuel cell (cell made of proposed modified material)

1.3.1 Electrochemical grafting of monofunctional sulfonimide electrolyte onto glassy carbon substrate via diazonium salt

Electrochemical grafting of functional groups (either electrolyte or non-electrolyte) onto the planar glassy carbon and other substrates via pre-formed or *in-situ* generated diazonium salts is well documented in the literature.[33-37] The electrochemical grafting strategy has advantages of better control of the grafting, and the grafted layers can be probed by electrochemical methods and other surface analytical methods (such XPS, SEM, TEM, and EDX) for basic study. So, for basic study purpose, a superacid of aryl perfluorosulfonimide is grafted onto glassy carbon electrode by an electrochemical method, and the properties of the graft on the electrode are investigated.

1.3.2 Chemical grafting of monofunctional and polymeric electrolyte onto mesoporous carbon

While electrochemical grafting of electrolyte onto glassy carbon electrode is easy and good for basic study of the grafted layer or the grafted electrode, electrochemical grafting is usually not practical for porous powdery carbon support used in PEMFCs. For grafting electrolyte (functional groups) onto porous powdery carbon supports, chemical grafting is preferred. Relatively few publications[38-43] are seen in literature grafting of electrolytes onto Pt-loaded carbon blacks via different chemistry for fuel cell applications. Diminished electrolyte (such as less Nafion) in the electrode is needed or moderate performance improvement was obtained using such electrolyte-grafted materials in fuel cell tests. A further study of grafting electrolyte onto carbon support itself via covalent bonding is logical and interesting. Aryl fluorosulfonimide is a superacid with desired properties as electrolyte developed in Clemson. Different aryl fluorosulfonimide zwitterions have been synthesized. Chemical grafting of functional groups onto carbon materials has recently attracted much attention[36, 44-47] and a possible reaction mechanism was discussed. Transfer of this grafting method via diazonium salts to porous powdery carbon substrates is a reasonable strategy to study the effects of grafting on the fuel cell performance. So grafting onto mesoporous carbons (such as carbon xerogel and carbon black) of aryl perfluorosulonimide superacid (electrolyte) was pursued in this work.

The optimal amount Nafion (around 30 wt% in the electrode) needed in the thin-film made electrode is reported in many papers. While monofunctional electrolyte grafting helps increase of the three-phase zone in the electrode, the electrolyte grafted onto the

carbon support is usually less than the optimal amount of electrolyte for optimal electrode performance. To overcome this, a polymeric electrolyte grafted onto carbon (electrode) might work. Polymer grafting on carbon substrates has been reported,[48] but polymer electrolyte grafting onto carbon support for PEMFC application is little reported. One paper[49] shows marginal performance increase after grafting methylsulfonic acid polymer electrolyte on the Pt loaded carbon black. Much work is needed for grafting polymer electrolytes on electrodes for fuel cell applications.

Sulfonated poly(arylene ether sulfones) posses many properties such as good thermal stability, high mechanical strength, high proton conductivity. They have been intensively investigated by many groups as alternative membrane materials[48-54] for PEMFCs especially in Virginia Tech. So, development of grafting sulfonated poly(arylene ether sulfone) onto mesoporous carbons is investigated in this work via the *in-situ* step-growth polymerization method and its application in fuel cells is also evaluated.

Lastly, because the PEMFC cell performance is in large extent affected by the Pt catalyst in the electrode and the way the electrode is fabricated, fair comparison of fuel cell applications of different carbon supports, and electrolyte (monofunctional or polymeric) grafted carbon supports is complicated by the Pt catalyst deposition and the electrode fabrication methods. Therefore, except for the need of optimization Pt catalyst deposition and electrode manufacture methods, development of characterization methods (e.g. impedance spectroscopy) to differentiate these effects is needed before any final conclusions can be made. It is clear while simple in principle, PEM fuel cells as power plants are complicated and delicate systems, and their performance is a balance of

different parameters (perhaps conflicting each other) of the Pt catalyst, the catalyst support, the electrolyte in the electrode, the membrane, the gas diffusion layer, and others.

1.4 The scope of this work

This document focuses on (1) the synthesis of mesoporous carbon materials such as carbon xerogel, silica-templated carbon, (2) application of these mesoporous carbons as alternative catalyst supports instead of carbon black in PEMFCs, (3) grafting monofunctional or polymeric electrolyte onto these mesoporous carbons and their application as PEMFC electrodes. The work also involves in evaluation of blended and cross-linked sulfonimide polymers as membrane materials in PEMFCs.

Specifically, Chapter 2 is about deposition of Pt catalyst onto the most commonly used carbon support, carbon black Vulcan XC-7R and its application as electrodes in PEMFC. Through this application, the catalyst deposition method, electrode (MEA) fabrication method, and fuel cell testing protocols are verified.

Chapters 3 and 4 present respectively the employment of carbon xerogel and silica-templated mesoporous carbon as catalyst supports in PEMFC applications. Their performance as catalyst supports is compared with the commercially obtained support, Vulcan XC-72R.

Chapter 5 presents the electrochemical grafting of aryl fluorosulfonimide electrolyte onto a glassy carbon (GC) electrode. The properties of the grafted layer on the GC electrode are characterized with electrochemical probes, XPS and the stability of the

grafted electrolyte on GC in high temperature, humid, or superacid environment is also investigated.

Chapter 6 and 7 describe respectively the grafting of monofunctional sulfonimide superacid and polymeric sulfonated poly(arylene ether sulfone) electrolyte onto carbon xerogel and carbon black supports and their application as electrodes in PEMFCs in comparison with un-grafted carbon supports.

Chapter 8 reports the evaluation of blended and cross-linked sulfonimide polymers as membrane materials in PEMFCs.

1.5 References

1. S. Litster and G. McLean, *Journal of Power Sources*, 2004, **130**, 61-76.

2. J. H. Wee, K. Y. Lee and S. H. Kim, *Journal of Power Sources*, 2007, **165**, 667-677.

3. N. P. Brandon and D. J. Brett, *Philosophical Transactions of the Royal Society A: Mathematical, Physical and Engineering Sciences*, 2006, **364**, 147-159.

4. A. L. Dicks, *Journal of Power Sources*, 2006, **156**, 128-141.

5. A. G. Pandolfo and A. F. Hollenkamp, *Journal of Power Sources*, 2006, **157**, 11-27.

6. E. Auer, A. Freund, J. Pietsch and T. Tacke, *Applied Catalysis A-General*, 1998, **173**, 259-271.

7. D. A. J. Rouquerol, C. W. Fairbridge, D. H. Everett, J. M. Haynes, N. Pernicone, J. D. F. Ramsay, K. S. W. Sing and K. K. Unger *Pure and Applied Chemistry*, 1994, **66**, 1739-1758.

8. M. E. Davis, *Nature*, 2002, **417**, 813-821.

9. K. Y. Chan, J. Ding, J. W. Ren, S. A. Cheng and K. Y. Tsang, *Journal of Materials Chemistry*, 2004, **14**, 505-516.

10. K. Kinoshita, *Carbon: Electrochemical and Physichemical Properties*, Wiley, New York, 1988.

11. R. W. Pekala, US Patent 4873218, 1989.

12. R. W. Pekala, *Journal of Materials Science*, 1989, **24**, 3221-3227.

13. R. W. Pekala and F. M. Kong, *Polym. Prepr*, 1989, **30**, 221.

14. R. W. Pekala, C. T. Alviso, F. M. Kong and S. S. Hulsey, *Journal of Non-Crystalline Solids*, 1992, **145**, 90-98.

15. T. Horikawa, J. Hayashi and K. Muroyama, *Carbon*, 2004, **42**, 1625-1633.

16. R. Saliger, V. Bock, R. Petricevic, T. Tillotson, S. Geis and J. Fricke, *Journal of Non-Crystalline Solids*, 1997, **221**, 144-150.

17. D. Wu, R. Fu, S. Zhang, M. S. Dresselhaus and G. Dresselhaus, *Carbon*, 2004, **42**, 2033-2039.

18. M. Glora, M. Wiener and J. Fricke, *New Materials for Electrochemical Systems IV. Extended Abstracts of the Fourth International Symposium on New Materials for Electrochemical Systems*, 2001, 366-367|.

19. J. Marie, S. Berthon-Fabry, P. Achard, M. Chatenet, A. Pradourat and E. Chainet, *Journal of Non-Crystalline Solids*, 2004, **350**, 88-96.

20. A. Smirnova, X. Dong, H. Hara, A. Vasiliev and N. Sammes, *International Journal of Hydrogen Energy*, 2005, **30**, 149-158.

21. A. Smirnova, X. Dong, H. Hara and N. Sammes, *Journal of Fuel Cell Science and Technology*, 2006, **3**, 477-481.

22. C. Arbizzani, S. Beninati, E. Manferrari, F. Soavi and M. Mastragostino, *Journal of Power Sources*, 2007, **172**, 578-586.

23. M. Chatenet, E. Guilminot, F. Fischer, A. Rigacci, S. Berthon-Fabry, P. Achard and E. Chainet, *Journal of Power Sources*, 2007, **166**, 104-111.

24. H. D. Du, L. Gan, B. H. Li, P. Wu, Y. L. Qiu, F. Y. Kang and Y. Q. Zeng, *Journal of Physical Chemistry C*, 2007, **111**, 2040-2043.

25. H. D. Du, B. H. Li, F. Y. Kang, R. W. Fu and Y. Q. Zeng, *Carbon*, 2007, **45**, 429-435.

26. K. Feiyu, D. Hongda, L. Baohua, R. Fu and Z. Yuqun, *Carbon*, 2007, **45**, 429-435.

27. N. Job, J. Marie, S. Lambert, S. Berthon-Fabry and P. Achard, *Energy Conversion and Management*, 2008, **49**, 2461-2470.

28. J. Marie, R. Chenitz, M. Chatenet, S. Berthon-Fabry, N. Cornet and P. Achard, *Journal of Power Sources*, 2009, **190**, 423-434.

29. D. R. Rolison, *Science*, 2003, **299**, 1698-1701.

30. J. B. Joo, P. Kim, W. Kim, J. Kim and J. Yi, *Catal. Today*, 2006, **111**, 171-175.

31. P. Kim, H. Kim, J. B. Joo, W. Kim, I. K. Song and J. Yi, *J. Power Sources*, 2005, **145**, 139-146.

32. J. Joo, P. Kim, W. Kim and J. Yi, *Journal of Electroceramics*, 2006, **17**, 713-718.

33. C. Louault, M. D'Amours and D. Belanger, *Chemphyschem*, 2008, **9**, 1164-1170.

34. J. Haccoun, C. Vautrin-Ul, A. Chausse and A. Adenier, *Progress in Organic Coatings*, 2008, **63**, 18-24.

35. F. Le Floch, A. Thuaire, G. Bidan and J. P. Simonato, *Nanotechnology*, 2009, 145705-145712.

36. S. Baranton and D. Belanger, *Electrochimica Acta*, 2008, **53**, 6961-6967.

37. P. Allongue and J. Pinson, *Actualite Chimique*, 2009, 98-103.

38. E. B. Easton, Z. Qi, A. Kaufman and P. G. Pickup, *Electrochemical and Solid-State Letters*, 2001, **4**, A59-A61.

39. N. Jia, R. B. Martin, Z. Qi, M. C. Lefebvre and P. G. Pickup, *Electrochimica Acta*, 2001, **46**, 2863-2869.

40. Z. Xu, Z. Qi and A. Kaufman, *Journal of Power Sources*, 2003, **115**, 49-53.

41. Z. Xu, Z. Qi and A. Kaufman, *Electrochemical and Solid-State Letters*, 2003, **6**, A171-A173.

42. Z. Q. Xu, Z. G. Qi and A. Kaufman, *Chemical Communications*, 2003, 878-879.

43. Z. Xu, Z. Qi and A. Kaufman, *Electrochemical and Solid-State Letters*, 2005, **8**, A313-A315.

44.   F. Barriere and A. J. Downard, *Journal of Solid State Electrochemistry*, 2008, **12**, 1231-1244.

45.   E. Bekyarova, M. E. Itkis, P. Ramesh, C. Berger, M. Sprinkle, W. A. de Heer and R. C. Haddon, *Journal of the American Chemical Society*, 2009, **131**, 1336-1337.

46.   C. Mangeney, Z. Qin, S. A. Dahoumane, A. Adenier, F. Herbst, J. P. Boudou, J. Pinson and M. M. Chehimi, *Diamond and Related Materials*, 2008, **17**, 1881-1887.

47.   J. M. Seinberg, M. Kullapere, U. Maeorg, F. C. Maschion, G. Maia, D. J. Schiffrin and K. Tammeveski, *Journal of Electroanalytical Chemistry*, 2008, **624**, 151-160.

48.   N. Tsubokawa, *Bulletin of the Chemical Society of Japan*, 2002, **75**, 2115-2136.

49.   H. Kuroki and T. Yamaguchi, *Journal of the Electrochemical Society*, 2006, **153**, A1417-A1423.

CHAPTER 2

SYNTHESIS OF CARBON-BLACK-SUPPORTED PT CATALYST FOR POLYMER ELECTROLYTE MEMBRANE FUEL CELL APPLICATION

2.1   Introduction

In the past decades, polymer electrolyte membrane fuel cells (PEMFCs) were extensively studied around the World as potential power sources for mobile, stationary and portable applications. They are in the edge of commercialization, but there are barriers yet to be overcome. High cost among them is the most significant factor affecting the commercialization. Catalyst is about half of the cost of the stack system in the PEMFCs. For now, Pt is still the most efficient catalyst in PEMFCs. Pt is expensive and limited in resources. In order to reduce the cost, a lower Pt loading but more active catalyst is needed in electrodes. Usually, Pt catalyst is dispersed as small-size nanoparticles onto a high-surface-area conductive support (the most commonly used support in PEMFC is carbon black Vulcan XC-72/72R) to increase the active surface area and stability of the catalyst, and therefore the activity and durability of the electrode. This in turn can reduce the cost for the PEMFC system. There are mainly four basic methods to deposit Pt (or Pt alloy) catalysts onto supports: impregnation method, colloidal method, micro-emulsion method, and electro-deposition method.[1] Impregnation is the simplest method among them.

This chapter discusses the placement of the Pt catalyst on commercially obtained carbon support, carbon black Vulcan XC-72R by the common impregnation-reduction

method. The prepared XC-72R-supported Pt catalyst was characterized in comparison with commercial carbon black Vulcan XC-72R supported Pt catalyst by powder X-ray diffractometry (XRD), transmission electron microscopy (TEM), *ex-situ* and *in-situ* cyclic voltammetry (CV) of H-adsorption/desorption method, and *ex-situ* CO stripping method. Both the prepared and commercial carbon black support Pt catalysts were fabricated in membrane electrode assemblies (MEAs) by the thin-film decal method, and the performance of these MEAs was tested on a single cell test station and compared.

2.2   Experimental

2.2.1   Catalyst deposition onto carbon black XC-72R

Carbon black, Vulcan XC-72R (Cabot, fluffy form, XC-72R) was used as catalyst support for Pt deposition. In a typical synthesis, 0.1 g XC-72R was suspended in 50 mL deionized (DI) water, and sonicated for 15 min. Then, a diluted H_2PtCl_6 (Acros Organics, 40% Pt) solution was added into the carbon black powder suspension and sonicated for another 30 min. The mass of platinum salt added to the XC-72R sample corresponded to 20 wt% of platinum metal in the final material. After sonication, the pH of the mixture was adjusted to 11 using a 4 mol L^{-1} NaOH solution and an excess amount (10x) of formaldehyde was diluted in DI water (2 mL) and added drop by drop into the carbon black suspension under stirring. The mixture was kept stirring for another 15 min at room temperature, then the reaction temperature was raised to 90 ºC and kept at 90 ºC for 2 h under stirring. Then the reaction was cooled down to room temperature and diluted HCl (2 mol L^{-1}) was added to promote precipitation of Pt catalyst onto carbon powders. The Pt deposited XC-72R (Pt/XC-72R$_s$) was then filtered, thoroughly washed with DI water, and

dried at 100 °C under vacuum. The final Pt content in Pt/XC-72R$_s$ was measured by thermogravimetric analysis (TGA) under O$_2$ atmosphere.

2.2.2 Characterization of materials

2.2.2.1 N$_2$ adsorption/desorption method

The specific surface area and pore texture of the carbon black Vulcan XC-72R were characterized by the analysis of nitrogen adsorption–desorption isotherms, performed at 77 K with a Micromeritics ASAP 2010 apparatus. The sample was degassed at 200 ºC for one day before measurement. The specific surface area (S$_{BET}$) of XC-72R sample was obtained using the Brunauer-Emmett-Teller (BET) model[2], micropore properties (microporous volume V$_{micro}$, microporous surface area S$_{micro}$) were obtained using the t-plot method[3, 4] and the Barrett-Joyner-Halenda (BJH) model[5] was used to evaluate the mesopore properties (mesoporous volume V$_{meso}$, mesoporous surface area S$_{meso}$ pore size and distribution (PSD). The total pore volume (V$_{total}$) was recorded at P/P$_0$ of near saturation.

2.2.2.2 Powder X-ray diffractometry

X-ray powder diffractograms of Pt/XC-72R$_s$ and commercially obtained Pt/XC-72R (20% Pt, Alfa Aesar, Pt/XC-72R$_c$) samples were obtained using a Scintag XDS2000 powder x-ray diffractometer using Cu Kα radiation of wavelength 0.1540 nm. The tube current was 100 mA, and tube voltage was 40 kV. The 2θ angular range between 5 and 90 degrees was scanned at 0.5 s per step in 0.02 º steps.

2.2.2.3 Electron microscopy

Scanning electron microscopy (SEM) measurements on Pt/XC-72R$_s$ and Pt/XC-72R$_c$ samples were performed using a Hitachi S-4800 microscope equipped with an Oxford INCA EDS detector. The powder sample was mounted on a double-sided carbon sticky tape. TEM measurements were performed on Pt/XC-72R$_s$ and Pt/XC-72R$_c$ samples using a Hitachi H7600T transmission electron microscope which was operated at an accelerating voltage of 200 kV. The samples were prepared by dispersing a small amount of the catalyst powder in ethanol with ultrasonic treatment. Several drops of the dispersion were taken using a pipette and put on a holey carbon copper grid, followed by drying in air at room temperature overnight.

2.2.2.4 Thermogravimetry analysis

The Pt contents of Pt/XC-72R$_s$ and Pt/XC-72R$_c$ samples were determined from the residual mass following TGA under O_2 atmosphere at 850 °C with a heating rate of 15 °C min^{-1} using a Mettler Toledo TGA/SDA 851e analyzer. Residual mass for Pt-containing samples is assumed to be Pt metal. TGA runs on Pt-free XC-72R samples showed very low residual masses.

2.2.2.5 *Ex-situ* cyclic voltammetry and CO stripping voltammetry

Ex-situ cyclic voltammetry (*ex-situ* CV) was employed to characterize the electrochemically active surface area (ESA) of Pt catalysts on carbon-supported samples. CV measurements were made using a CH Instruments model 660A electrochemical workstation with picoamp booster and Faraday cage with a standard three-electrode cell. The home-made Hg/Hg$_2$SO$_4$ (0.1 mol L^{-1} H$_2$SO$_4$) electrode and a Pt wire served as

reference and counter electrodes respectively. The working electrode (WE) was a glassy carbon (GC) plate electrode made by attaching a graphite rod with graphite adhesive to the back of a square GC plate (5 mm each side, geometric surface area 0.025 cm^2). All GC electrodes were cleaned prior to use and cleanliness was checked by CV in 0.5 mol L^{-1} H$_2$SO$_4$ solution. A thin layer electrode was formed on the GC surface by evaporation of 10 µL of an ink suspension consisting of well-mixed supported catalyst and solubilized Nafion solution in isopropanol (0.5 mL isopropanol, 10 mg Pt/C catalyst, and 50 mg 5% Nafion (EW 1100, Solution technology) mixed together and stirred overnight). The mass of the catalyst layer deposited onto GC was determined by weighing a drop of 10 µL of the same suspension placed on a Teflon template and processed the same as the GC plate electrode assuming the two pipeted volumes are the same. *Ex-situ* CV measurements were performed by partial immersion of the GC electrode in 0.5 mol L^{-1} H$_2$SO$_4$ solutions. Before recording the CVs used to determine ESA, the potential was repeatedly cycled until a stable voltammogram was obtained. The ESA was then calculated from the charge density for hydrogen desorption with subtraction of the double layer charging density as reported in literature.[6]

For CO stripping voltammetry, charge densities associated with stripping of adsorbed CO provide an alternative to H$_2$ adsorption/desorption for determining ESA. The same standard three-electrode cell setup as described above was used for CO stripping measurements. The cell was thoroughly degassed with nitrogen (UHP) prior to analysis, then pure CO gas was bubbled through the cell for 5 min with the WE held at -0.25 V (vs. Hg/Hg$_2$SO$_4$). After that, the cell was bubbled by nitrogen to remove residue CO in

solution while holding the WE at -0.25 V for 15 min. CO stripping cyclic voltammograms were obtained with a potential scan from -0.25 to -0.70 V then back to 0.45 V at a scan rate of 20 mV s^{-1}.

2.2.2.6 MEA fabrication

MEAs were prepared using the decal transfer method developed by Wilson and co-workers[7, 8] at Los Alamos National Laboratory. Detail of the method is given in published papers[7-9]. In brief, an ink was prepared by mixing of carbon supported catalyst (21% Pt/XC-72R$_s$, or 20% Pt/XC-72R$_c$), solubilized Nafion solution (5%, EW 1100), isopropanol, glycerol and tetrabutyl ammonium hydroxide solution (1 mol L^{-1} in methanol) in a small vial with cap, under stirring. The dry mass ratio of carbon plus catalyst to Nafion was 5:2. After mixing the ink was applied by painting in thin layers onto Teflon-coated fiberglass templates and then heating the ink-painted templates in an oven at 140 ºC for 30 min to remove solvent. The painting-heating sequence was repeated until a Pt catalyst loading in the range of 0.25 mg cm^{-2} was reached. An MEA was made by hot-pressing a Nafion 117 membrane with two ink-coated templates on each side at 200-210 ºC and 600 lbs force for 5 min. All membranes were pretreated before use by boiling in 0.5 mol L^{-1} NaOH for 1h to convert into Na$^+$ form, followed by boiling in DI water for 1 h and washing with DI water several times. Following hot pressing, the MEA was boiled in 0.5 mol L^{-1} sulfuric acid for 1 h to convert all ionomer back to the proton form, then boiled in DI water for 1 h and washed with DI water for several times. The MEAs were stored in DI water before use.

2.2.2.7 Single fuel-cell testing

The single-cell testing of MEAs was performed on a model 850C test station from Scribner Associates Company. Before assembling in the test fixture, the MEA was pulled dry and flat on a vacuum table at 60 °C for 20 min, and then the MEA was mounted on the test fixture by sandwiching the MEA between the two pieces of uncatalyzed gas diffusion backing (ELAT/NC, E-TEK). Humidified fuel (H_2) and oxidant (O_2 or air) gases were supplied to the test fixture by the test station. The cell was operated under ambient pressure on both the anode and cathode. Cells were broken in at a cell voltage of 0.5 V overnight, after which a series of polarization curves was acquired in controlled voltage mode under different operating conditions. The cell open circuit voltage was close to or above 1.0 V for all MEAs. The cell resistance was monitored during acquisition of the polarization curves using the current interrupt method (CI) and by high frequency impedance spectroscopy (HFR) at 1 kHz frequency.[10]

2.2.2.8 *In-situ* cyclic voltammetry

The *in-situ* CV measurement was used to obtain ESA values for the supported Pt catalysts in the MEAs in the fuel-cell test fixture[11]. For such a measurement the fuel-cell station operates in a two-electrode configuration in which the anode severed as both pseudo-reference and counter electrodes, and the cathode served as the working electrode. The anode was fed with high purity H_2 gas (humidified) and the cathode was fed with high purity N_2 gas (humidified). The gas flow of both N_2 and H_2 was kept at 50 mL min^{-1} during the measurements. The Solartron 1280B was used as a potentiostat. The potential was cycled between 0 to 0.8 V with a scan rate of 40 mV s^{-1}.

27

2.3   Results and discussion

The surface area, pore size, pore size distribution (PSD) and other textural properties of the carbon black Vulcan XC-72R sample (which was used as catalyst support in both our synthesis and commercial Pt/XC-72R catalyst) were characterized by their N_2 physisorption method. The N_2 adsorption and desorption isotherm is shown in Figure 2.1 The XC-72R sample shows a type IV, H2 isotherm according to IUPAC classification[12] indicating that mesopores exist in the sample. The nominal BET surface area of XC-72R sample is 250 m^2 g^{-1}, and our measured value is 237 m^2 g^{-1}. They are in consistency. The PSD deduced from the BJH method for XC-72R samples is shown on the inset in Figure 2.1
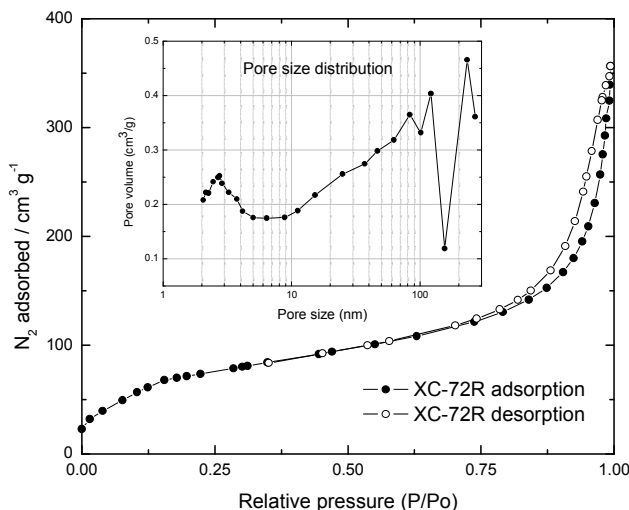
Figure 2.1 N_2 adsorption/desorption isotherm of carbon black Vulcan XC-72R and pore size distribution by BJH method (inset)

The XC-72R sample has a very broad pore size distribution, which was reported in literature and reflects its aggregate and agglomerate structure. Other textural properties of XC-72R are listed on Table 2.1. From Table 2.1, it is seen that the total pore volume of

XC-72R is not high, but the mesoporosity is about 90%; the micropore volume is low but its microporous surface area is not low, which may indicate many small size micropores in the XC-72R sample.

Table 2.1 Textural properties of carbon black Vulcan XC-72R

Carbon	S_{BET}	S_{micro}	$S_{micro}/$	V_{total}	V_{micro}	V_{meso}	$V_{meso}/$	d_{BET}	d_{BJHads}	d_{BJHdes}
	m^2g^{-1}	m^2g^{-1}	S_{BET}	cm^3g^{-1}	cm^3g^{-1}	cm^3g^{-1}	V_{total}	nm	nm	nm
XC-72R	237	83	0.35	0.62	0.04	0.55	0.89	10.4	17.6	22.7

S_{BET}: BET surface area, S_{micro}:micropore surface area by t-plot, V_{total}:total pore volume at near saturation pressure, V_{meso}:cumulative volume of pores between 1.7 and 300 nm by BJH adsorption branch, d_{BET}, d_{BJHads}, d_{BJHdes}:average pore width by 4V/A

The Pt content in the prepared Pt/XC-72R$_s$ was obtained by TGA method was 21%, Pt in content in commercial Pt/XC-72R (Pt/XC-72R$_c$) was 20% (nominal 20% Pt). Both the prepared and commercial Pt/XC-72R catalysts were subjected to further analyses as discussed below. Powder XRD analysis of the Pt/XC-72R$_s$ samples was employed to confirm Pt deposition and allow for estimation of Pt particle sizes. The XRD graphs of a representative Pt/XC-72R$_s$ sample and a commercial Pt/XC-72R$_c$ sample are shown in Figure 2.2. The diffractogram shows features expected for Pt as labeled on the graph; the feature near 25 degrees 2-theta is from the carbon black graphitic nature. The Pt diffraction lines are slightly narrower for the Pt/XC-72R$_s$ sample relative to and commercial Pt/XC-72R$_c$ sample, which suggests that slightly larger Pt particles for Pt/XC-72R$_s$ sample by XRD.
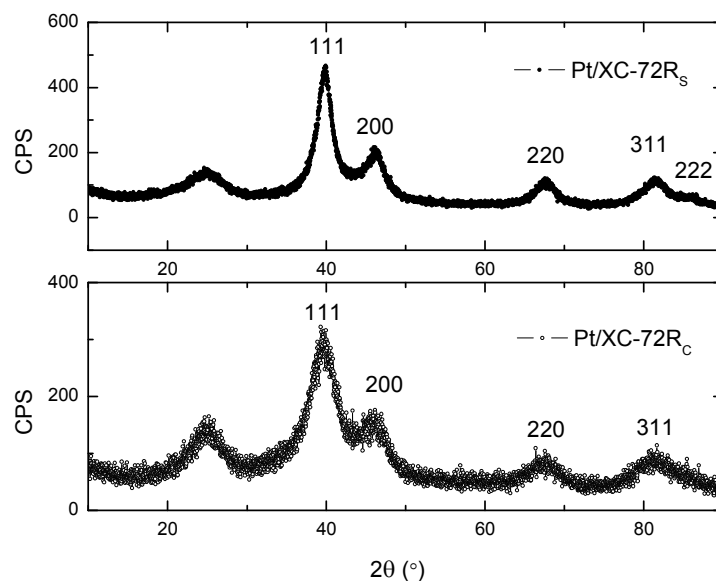
Figure 2.2 XRD diffractograms of prepared Pt/XC-72R$_s$ and commercial Pt/XC-72R$_c$

Nanoparticle sizes may be estimated from powder XRD data using the Scherer equation. The Pt (220)[13] line is used for the calculation. According to the Scherer equation (Equation 2.1)[14], , the Pt particle size may be estimated.

$$d(\mathrm{nm}) = \frac{0.9\lambda}{B\cos(\theta)} \tag{2.1}$$

In this equation d is the Pt crystal size (diameter), λ is the X-ray wavelength (0.1540 nm), B is the full width at half height for the diffraction peak in radians and θ is half of the diffraction angle. Particle size values obtained in this way for Pt/XC-72R$_s$ and Pt/XC-72R$_c$ are given in Table 2.2. As expected, Pt particle diameters are larger for the Pt/XC-72R$_s$ sample (3.8 nm) and the Pt/XC-72R$_c$ (2.2 nm).

From the particle size obtained as described above, the Pt specific surface area may be calculated using Equation 2.2:

$$S(\text{m}^2\text{g}^{-1}) = \frac{6000}{\rho d} \qquad\qquad (2.2)$$

In this equation d is the Pt particle diameter (nm), and ρ is the Pt density (21.4 g cm^{-3}).

Pt specific surface areas calculated in this way are listed in Table 2.2 for Pt/CX and

Pt/XC-72R samples. These values will be compared with Pt specific surface area values

obtained from TEM estimates of Pt particle size, and also with ESA values obtained by

ex-situ and *in-situ* CV measurements.

Table 2.2 Pt nanoparticle size and specific surface area by different methods (XRD, TEM, *ex-situ* CV (H), *ex-situ* CV (CO) and *in-situ* CV (H)

Sample	d_{XRD}	S_{XRD}	d_{TEM}	S_{TEM}	S_H	S_{CO}	$S_{in\text{-}situ}$
	nm	m^2g^{-1}	nm	m^2g^{-1}	m^2g^{-1}	m^2g^{-1}	m^2g^{-1}
Pt/XC-72R$_s$	3.8	74	2.7	104	60	52	35
Pt/XC-72R$_c$	2.2	127	2.8	100	67	66	65

d_{XRD}: particle size by XRD, d_{TEM}: particle size by TEM, S_{XRD},S_{TEM}: the specific surface area calculated from the equation (2.2) from XRD and TEM respectively, S_H: specific surface area from *ex-situ* CV (H desorption charge), S_{CO}: surface area from CO stripping CV, $S_{in\text{-}situ}$: surface area from *in-situ* CV (in MEA)

TEM was also used to characterize catalyst supports, and provide an alternate estimate

of Pt particle size and particle size distribution. The TEM micrographs and the histogram

graphs of Pt particle size for the Pt/XC-72R$_s$ and Pt/XC-72R$_c$ samples are shown in

Figures 2.3 and 2.4 respectively. The typical structure for carbon black of aggregates of

small carbon primary particles is shown in the micrographs (Figure 2.3). For both

samples Pt particles appear to be well distributed all throughout the carbon black support,

but for Pt/XC-72R$_s$, it shows some Pt aggregates on the carbon support surface. The

mean Pt diameter for Pt/XC-72R$_s$ and Pt/XC-72R$_c$ samples is estimated to be 2.7 ± 0.9 nm and 2.8 ± 0.7 nm respectively by counting more than 200 particles from each TEM image using ImageJ software[15]. Error estimates are standard deviations from which a slightly broader Pt size distribution for Pt/XC-72R$_s$ is seen. The mean Pt particle diameter of Pt/XC-72Rs is slightly smaller by TEM than XRD, in which the Pt agglomeration may be reflected showing larger Pt particle size. The specific surface area (SA) of Pt could be calculated according to Equation (2.2) from the Pt particle size measured by TEM or XRD on the Pt/XC-72R$_s$ and Pt/XC-72R$_c$ samples, and the values are listed on Table 2.2 in comparison with the ESA measured by *ex-situ* and *in situ* CVs. Pt specific SA of Pt/XC-72R$_s$ is comparable to that of Pt/XC-72R due to comparable Pt particle size on Pt/XC-72R(by TEM). Usually the Pt catalyst specific surface area from TEM and XRD are larger than that measured by *ex-situ* or *in-situ* CV because TEM or XRD measurement includes electrochemically-inaccessible Pt particle. Also the ESA measured *ex-situ* (in a half cell) is commonly higher than that measured *in-situ* (in a full cell) due to better ion conduction by help from free acid (H$_2$SO$_4$) in the half-cell measurement. These will be evident in the following discussion.
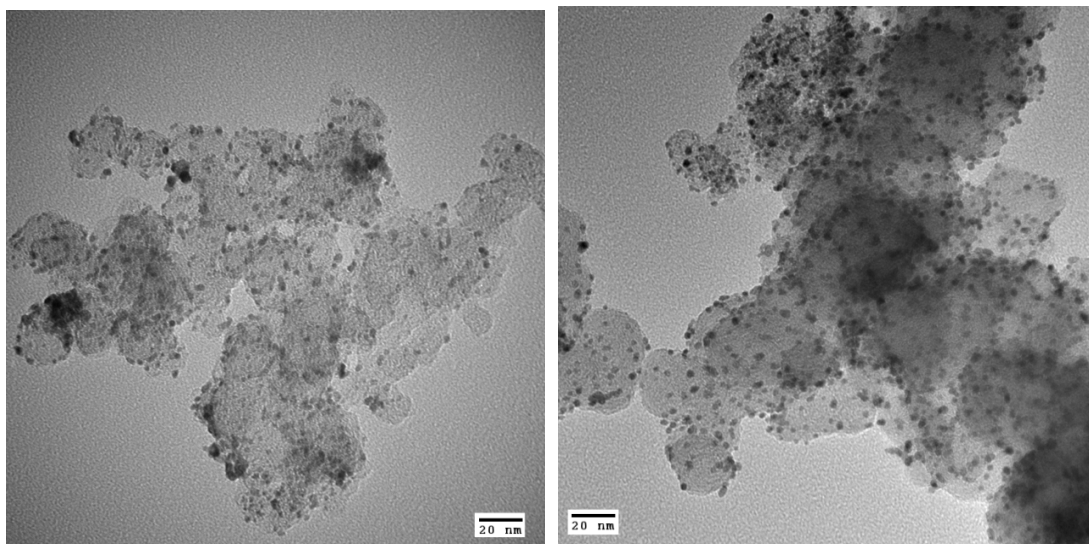
Figure 2.3 TEM graphs of prepared Pt/XC72R$_s$ (left) and commercial Pt/XC72R$_c$ (right) catalysts
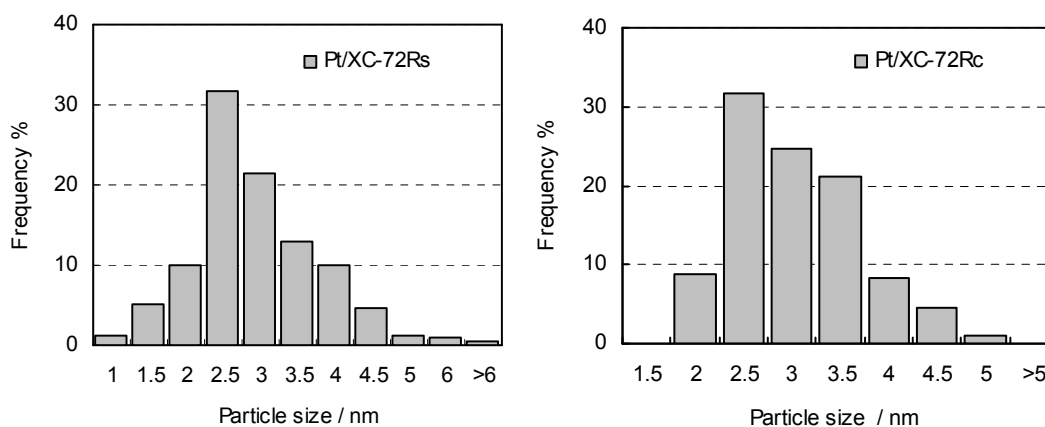
Figure 2.4 Pt particle size histogram of prepared Pt/XC-72R$_s$ (d mean=2.7 ± 0.9 nm) and commercial Pt/XC72R$_c$, (d mean=2.8 ± 0.7 nm (SD))

Ex-situ CV is commonly used to estimate electrochemically active Pt surface area (ESA) for comparison with areas calculated from Pt particle sizes. Estimates may be obtained from H adsorption/desorption or CO stripping. For the case of H adsorption/desorption, the ESA (S_{ESA} m^2 g^{-1} Pt) may be calculated from Equation 2.3:[16]

$$S_{ESA}(\text{m}^2\text{g}^{-1}\text{Pt}) = 100 \frac{q}{\Gamma L_{Pt}} \qquad (2.3)$$

In this equation q is the hydrogen adsorption or desorption charge density determined by CV (mC cm^{-2}), Γ (210 µC cm^{-2}) is the well-established quantity for the charge to reduce a monolayer of protons on Pt, L_{Pt} is the Pt loading in the electrode (mg cm^{-2}). Figure 2.5 (top) presents CVs for Pt/XC-72R$_s$ and Pt/XC-72R$_c$ samples for the H adsorption or desorption region. The CV shapes are as expected for Pt on carbon. ESA values estimated are given in Table 2.2. The SA for Pt/XC-72R$_s$ by *ex-situ* CV is slightly lower but close to that of Pt/XC-72R$_c$ by the same method. This finding indicates the similar Pt accessibility in free acid in both synthesized and commercial Pt/XC-72R.

Figure 2.5 (bottom) shows CVs for CO stripping for Pt/XC-72R$_s$ and Pt/XC-72R$_c$ samples. ESA values were again obtained using Equation 2.3 but with a Γ value of (420 µC cm^{-2})[16] which is appropriate for CO stripping. ESA values from CO stripping are in good agreement with those from hydrogen adsorption or desorption, which serves to validate both methods.

In-*situ* CV may be used to estimate Pt ESA in intact electrodes in MEAs. Comparison of ESAs for such samples with those obtained by *ex-situ* CV provides information on catalyst utilization in the MEA. Generally, the cathode is of most interest because of the sluggish reaction kinetics of the oxygen reduction. The *in-situ* CVs of both Pt/XC-72R$_s$ and Pt/XC-72R$_c$ are shown in Figure 2.6. Surprisingly, the ESA values measured *in-situ* for Pt/XC-72R$_s$ are lower than those measured *ex-situ* by H-adsorption/desorption or CO stripping, while for Pt/XC-72R$_c$ samples the *in-situ* SA is very close to those measured *ex-situ* using both H adsorption/desorption and CO stripping. This may indicate possible

high catalyst utilization in MEAs fabricated by Pt/XC-72R$_c$ samples, but the cell

performance test gave different results as seen in the following discussion.
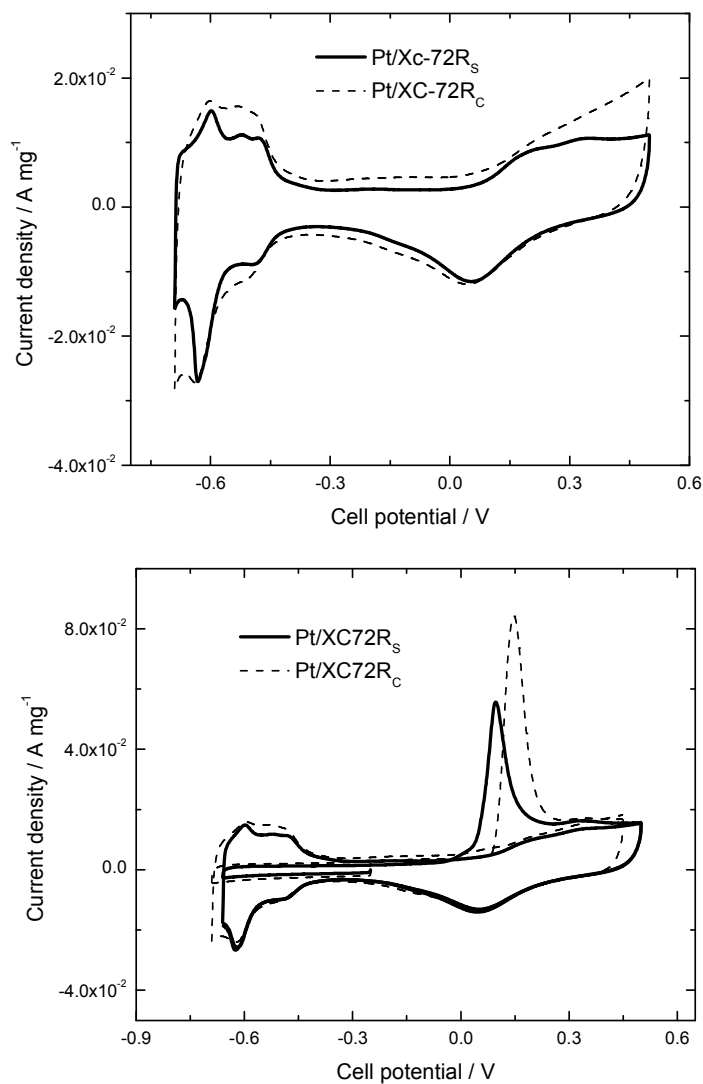
Figure 2.5 *Ex-situ* H-adsorption/desorption CVs and CO stripping CVs of prepared
Pt/XC-72R$_s$ and commercial Pt/XC-72R$_c$ WE: thin-film-catalyst coated GC, RE:
Hg/Hg$_2$SO$_4$, CE: Pt wire; scan rate: 20 mV s^{-1}
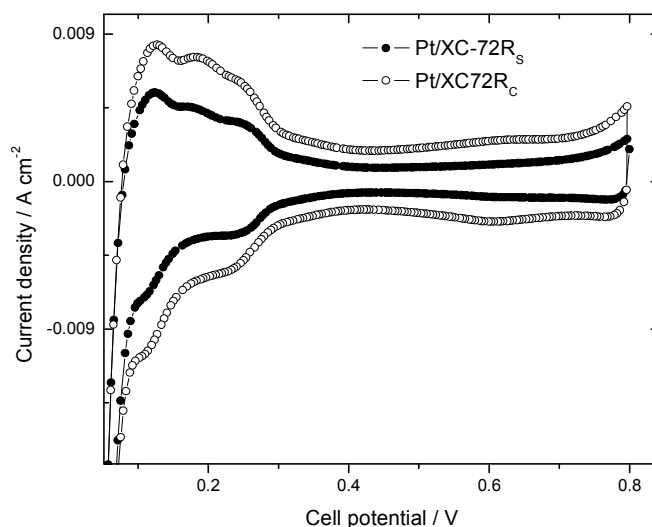
Figure 2.6 *In-situ* CVs from prepared Pt/XC-72R$_s$ (●) and commercial Pt/XC-72R$_c$ (○), Anode: H$_2$, 50 mL min^{-1}, Cathode: N$_2$, 50 mL min^{-1}, cell temperature 30 ℃, potential range 0-0.8 V, scan rate 40 mV s^{-1}

The MEAs fabricated with both catalyst Pt/XC-72R$_s$ and Pt/XC-72R$_c$ were tested in H$_2$/O$_2$ and H$_2$/air cells at 50 ℃ and 80 ℃ respectively and under atmospheric pressure conditions. The polarization and resistance curves are shown in Figures 2.7, and 2.8, 2.9 respectively. The performance of Pt/XC-72R$_s$ is slightly higher than that of Pt/XC-72R$_c$ in H$_2$/O$_2$ cells at 50 and 80 ℃. The performance of Pt/XC-72R$_s$ is slightly lower than that of Pt/XC-72R$_c$ in H$_2$/air cells, at 50 and 80 ℃. The same trend of much lower performance in H$_2$/air cells than H$_2$/O$_2$ cells was observed in both prepared and commercial Pt/XC-72R catalysts both at 50 and 80 ℃.

From Figures 2.8 and 2.9, the areal resistance for Pt/XC-72R$_s$ is lower than that of Pt/XC-72R$_c$ by both the CI and HFR methods. Because the two MEAs were tested using similar Nafion 117 membranes, the resistance difference should be caused by the active

catalyst layer and not the membrane. This finding may therefore indicate the catalyst prepared by different methods has different effects on the cell performance.
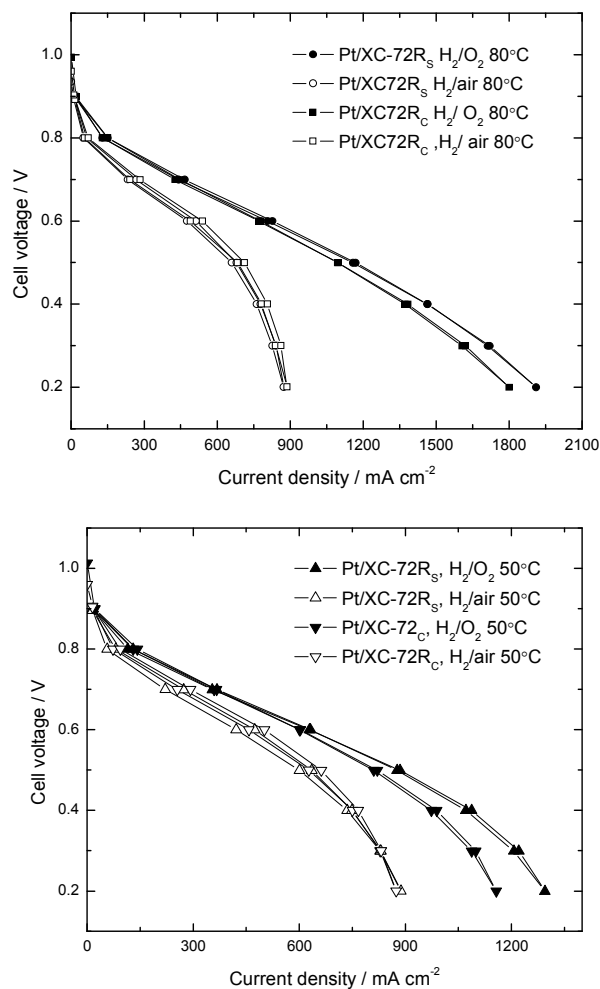
Figure 2.7 Polarization curves of prepared Pt/XC72R$_s$ at 80 ºC (O$_2$ ●, air ○) and at 50 ºC (O$_2$ ▲, air Δ) and commercial Pt/XC72R$_c$ at 80 ºC (O$_2$ ■, air □) and 50 ºC (O$_2$ ▼, air, ∇), measurement conditions: H$_2$/O$_2$ or air, cell temperature 80 or 50 ºC, stoichiometric ratio, H$_2$ 1.25, O$_2$ 1.5, or air 4.0, all measurements at atmospheric pressure, and Pt around 0.25 mg cm^{-2} in both anode and cathode, respectively
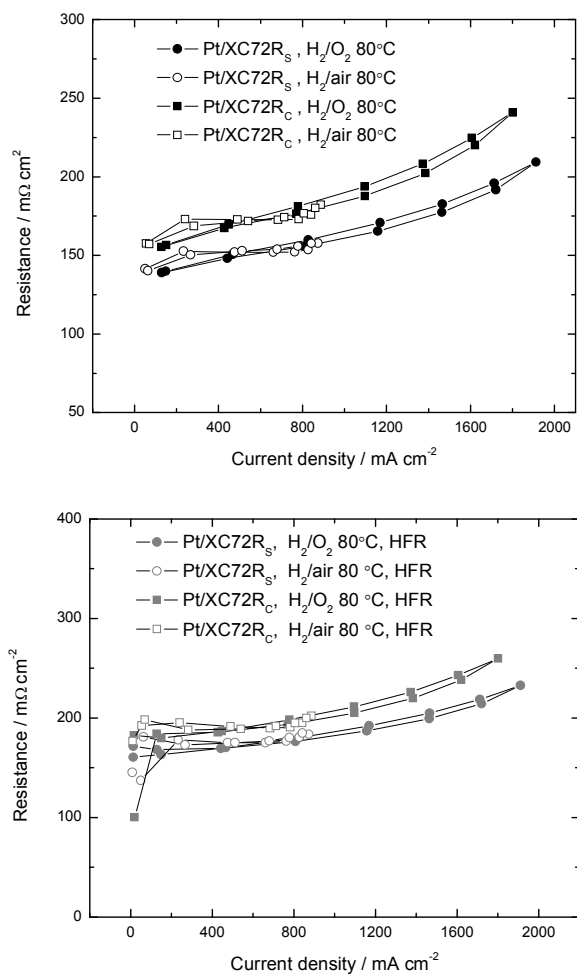
Figure 2.8 CI-Resistance of prepared Pt/XC72R$_s$ (O$_2$ ●, air ○) at 80 °C and commercial Pt/XC72R $_c$ (O$_2$ ■, air □) at 80 °C and HF-Resistance of prepared Pt/XC72R$_s$ (O$_2$ ●, air ○) at 80 °C and commercial Pt/XC72R$_c$ (O$_2$,■ air□) at 80 °C, measurement conditions same as that in Figure 2.7, for HFR, frequency at 1 kHz
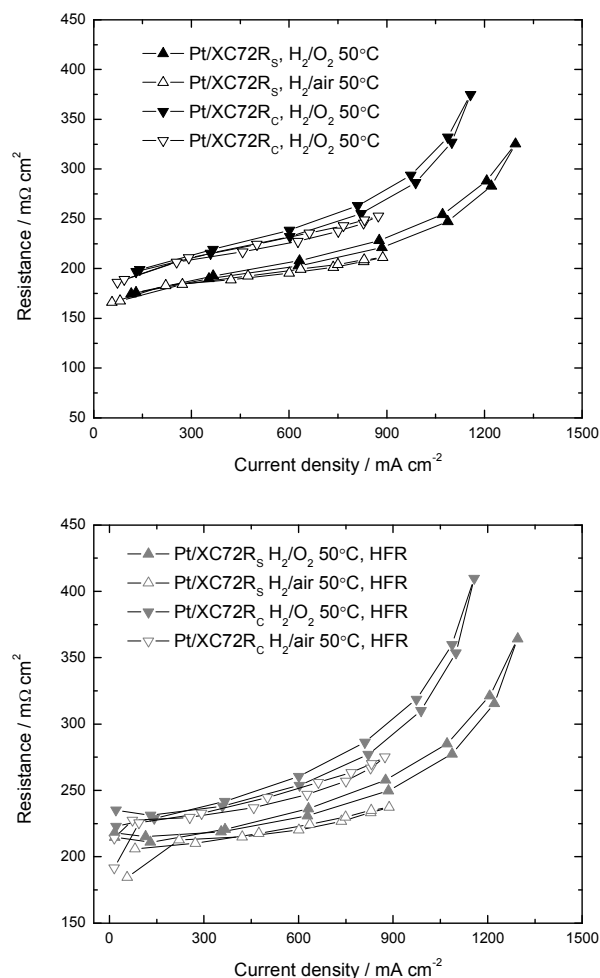
Figure 2.9 CI-Resistance of prepared Pt/XC72R$_s$ (O$_2$ ▲, air Δ) and commercial Pt/XC72R (O$_2$ ▼, air, ∇), and HF-Resistance of prepared Pt/XC72R$_s$ (O$_2$ ▲, air Δ) and commercial Pt/XC72R$_c$ (O$_2$ ▼, air ∇), at 50 °C, measurement conditions same as that in Figure 2.7, for HFR, frequency at 1 kHz

2.4 Conclusions

Pt catalyst was successfully deposited onto carbon black support Vulcan XC-72R by the common impregnation-reduction method. The prepared Pt catalyst (Pt/XC-72R$_s$) was characterized with XRD, SEM, TEM, *ex-situ* and *in-situ* cyclic voltammetry in comparison with commercial obtained Pt catalyst Pt/XC-R$_c$ A similar Pt particle size was observed in Pt/XC-72R$_s$ to that in Pt/XC-72R$_c$ (by TEM); the ESAs obtained by *ex-situ*

cyclic voltammetry for both samples are very close, but unexpectedly, the ESA measured by *in-situ* CV for Pt/XC-72R$_s$ is lower than that in Pt/XC-72R$_c$. The performance of the catalyst Pt/XC-72R$_s$ and Pt/XC-72R$_c$ was also tested in a MEA format in a single cell test station and the results show very close or a slightly better performance for Pt/XC-72R$_s$ than that for commercial Pt/XC-72R catalyst.

From the above-mentioned results, it is inferred that the catalyst deposition method, MEA fabrication and fuel cell testing methods employed in the experiments are all reliable. These methods will apply in following experiments in the following chapters.

2.5   References

1.   H. Liu, C. Song, L. Zhang, J. Zhang, H. Wang and D. P. Wilkinson, *Journal of Power Sources*, 2006, **155**, 95-110.

2.   S. Brunauer, P. H. Emmett and E. Teller, *Journal of the American Chemical Society*, 1938, **60**, 309-319.

3.   B. C. Lippens and J. H. de Boer, *Journal of Catalysis*, 1965, **4**, 319-323.

4.   R. S. Mikhail, S. Brunauer and E. E. Bodor, *Journal of Colloid and Interface Science*, 1968, **26**, 45-53.

5.   E. P. Barrett, L. G. Joyner and P. P. Halenda, *Journal of the American Chemical Society*, 1951, **73**, 373-380.

6.   A. Pozio, M. De Francesco, A. Cemmi, F. Cardellini and L. Giorgi, *Journal of Power Sources*, 2002, **105**, 13-19.

7.   M. S. Wilson, J. A. Valerio and S. Gottesfeld, *Electrochimica Acta*, 1995, **40**, 355-363.

8.   M. S. Wilson and S. Gottesfeld, *Journal of Applied Electrochemistry*, 1992, **22**, 1-7.

9.   S. C. Savett, J. R. Atkins, C. R. Sides, J. L. Harris, B. H. Thomas, S. E. Creager, W. T. Pennington and D. D. DesMarteau, *Journal of the Electrochemical Society*, 2002, **149**, 1527-1532.

10.   K. R. Cooper and M. Smith, *Journal of Power Sources*, 2006, **160**, 1088-1095.

11.   K. R. Cooper, V. Ramani, J. M. Fenton and H. R. Kunz, *Experimental methods and data analyses for polymer electrolyte fuel cells*, 1.5 edn., Scribner Associates, Inc., 2007.

12.   K. S. W. Sing, D. H. Everett, R. A. W. Haul, L. Moscou, R. A. Pierotti, J. Rouquerol and T. Siemieniewska, *Pure and Applied Chemistry*, 1985, **57**, 603-619.

13.   Z.-H. Teng, G. Wang, B. Wu and Y. Gao, *Journal of Power Sources*, 2007, **164**, 105-110.

14.   J. I. Langford and A. J. C. Wilson, *Journal of Applied Crystallography*, 1978, **11**, 102-113.

15.   http://rsb.info.nih.gov/ij/, accessed on August 4, 2009.

16.   T. Vidakovic, M. Christov and K. Sundmacher, *Electrochimica Acta*, 2007, **52**, 5606-5613.

CHAPTER 3

CARBON XEROGELS AS PT CATALYST SUPPORTS FOR PEM FUEL CELL APPLICATIONS

3.1 Introduction

One of the 'quantum jumps' in polymer electrolyte membrane fuel cell (PEMFC) science and technology development is the jump of a 10- to 100-fold catalyst (Pt or Pt alloy) loading reduction in electrodes by using high-surface-area-carbon-supported catalyst instead of unsupported catalyst in the active catalyst layers in the electrodes in PEMFCs. The use of carbon-supported catalysts not only decreases significantly the production cost but also increases the catalyst (Pt or Pt alloy) utilization and thus the cell performance in fuel cells.[1] The requirements for a catalyst support for PEMFCs include the following: (1) high surface area; (2) suitable porosity with mainly mesopores (2-50 nm); (3) high electrical conductivity; and (4) good chemical, thermal and electrochemical stability under the harsh fuel cell conditions (under H_2, O_2, heat, humid, acid or alkaline conditions).[2, 3] Conventionally, carbon black (e.g. Vulcan XC-72/72R from Cabot Company) is the most commonly used catalyst support in PEMFCs. Due to the importance of the catalyst support materials in fuel cell applications, much research effort has been put on supports other than carbon blacks, such as activated carbon, carbon nanotubes, carbon nanofibers, ordered mesoporous carbons, carbon aerogels, etc. in order to discover better support materials for better fuel cell performance and durability.[2, 3] Activated carbon is very highly microporous which can result in Pt particles being trapped where they are not in contact with electrolyte or fuel, so it is expected not to be a

good support candidate. Better performance on carbon nanotubes and nanofibers as supports in fuel cells has been reported, but the production cost for these materials is very high which may prevent the immediate application of these supports in practice.

The structure of carbon aerogel is very different from that of carbon black. Carbon black consists of carbon agglomerates formed from weak van der Waals forces between aggregates of primary particles. The primary particles in the aggregates are fused together by strong covalent bonding. Carbon aerogel's structure can be described as three-dimensional consisting of interconnected carbon nanoparticles and interconnected nanopores. Carbon aerogel was first synthesized by Pekela[4, 5] in 1989 using resorcinol (R) and formaldehyde (F) as reactants polymerized using sodium carbonate catalyst (C) to form a precursor RF hydrogel. This precursor hydrogel is then subjected to supercritical CO_2 drying and carbonization at about 1050 ºC under inert atmosphere to produce the carbon aerogel. The aerogel structure (specific surface area, pore size, pore size distribution, porosity, density, etc.) can be tuned by varying synthesis conditions such as RF content in the reaction mixture (the combined weight percent of R and F relative to the weight of the overall reaction mixture including water), the ratio of C to R in the reaction mixture, pH, etc.[6, 7] Due to these special properties of carbon aerogels mentioned above, they have been pursued as gas diffusion layers[8] and as catalyst supports in the active catalyst layer[9, 10] in PEMFCs. High performance of aerogels as supports in catalyst layers was reported[9], but supercritical drying is expensive and time consuming. Carbon xerogels with similar structure and properties to carbon aerogels could be

prepared under ambient pressure drying after careful control of the synthesis conditions.[11-13] The ambient-pressure drying is simple and cost-effective.

Several groups have described work using carbon aerogels and xerogels as Pt catalyst supports in PEM fuel cells[9, 10, 14-22]. In many cases materials have been well characterized but comparisons have not been made with conventional Pt-on-carbon-black materials, and/or the materials have not been used to fabricate membrane electrode assemblies (MEAs). In cases where MEAs were fabricated and tested, the results have been mixed. In some cases the catalysts with aerogel/xerogel supports work as well or better than conventional Pt-on-carbon black catalysts, whereas in other cases the performance is worse. Critical issues appear to include the Pt particle size and penetration of catalyst particles, electrolytes and fuels into and out of aerogel/xerogel supports. Each approach is unique and the results have varied from one group to another.

In this chapter, carbon xerogels with BET surface area of 462 $m^2 g^{-1}$ and peak pore size 14 nm were produced by modifying a previously described ambient-pressure drying method[12, 13] and explored as Pt catalyst supports for H_2/O_2 (air) PEMFCs. The carbon xerogel supported Pt catalysts (Pt/CX) were characterized by thermogravimetry (TGA), powder X-ray diffractometry (XRD), electron microscopy (SEM, TEM) and *ex-situ* cyclic voltammetry (CV) for thin-film electrode samples supported on glassy carbon and studied in a sulfuric acid electrolyte. Pt/CX samples were studied in comparison with commercially obtained samples of Pt catalyst supported on a Vulcan XC-72R carbon black support (Pt/XC-72R). The Pt/CX samples were also used to fabricate MEAs which were tested in a single-cell test station.

3.2 Experimental

3.2.1 Synthesis of carbon xerogel

Carbon xerogels were synthesized by the RF sol-gel method using ambient-pressure evaporative drying.[12, 13] The R/F mole ratio was kept at 1:2 and C/R mole ratio was at 1:1500. The RF content was 30 wt%. A typical preparation proceeded as follows: calculated amounts of resorcinol (98%, Aldrich) and formaldehyde (37 wt%, ACS Reagent, Aldrich) were mixed in a glass test tube (approx 50 mL) with DI water using sodium carbonate as polymerization catalyst. The solution pH was adjusted to near 7 before the test tube was sealed with a rubber septum. The sol was cured at room temperature, 50 °C and 90 °C, one day each, then the gel was exchanged with acetone three times to remove water from inside the pores. The acetone-filled RF gel was then dried in air. Finally the carbon xerogel product was obtained after carbonizing the dried organic RF gel at 1050°C under flowing N_2 for 4 h.

3.2.2 Catalyst deposition onto carbon xerogel

Carbon aerogel (CX) samples (about 0.1 g) were ground in an agate mortar to a fine powder, and the resulting powders were sonicated in 30 mL DI water for 15 min. Then, a diluted H_2PtCl_6 (Acros Organics, 40% Pt) solution was added into the carbon powder suspension and sonicated for another 30 min. The mass of platinum salt added to the CX sample corresponded to 20 wt% of platinum metal in the final material. After sonication, the mixture pH was adjusted to 11 and an excess amount (10x) of formaldehyde was diluted in DI water (2 mL) and added drop by drop into the carbon suspension under stirring. The mixture was kept stirring for another 15 min at room temperature, then the

reaction temperature was raised to 90 ºC and kept at 90 ºC for 2 h under stirring. Then the reaction was cooled down to room temperature and diluted HCl (2 mol L^{-1}) was added to promote precipitation of Pt catalyst onto carbon powders. The Pt deposited carbon xerogel powder (Pt/CX) was then filtered, thoroughly washed with deionized (DI) water, and dried at 100 °C under vacuum. For all Pt/CX samples subjected to further analysis, the final Pt content was approximately 20% weight percent as measured by thermogravimetric analysis (TGA) under O_2 atmosphere.

3.2.3 Characterization of the materials

3.2.3.1 N_2 adsorption/desorption method

The specific surface area and pore texture of the carbon xerogels were characterized by the analysis of nitrogen adsorption–desorption isotherms, performed at 77 K with a Micromeritics ASAP 2010 apparatus. The sample was degassed at 200 ºC for one day before measurement. The specific surface area (S_{BET}) of carbon xerogel samples was obtained using the Brunauer-Emmett-Teller (BET) model[23], micropore properties (microporous volume V_{micro}, microporous surface area S_{micro}) were obtained using the t-plot method[24, 25] and the Barrett-Joyner-Halenda (BJH) model[26] was used to evaluate the mesopore properties (mesoporous volume V_{meso}, mesoporous surface area S_{meso} pore size and distribution (PSD). The total pore volume (V_{total}) was recorded at P/P$_0$ of near saturation. As a comparison, a commercial support Vulcan XC-72R from Cabot Company (without Pt) was also characterized by the N_2 adsorption/desorption method.

3.2.3.2   Powder X-ray diffractometry

X-ray powder diffractograms of Pt/CX and Pt/XC-72R (20% Pt, Alfa Aesar) samples were obtained using a Scintag XDS2000 powder x-ray diffractometer using Cu Kα radiation of wavelength 0.1540 nm. The 2θ angular range between 5 and 90 degrees was scanned at 0.5 s per step in 0.02 º steps.

3.2.3.3   Electron microscopy

Scanning electron microscopy (SEM) measurements on Pt/CX samples were performed using a Hitachi S-4800 microscope equipped with an Oxford INCA EDS detector. Pt mapping was done with EDS. The powder sample was mounted on a double-sided carbon sticky tape. Transmission electron microscopy (TEM) measurements were performed on Pt/CX and Pt/XC-72R samples using a Hitachi H7600T transmission electron microscope which was operated at an accelerating voltage of 200 kV. The samples were prepared by dispersing a small amount of the catalyst powder in ethanol with ultrasonic treatment. Several drops of the dispersion were taken using a pipette and put on a holey carbon copper grid, followed by drying in air at room temperature overnight.

3.2.3.4   Thermogravimetry analysis

The Pt contents of Pt/CX and Pt/XC-72R samples were determined from the residual mass following TGA under O_2 atmosphere at 850 °C with a heating rate of 15 ºC min^{-1} using a Mettler Toledo TGA/SDA 851e analyzer. Residual mass for Pt-containing samples is assumed to be Pt metal. TGA runs on Pt-free carbon samples showed very low residual masses (< 1%).

3.2.3.5 *Ex-situ* cyclic voltammetry and CO stripping voltammetry

Ex-situ cyclic voltammetry (CV) was employed to characterize the electrochemically active surface area (ESA) of Pt catalysts. CV measurements were made using a CH Instruments model 660A electrochemical with a standard three-electrode cell with home-made Hg/Hg_2SO_4 (0.1 mol L^{-1} H_2SO_4) reference and Pt wire counter electrodes. The working electrode was a freshly cleaned glassy carbon (GC) plate electrode onto which a thin layer electrode was formed by evaporation of 10 µL of a well-mixed ink suspension consisting of supported catalyst and solubilized Nafion solution in isopropanol (0.5 mL isopropanol, 10 mg Pt/C catalyst, and 50 mg 5% Nafion (EW 1100, Solution technology) mixed together and stirred overnight). *Ex-situ* CV measurements were performed by partial immersion of the GC electrode in 0.5 mol L^{-1} deaerated H_2SO_4 solutions with N_2 blanket on the top. Before recording the CVs used to determine ESA, the potential was repeatedly cycled until a stable voltammogram was obtained. In the case of CO stripping, electrodes were exposed to CO by brief bubbling with CO gas with the electrode held at -0.25 V (vs. Hg/Hg_2SO_4) prior to voltammetric analysis.

3.2.3.6 MEA fabrication

Membrane electrode assemblies (MEAs) were prepared using the decal transfer method developed by Wilson and co-workers[27, 28]. In brief, an ink was prepared by mixing carbon supported catalyst (20% Pt/CX, or 20% Pt/XC-72R), solubilized Nafion solution (5%, EW 1100), isopropanol, glycerol and tetrabutyl ammonium hydroxide solution (1mol L^{-1} in methanol, Aldrich) with a dry mass ratio of Pt/carbon to Nafion of 5:2. The ink was applied via several steps of painting thin layers of ink onto Teflon-coated fiberglass

templates followed by heating at 140 ºC for 30 min to remove solvent, to achieve a Pt catalyst loading in the range of 0.25 mg cm^{-2}. An MEA was then made by hot-pressing a Nafion 117 membrane in Na^{+} form with two ink-coated templates (one on each side) at 200-210 ºC and 600 lbs force for 5 min. Following hot pressing, the MEA was boiled in 0.5 mol L^{-1} sulfuric acid for 1 hr to convert all ionomer back to the proton form, then boiled in DI water for 1 h and washed with DI water several times. The MEAs were stored in DI water before use.

3.2.3.7 Single fuel-cell testing

The single-cell testing of MEAs was performed on a model 850C test station from Scribner Associates Company. Before assembling in the test fixture, the MEA was pulled dry and flat on a vacuum table at 60 °C for 20 min, and then the MEA was mounted on the test fixture by sandwiching the MEA between the two pieces of uncatalyzed gas diffusion backing (ELAT/NC, E-TEK). The active area of an MEA is 5 cm^{2}. Humidified fuel (H$_2$) and oxidant (O$_2$ or air) gases were supplied to the test fixture by the test station. The cell was operated under ambient pressure on both the anode and cathode. Cells were broken in at a cell voltage of 0.5 V overnight, after which a series of polarization curves was acquired in controlled voltage mode under different operating conditions. The cell open circuit voltage was close to or above 1.0 V for all MEAs. The cell resistance was monitored during acquisition of the polarization curves using the current interrupt method (CI) and by high frequency impedance spectroscopy (HFR) at 1 kHz frequency.[29]

3.2.3.8 *In-situ* MEA cyclic voltammetry

The *in-situ* CV measurement was used to obtain ESA values for the supported Pt catalysts in the MEAs in the fuel-cell test fixture [30]. For such a measurement the fuel-cell station operated in a two-electrode configuration in which the anode severed as both pseudo-reference and counter electrodes, and the cathode served as the working electrode. The anode was fed with high purity H_2 gas (humidified) and the cathode was fed with high purity N_2 gas (humidified). The gas flow of both N_2 and H_2 was kept at 50 mL min^{-1} during the measurements. The Solartron 1280B electrochemical measurement unit was used as a potentiostat. The potential was cycled between 0 to 0.8 V with a scan rate of 40 mV s^{-1}.

3.3 Results and discussion

The CX samples synthesized as described above were characterized via their N_2 adsorption and desorption isotherms in comparison with the commercial carbon black support Vulcan XC-72R (which was used as the catalyst support for the commercially obtained Pt/XC-72R samples). The N_2 adsorption and desorption isotherms are shown in Figure 3.1. The CX sample shows a type IV, H2 isotherm according to IUPAC classification[31] indicating that mesopores exist in the sample. The pore size distribution (PSD) deduced from the BJH method for both CX and XC-72R samples is shown in Figure 3.2. The CX sample has a relatively sharp pore size distribution, with pore sizes between 5-30 nm while XC-72R carbon shows a broad PSD of about 2-300 nm. The XC-72R broad PSD was reported in literature and reflects its aggregate and agglomerate structure. Other textural properties of CX and XC-72R are listed on Table 3.1. From

Table 3.1 it is seen that CX has nearly double the BET surface area of XC-72R while the mesoporosity (V_{meso}/V_{total}) for both samples is nearly the same. The CX sample has more micropore surface area (higher S_{micro}/S_{BET}) although for both supports, the micropore volume is low.

Table 3.1 Textural property of carbon xerogel and carbon black

Carbon	S_{BET} m^2g^{-1}	S_{micro} m^2g^{-1}	$S_{micro}/$ S_{BET}	V_{total} cm^3g^{-1}	V_{micro} cm^3g^{-1}	V_{meso} cm^3g^{-1}	$V_{meso}/$ V_{total}	d_{BET} nm	d_{BJHads} nm	d_{BJHdes} nm
CX	462	197	0.43	0.81	0.09	0.70	0.86	7.0	10.4	9.9
XC-72R	237	83	0.35	0.62	0.04	0.55	0.89	10.4	17.6	22.7

S_{BET}: BET surface area, S_{micro}:micropore surface area by t-plot, V_{total}:total pore volume at near saturation pressure, V_{meso}:cumulative volume of pores between 1.7 and 300 nm by BJH adsorption branch, d_{BET}, d_{BJHads}, d_{BJHdes}:average pore width by 4V/A

Figure 3.1 N_2 sorption isotherms of carbon xerogel (CX) (●) and XC-72R (○)
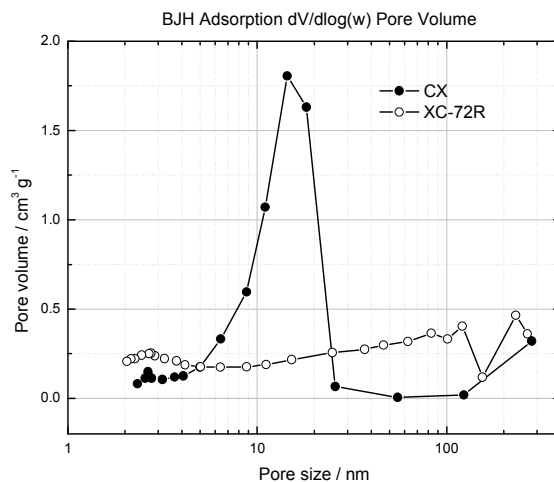
Figure 3.2 The pore size distribution of carbon xerogel (CX) (●) and XC-72R (○)

The Pt catalyst was deposited onto CX powder samples by the impregnation-reduction method using hexachloroplatinic acid as a Pt precursor and formaldehyde as a reducing agent.[32, 33] TGA analysis showed the Pt contents in most Pt/CX samples were close to the 20 wt % value expected from the amount of hexachloroplatinic acid used in the Pt deposition step. This finding confirms that Pt reduction/deposition proceeds with high efficiency.
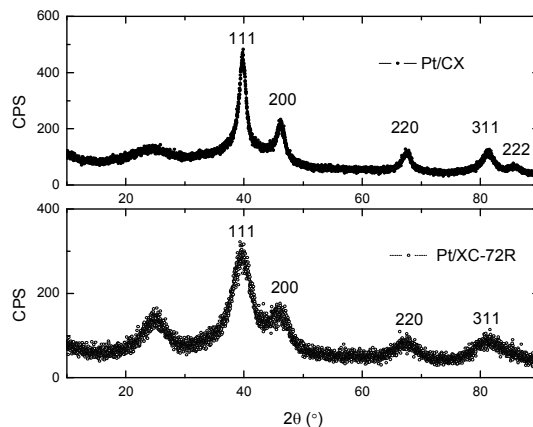
Figure 3.3 XRD graphs of carbon supported catalysts Pt/CX (top) and Pt/XC-72R (bottom)

The Pt/CX samples were subjected to powder XRD analysis to confirm Pt deposition and allow for estimation of Pt particle sizes. The XRD graphs of a representative Pt/CX sample and a commercial Pt/XC-72R sample are shown in Figure 3.3. The diffractogram shows features expected for Pt as labeled on the graph; the feature near 25 degrees 2-theta is from the carbon substrate. The Pt diffraction lines are generally narrower for the Pt/CX sample relative to the Pt/XC-72R sample, which suggests that the Pt particles on the Pt/CX sample are larger.

Table 3.2 Pt nanoparticle size and specific surface area by different methods (XRD, TEM, *ex-situ* CV (H), *ex-situ* CV (CO) and *in-situ* CV (H)

Sample	d_{XRD}	S_{XRD}	d_{TEM}	S_{TEM}	S_H	S_{CO}	$S_{in-situ}$
	nm	$m^2 g^{-1}$	nm	$m^2 g^{-1}$	$m^2 g^{-1}$	$m^2 g^{-1}$	$m^2 g^{-1}$
Pt/CX	4.5	62.3	3.3	85	67	63	55
Pt/XC-72R	2.2	127.4	2.8	100.1	67	66	65

d_{XRD}: particle size by XRD, d_{TEM}: particle size by TEM, S_{XRD}, S_{TEM}: the specific surface area calculated from the equation (2) from XRD and TEM respectively, S_H: specific surface area from *ex-situ* CV (H desorption charge), S_{CO}: surface area from *ex-situ* CO stripping CV, $S_{in-situ}$: surface area from *in-situ* CV (in MEA)

Nanoparticle sizes may be quantified from powder XRD data using the Scherer equation. For the case of Pt on carbon it is common to use the Pt (220) line for this analysis. According to the Scherer equation (Equation 3.1),[34] from the line broadening of the Pt crystal face 220[35], the Pt particle size may be estimated.

$$d(nm) = \frac{0.9\lambda}{B\cos(\theta)} \qquad (3.1)$$

In this equation d is the Pt crystal size (diameter), λ is the X-ray wavelength (0.1540 nm), B is the full width at half height for the diffraction peak in radians and θ is half of the diffraction angle. Particle size values obtained in this way for Pt/CX and Pt/CX-72R are given in Table 2. As expected, Pt particle diameters are higher for the Pt/CX sample (4.5 nm) than the Pt/XC-72R (2.2 nm).

From the particle size obtained as described above, the Pt specific surface area may be calculated using Equation 3.2:

$$S(\text{m}^2\text{g}^{-1}) = \frac{6000}{\rho d} \qquad (3.2)$$

In his equation d is the Pt particle diameter (nm), and ρ is the Pt density (21.4 g cm^{-3}). Pt specific surface areas calculated in this way are listed in Table 2 for Pt/CX and Pt/XC-72R samples. These values will be compared with Pt specific surface area values obtained from TEM estimates of Pt particle size, and also with ESA values obtained by *ex-situ* and *in-situ* CV measurements.

An SEM micrograph and Pt map (by EDX) of a Pt-deposited carbon xerogel sample are seen in Figure 3.4. The ground CX sample consists of a broad range of particle sizes, from submicron to several tens of microns. This finding is in sharp contrast to carbon black supports which are generally very fine powders. The Pt spatial distribution on the CX supports is shown in the Pt EDX map to be relatively homogeneous on the length scale shown in the figure. The Pt/CX powder samples were ground a second time before using them to make the catalyst ink for MEA fabrication, and also the thin-film

electrodes used for *ex-situ* CV experiments. This was done to make the MEA active

layers more homogeneous and thin.
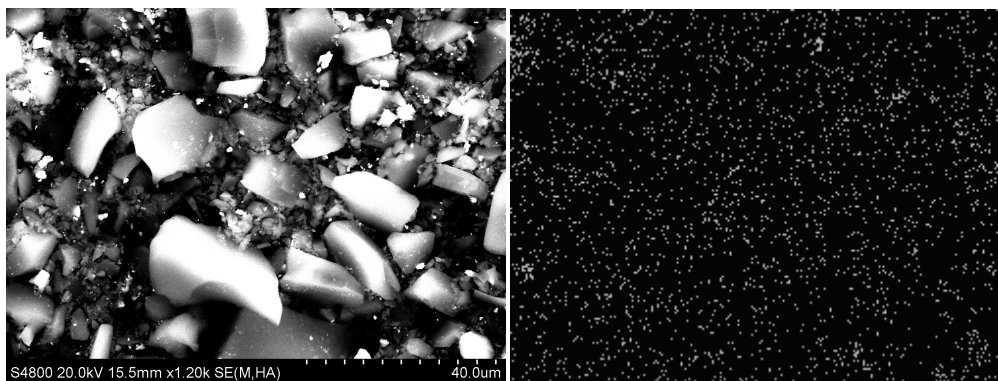
Figure 3.4 SEM micrograph and Pt mapping of Pt/CX, left: SEM, right: Pt map (white spot: Pt particle)
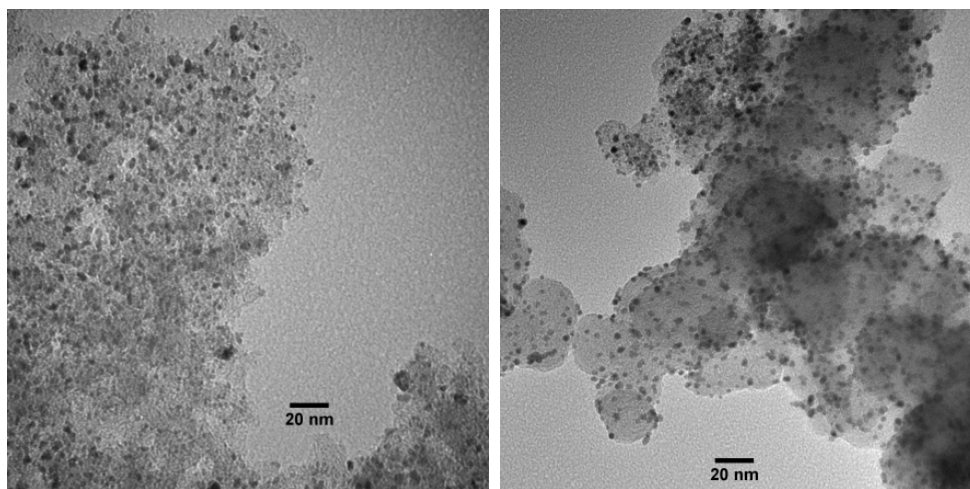
Figure 3.5 TEM micrographs of Pt/CX (left) and Pt/XC-72R (right)
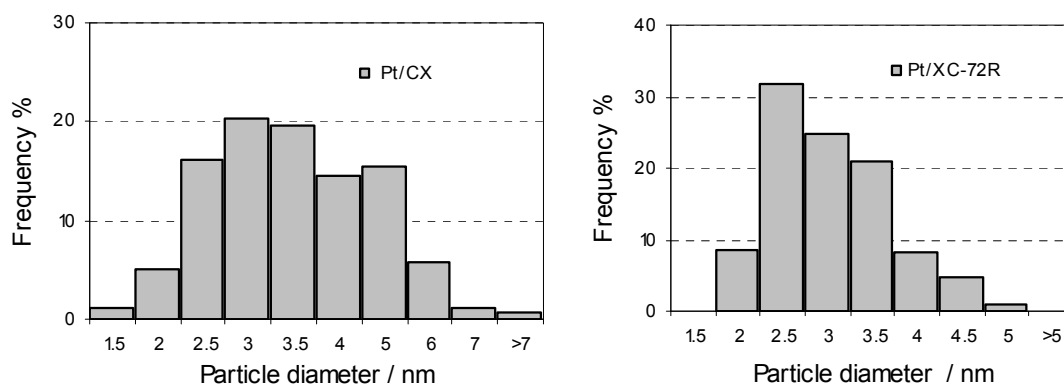
Figure 3.6 Pt Particle size histogram of carbon supported catalysts by TEM, Pt/CX (left, $d_{mean} = 3.3 \pm 1.1$ nm), and Pt/XC-72R (right, $d_{mean} = 2.8 \pm 0.7$ nm)

Transmission electron microscopy (TEM) was used to characterize catalyst supports on a much finer length scale than SEM, and to provide an alternate estimate of Pt particle size. The TEM micrographs and the histogram graphs of Pt particle size for the Pt/CX and Pt/XC-72R samples are shown in Figures 3.5 and 3.6 respectively. The micrograph for Pt/XC-72R shows the typical structure expected for carbon black of aggregates of small carbon primary particles. The Pt/CX sample does not show this structure; rather it consists of larger regions of porous carbon. Lower magnification TEM micrographs (not shown) support this view of the CX samples as consisting of relatively large particles with internal porosity. Both TEM micrographs also clearly show the supported Pt particles. In both cases but particularly for the Pt/CX sample, the Pt particles appear to be distributed all throughout the carbon support, and not just on the carbon particle surface. The mean Pt diameter for Pt/CX and Pt/XC-72R samples is estimated to be 3.3 ± 1.1 nm and 2.8 ± 0.7 nm respectively by counting more than 200 particles from each TEM image using ImageJ software.[36] Error estimates are standard deviations from which a slightly broader Pt size distribution for Pt/CX is seen. The specific surface area (SA) of Pt could

be calculated according to Equation (2) from the Pt particle size measured by TEM or XRD on the Pt/CX and Pt/XC-72R samples, and the values are listed on Table 3.2 in comparison with the ESA measured by *ex-situ* and *in situ* CVs. Pt specific SA of Pt/CX is smaller than that of Pt/XC-72R due to smaller Pt particle size on Pt/XC-72R. Usually the Pt catalyst specific surface area from TEM and XRD are larger than that measured by *ex-situ* or *in-situ* CV because TEM or XRD measurement includes electrochemically-inaccessible Pt particle. Also the ESA measured *ex-situ* (in a half cell) is commonly higher than that measured *in-situ* (in a full cell) due to better ion conduction by help from free acid (H_2SO_4) in the half–cell measurement. These will be seen in following discussion.

Ex-situ CV is commonly used to estimate electrochemically active Pt surface area (ESA) for comparison with areas calculated from Pt particle sizes. Estimates may be obtained from H adsorption/desorption or CO stripping. For the case of H adsorption/desorption, the ESA (S_{ESA} m^2 g^{-1} Pt) may be calculated from Equation 3.3:[37]

$$S_{ESA}(\text{m}^2\text{g}^{-1}\text{Pt}) = 100\frac{q}{\Gamma L_{Pt}}$$

(3.3)

In this equation q is the hydrogen adsorption or desorption charge density determined by CV (mC cm^{-2}), Γ (210 μC cm^{-2}) is the well-established quantity for the charge to reduce a monolayer of protons on Pt, L_{Pt} is the Pt loading in the electrode (mg cm^{-2}). Figure 3.7 (left) presents CVs for Pt/CX and Pt/ XC-72R samples for the H adsorption or desorption region. The CV shapes are as expected for Pt on carbon. Estimates of the hydrogen adsorption or desorption charge density were made as described in references [37, 38], and ESA values are given in Table 3.2. Somewhat surprisingly, ESA values are

nearly identical for the two samples despite previous findings that Pt particles sizes are smaller for the Pt/XC-72R sample. We believe that this finding reflects the possible presence of Pt particles in micropores of the Pt/XC-72R sample that may be inaccessible to even liquid electrolyte. It is possible that Pt particles did not enter into micropores in the Pt/CX sample due to the technique used to make Pt particles and deposit them.
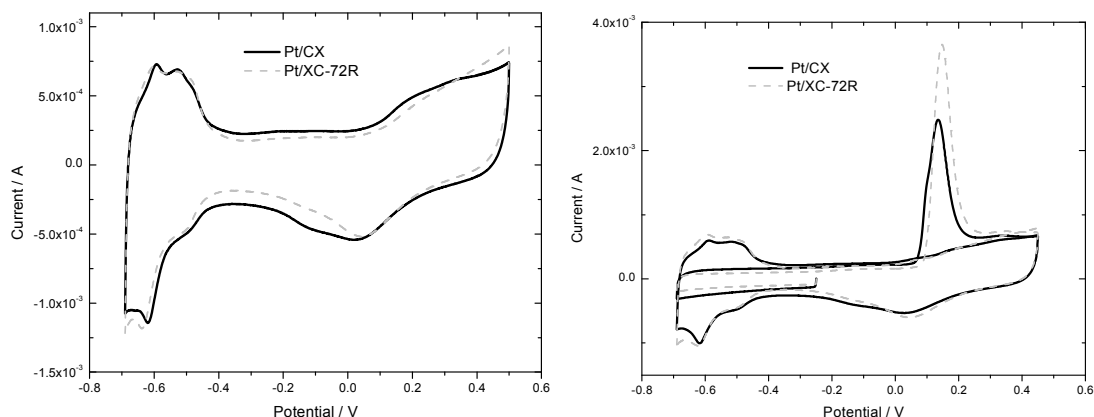
Figure 3.7 *Ex-situ* CVs (left) and CO stripping CVs (right) of Pt/CX (solid line) and commercial Pt/XC-72R (dash line), WE: thin-film-catalyst coated GC, RE: Hg/Hg$_2$SO$_4$, CE: Pt wire; scan rate: 20 mV s^{-1}

Figure 3.7 (right) shows *ex-situ* CVs for CO stripping for Pt/CX and Pt/ XC-72R samples. ESA values were again obtained using Equation 3.3 but with a Γ value of (420 $\mu C \ cm^{-2}$)[37] which is appropriate for CO stripping. ESA values from CO stripping are in relatively good agreement with those from hydrogen adsorption or desorption (i.e. agreement to within ten percent which is as good as can be expected given the uncertainties associated with baseline subtraction in CV integration, sample weighing and volume measurement by micro-pipette), which serves to validate both methods. We note that the onset and peak potentials for CO oxidation are shifted slightly negative for Pt/CX

59

relative to Pt/XC-72R. This shift is consistent with expectations if the Pt particles are slightly larger in the Pt/CX catalyst.[39]
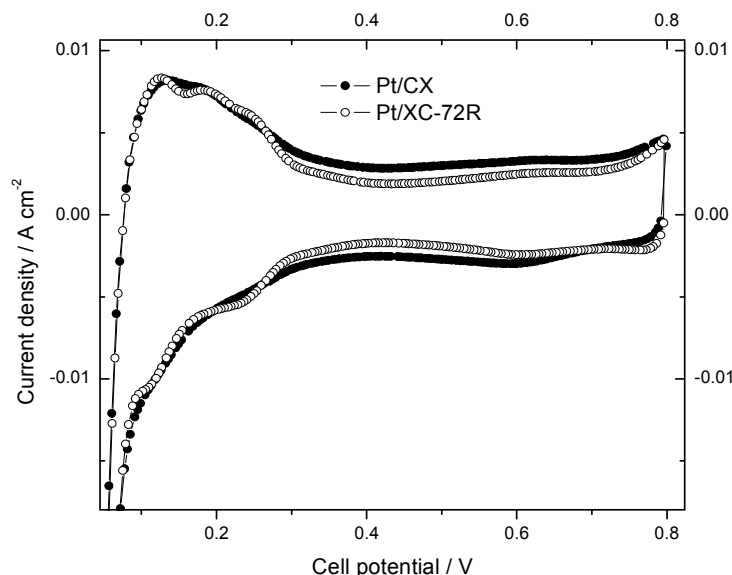
Figure 3.8 *In-situ* CVs of Pt/CX and commercial Pt/XC-72R catalysts; Anode: H_2, 50 mL min^{-1}, Cathode: N_2, 50 mL min^{-1}, cell temperature 30 ºC, potential range 0-0.8 V, scan rate 40 mV s^{-1}

In-*situ* CV may be used to estimate Pt ESA in intact electrodes in MEAs. Comparison of ESAs for such samples with those obtained by *ex-situ* CV provides information on catalyst utilization in the MEA. Generally, the cathode is of most interest because of the sluggish reaction kinetics of the oxygen reduction. *In-situ* CV (Figure 3.8) yielded ESA values for Pt/XC-72R cathodes that were similar to those obtained by *ex-situ* CV in sulfuric acid, suggesting that Pt utilization is high in these electrodes (notwithstanding the comment above regarding the possible presence of Pt trapped in micropores in Pt/XC-72R which would be inaccessible to both *in-situ* and *ex-situ* CV). In contrast, *in-situ* CV (Figure 3.8) for Pt/CX cathodes revealed a smaller ESA value, e.g. 55 m^2 g^{-1}, than was

obtained by *ex-situ* CV, e.g. 63 - 67 m^2 g^{-1}. This finding suggests that access of Nafion

electrolyte to Pt particles in Pt/CX electrodes is diminished relative to that for Pt/XC-72R

electrodes.
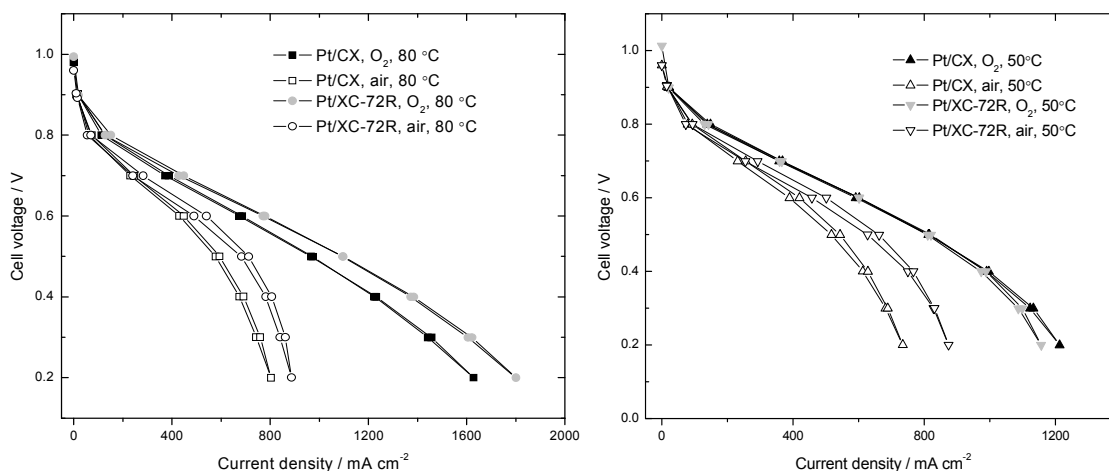
Figure 3.9 Polarization curves of MEAs tested in H_2/O_2 or H_2/air cells, at 80 ºC (left) and
at 50 ºC (right) Measurement conditions: H_2/O_2 or air, cell temperature 80 or 50 ºC,
stoichiometric ratio, H_2 1.25, O_2 1.5, or air 4.0, all measurements at atmospheric pressure,
and Pt around 0.25 mg cm^{-2} in both anode and cathode, respectively

MEAs fabricated with both Pt/CX and Pt/XC-72R catalysts were tested at 50 ºC and 80

ºC in both H_2/O_2 and H_2/air cells under atmospheric pressure conditions. The polarization

and resistance curves are shown in Figures 3.9 and 3.10 respectively. In the following

discussion we consider two ways of analyzing these data. In one approach we consider

performance at high cell voltage (0.9 V) and low current density, where current is limited

principally by the catalyst intrinsic activity. This approach allows for quantitative

comparison of catalyst intrinsic activity with published values for related catalysts. The

second approach focuses on performance at higher current density and lower cell voltage.

These conditions are closer to those under which a cell would operate in a real-world

application. Comparison of performance under these two conditions allows for a more careful consideration of loss mechanisms under different operating conditions.

Table 3.3 Specific activity $I_{s(0.9V)}$ and mass activity $I_{m(0.9V)}$, of Pt/CX and Pt/XC-72R catalysts at 80 °C, H_2/O_2, 100% RH, atmospheric pressure

Sample	$ESA_{in\text{-}situ}$	Pt loading	$I_{(0.9\ V)}$	$I_{s(0.9V)}$	$I_{m(0.9V)}$	$I*_{s(0.9V)}$ 100kPa	$I*_{m(0.9V)}$ 100kPa
	$m^2\ g^{-1}$	$mg\ cm^{-2}$	$mA\ cm^{-2}$	$\mu A\ cm^{-2}$	$mA\ mg^{-1}$	$\mu A\ cm^{-2}$	$mA\ mg^{-1}$
Pt/CX	55	0.23	17.3	136	75	259	143
Pt/XC-72R	65	0.28	19.7	108	70	206	134

$I*_{s(0.9V)\ 100kPa}$ and $I*_{m(0.9V)\ 100kPa}$ values are after correction for the oxygen partial pressure which were made assuming a first-order dependence of cell current on oxygen partial pressure and a water partial pressure of 47.37 kPa which corresponds to saturation conditions at 80 °C and 100% RH
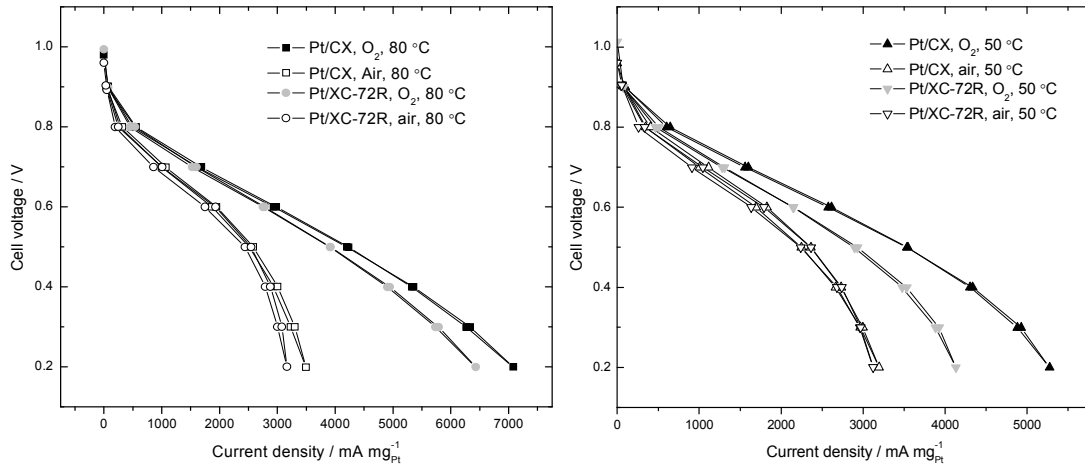
Figure 3.10 Polarization curve data from Figure 3.9 with currents normalized to Pt loading

Table 3.3 presents values for the intrinsic catalyst activity for Pt/CX and Pt/XC-72R cathodes at 80 °C in H_2/O_2 cells at 100% RH at atmospheric pressure. Values are given for both area-normalized and mass-normalized activity at 0.9 V cell voltage which

follows the recommended procedure for comparing intrinsic catalyst activities under conditions where ohmic and mass-transfer limits should be minimized.[40, 41] The lower values are without correction for the oxygen partial pressure (which is less than 1 atm due to the partial pressure of water vapor) and the higher values are after correction for the contribution of water partial pressure, assuming first-order dependence of current on oxygen partial pressure. Comparison with literature values shows that these catalysts have quite high activities. For example Gasteiger and co-workers[40] have suggested that an area-specific activity of 170-210 $\mu A\ cm^{-2}$ Pt is a good benchmark for comparison with new catalysts, and both our catalysts exceed this value. Significantly, the area-specific activity for the Pt/CX catalyst exceeds that of the Pt/XC-72R catalyst by approximately 20 percent. This finding is consistent with the fact that the Pt/CX catalyst has a slightly larger Pt particle size. Larger Pt particles have been shown to give higher area-specific activities.

Next, the cell performance at lower cell voltages is considered, near 0.3 - 0.6 V, where current densities are much higher, e.g. by up to 80 times, and mass transfer limitations are more prevalent. The performance of Pt/CX cells in H_2/O_2 at 80 ºC (as indicated by current density at a particular cell voltage) is slightly poorer than that of Pt/XC-72R. The performance of Pt/CX in H_2/O_2 at 50 ºC is close to that of Pt/XC-72R while performance in H_2/air at both 50 ºC and 80 ºC is poorer. Performance under such conditions is affected by many factors, one of which is Pt loading, and it is instructive to compare performance curves following normalization for Pt loading. Figure 3.10 presents the data from Figure 3.9 with just this normalization applied. It is clear that under all conditions, but especially

63

in H_2/O_2 at lower temperature, performance of the Pt/CX cell is slightly better than that of the Pt/XC-72R cell. We believe that this slightly improved performance of the Pt/CX cell under these higher current density conditions reflects a lower mass-transfer resistance in the Pt/CX catalyst.

The curves of areal resistance vs current density of MEAs made with Pt/CX and Pt/XC-72R are shown in Figure 3.11. The areal resistance for Pt/CX is slightly lower than that of Pt/XC-72R although Pt/XC-72R has the higher currents (see Figure 3.9). Because the two MEAs were tested using similar Nafion 117 membranes, the resistance difference should be caused by the active catalyst layer and not the membrane. This finding may therefore indicate a lower electrical contact resistance between the membrane and the catalyst layer in the Pt/CX sample.
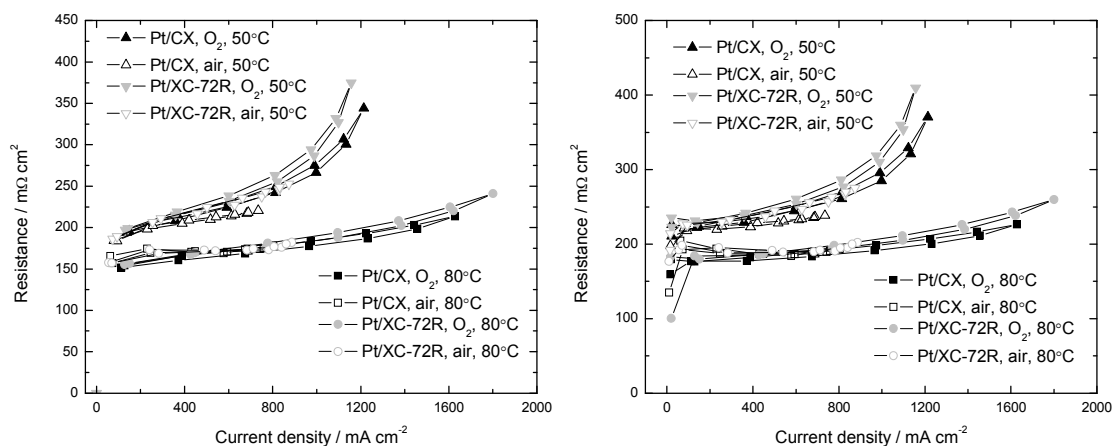
Figure 3.11 Resistance of the carbon supported catalysts by CI (left) and HFR (right) methods, measurement conditions same as that in Figure 3.9, for HFR, frequency at 1 kHz

3.4   Conclusions

Carbon xerogel with high surface area and a peak pore size 14 nm was synthesized by the RF sol-gel method using ambient pressure drying and explored as a catalyst support for polymer electrolyte fuel cells in comparison with a commercial carbon black XC-72R-supported catalyst. Both catalysts were characterized with XRD, SEM, TEM, cyclic voltammetry both *ex-situ* (thin film electrode supported on glassy carbon and immersed in electrolyte) and *in-situ* (in an MEA). The Pt/CX catalyst was shown to have slightly higher Pt particle sizes, slightly lower accessibility of Pt particles to Nafion electrolyte, and slightly higher intrinsic catalytic activity at 0.9 V cell voltage when normalized to Pt area. Cell performance at lower cell voltages/higher current densities was slightly lower for a Pt/CX MEA than for a Pt/XC72R MEA, however performance was slightly higher following normalization for Pt loading This finding may reflect a lower mass transfer resistance within the pores of the Pt/CX sample.

3.5   References

1.   P. Costamanga and S. Srinivasan, *Journal of Power Sources*, 2001, **102**, 242-252.

2.   H. Liu, C. Song, L. Zhang, J. Zhang, H. Wang and D. P. Wilkinson, *Journal of Power Sources*, 2006, **155**, 95-110.

3.   A. L. Dicks, *Journal of Power Sources*, 2006, **156**, 128-141.

4.   R. W. Pekala and F. M. Kong, *Polymer. Preprints*, 1989, **30**, 221.

5.   R. W. Pekala, *Journal of Materials Science*, 1989, **24**, 3221-3227.

6.   S. A. Al-Muhtaseb and J. A. Ritter, *Advanced Materials*, 2003, **15**, 101-114.

7.   J. Fricke and R. Petricevic, *Handbook of Porous Solids*, 2002, **3**, 2037-2062.

8.   M. Glora, M. Wiener, R. Petricevic, H. Pröbstle and J. Fricke, *Journal of Non-Crystalline Solids*, 2001, **285**, 283-287.

9.   A. Smirnova, X. Dong, H. Hara, A. Vasiliev and N. Sammes, *International Journal of Hydrogen Energy*, 2005, **30**, 149-158.

10.   A. Smirnova, X. Dong, H. Hara and N. Sammes, *Journal of Fuel Cell Science and Technology*, 2006, **3**, 477-481.

11.   J. L. Kaschmitter, S. T. Mayer, R. W. Pekala, US Patent 5601938, WO 9520246, 1995.

12.   R. Petricevic, G. Reichenauer, V. Bock, A. Emmerling and J. Fricke, *Journal of Non-Crystalline Solids*, 1998, **225**, 41-45.

13.   R. Saliger, V. Bock, R. Petricevic, T. Tillotson, S. Geis and J. Fricke, *Journal of Non-Crystalline Solids*, 1997, **221**, 144-150.

14.   R. Petricevic, M. Glora and J. Fricke, *Carbon*, 2001, **39**, 857-867.

15.   J. Marie, S. Berthon-Fabry, P. Achard, M. Chatenet, A. Pradourat and E. Chainet, *Journal of Non-Crystalline Solids*, 2004, **350**, 88-96.

16.   P. V. Samant, J. B. Fernandes, C. M. Rangel and J. L. Figueiredo, *Catalysis Today*, 2005, **102-103**, 173-176.

17.   J. L. Figueiredo, M. F. R. Pereira, P. Serp, P. Kalck, P. V. Samant and J. B. Fernandes, *Carbon*, 2006, **44**, 2516-2522.

18.   C. Arbizzani, S. Beninati, E. Manferrari, F. Soavi and M. Mastragostino, *Journal of Power Sources*, 2007, **172**, 578-586.

19.   H. Du, B. Li, F. Kang, R. Fu and Y. Zeng, *Carbon*, 2007, **45**, 429-435.

20.   E. Guilminot, F. Fischer, M. Chatenet, A. Rigacci, S. Berthon-Fabry, P. Achard and E. Chainet, *Journal of Power Sources*, 2007, **166**, 104-111.

21.   N. Job, J. Marie, S. Lambert, S. Berthon-Fabry and P. Achard, *Energy Conversion and Management*, 2008, **49**, 2461-2470.

22.   H.-J. Kim, W.-I. Kim, T.-J. Park, H.-S. Park and D. J. Suh, *Carbon*, 2008, **46**, 1393-1400.

23.   S. Brunauer, P. H. Emmett and E. Teller, *Journal of the American Chemical Society*, 1938, **60**, 309-319.

24. B. C. Lippens and J. H. de Boer, *Journal of Catalysis*, 1965, **4**, 319-323.

25. R. S. Mikhail, S. Brunauer and E. E. Bodor, *Journal of Colloid and Interface Science*, 1968, **26**, 45-53.

26. E. P. Barrett, L. G. Joyner and P. P. Halenda, *Journal of the American Chemical Society*, 1951, **73**, 373-380.

27. M. S. Wilson, J. A. Valerio and S. Gottesfeld, *Electrochimica Acta*, 1995, **40**, 355-363.

28. M. S. Wilson and S. Gottesfeld, *Journal of Applied Electrochemistry*, 1992, **22**, 1-7.

29. K. R. Cooper and M. Smith, *Journal of Power Sources*, 2006, **160**, 1088-1095.

30. K. R. Cooper, V. Ramani, J. M. Fenton and H. R. Kunz, *Experimental methods and data analyses for polymer electrolyte fuel cells*, 1.5 edn., Scribner Associates, Inc., 2007.

31. K. S. W. Sing, D. H. Everett, R. A. W. Haul, L. Moscou, R. A. Pierotti, J. Rouquerol and T. Siemieniewska, *Pure and Applied Chemistry*, 1985, **57**, 603-619.

32. J. H. Tian, F. B. Wang, Z. Q. Shan, R. J. Wang and J. Y. Zhang, *Journal of Applied Electrochemistry*, 2004, **34**, 461-467.

33. Z. Zhou, S. Wang, W. Zhou, L. Jiang, G. Wang, G. Sun, B. Zhou and Q. Xin, *Physical Chemistry Chemical Physics*, 2003, **5**, 5485-5488.

34. J. I. Langford and A. J. C. Wilson, *Journal of Applied Crystallography*, 1978, **11**, 102-113.

35. Z.-H. Teng, G. Wang, B. Wu and Y. Gao, *Journal of Power Sources*, 2007, **164**, 105-110.

36. http://rsb.info.nih.gov/ij/, accessed on August 4, 2009.

37. T. Vidakovic, M. Christov and K. Sundmacher, *Electrochimica Acta*, 2007, **52**, 5606-5613.

38. A. Pozio, M. De Francesco, A. Cemmi, F. Cardellini and L. Giorgi, *Journal of Power Sources*, 2002, **105**, 13-19.

39. F. Maillard, S. Schreier, M. Hanzlik, E. R. Savinova, S. Weinkauf and U. Stimming, *Physical Chemistry Chemical Physics*, 2005, **7**, 385-393.

40. H. A. Gasteiger, S. S. Kocha, B. Sompalli and F. T. Wagner, *Applied Catalysis B: Environmental*, 2005, **56**, 9-35.

41. H. A. Gasteiger, W. Gu, R. Makharia, M. F. Mathias and B. Sompalli, in *Handbook of Fuel Cells - Fundamentals, Technology and Applications,* Eds. W. Vielstich, H. A. Gasteiger and A. Lamm, John Wiley & Sons, Ltd., 2003, Vol. 3.

CHAPTER 4

SILICA-SOL-TEMPLATED MESOPOROUS CARBON AS CATALYST SUPPORT FOR POLYMER ELECTROLYTE MEMBRANE FUEL CELL APPLICATION

4.1 Introduction

Polymer electrolyte membrane fuel cells (PEMFCs) receive worldwide attention as power sources in transportation, stationary and portable applications due to their characteristics of high efficiency, high power density, and low emission to the environment. However to be commercially viable, many technical issues remain to be solved, especially the prohibitive product cost and the poor durability and reliability.[1, 2] Catalysts in the electrodes have great influence on the cost and performance of PEMFCs. Current convention for catalysts in PEMFC electrodes is supporting them on porous conductive carbon materials which can provide high dispersion and narrow size distribution for the nanocatalyst particles.[3, 4] The support material itself can affect the electrode (catalyst) durability, and the support material can interact with catalyst particles, which also affects the catalyst's activity.

According to the International Union of Pure and Applied Chemistry (IUPAC), pores are classified, depending on their width, as micropores (<2 nm), mesopores (2-50 nm), and macropores (>50 nm).[5] When used as catalyst supports in fuel cells, it is difficult for microporous carbon materials to form good three-phase contacts in electrodes because it is difficult for the reactants and large size proton conductor (e.g., Nafion electrolyte) to

69

access the micropores when Pt nanoparticles are deposited inside the micropores. Macroporous carbon materials with pore size larger than 50 nm usually have a lower surface area and a higher electrical resistance so they are also often not good candidates for catalyst supports in fuel cells. Mesoporous carbon (MC) materials with pore size between 2 and 50 nm exhibit an attractive structure property as a catalyst support, i.e., a large surface area with larger size mesopores and is expected to bring about better three-phase contacts and therefore better performance for electrodes.

Mesoporous carbon may be classified into two categories according to their structures and morphologies:[6] (1) ordered mesoporous carbon (OMC), which is constructed of regular arrays of uniform mesopores and usually synthesized by nanocasting ordered mesoporous silica templates or by directly templating triblock copolymer structure-directing species and (2) disordered mesoporous carbon (DOMC) with irregular pore structures. In regard to pore structure, OMC is preferred as catalyst support in terms of regular pore structure, specific surface area, electrical conductivity, and mass transport and has been extensively studied as catalyst supports for PEMFCs.[6] But OMCs are generally prepared using ordered mesoporous silicas as hard templates; the long, complex, expensive synthesizing ordered mesoporous silicas makes its widespread applications limited. Also, the control of pore diameter in OMC synthesis is not easy because the control of the pore diameter in the carbon is resulted from controlling the pore-wall thickness of the template which is not easy to execute in synthesis.[7]

This chapter presents the work to employ disordered mesoporous carbon prepared by a silica particle (sol) template method as catalyst supports in PEMFCs. The synthesis

process is easy and the resulting carbon has high surface area and large pore size and broad pore size distribution (10-100 nm). The performance of MC-supported Pt catalysts is compared to that of the most commonly used commercial Vulcan XC-72R supported Pt catalyst. Our work extends prior recent work by others, notably Joo and co-workers, on the use of mesoporous carbon as a PEMFC catalyst support.[8-10] The work here differs from this prior work because it involves samples with an especially high specific pore volume (over 4 cm^3 g^{-1}) and surface area and because it addresses the issue of pore volume in ink formulations, specifically regarding the importance of ionomer inside mesopores.

4.2   Experimental

4.2.1   Synthesis of mesoporous carbon

Mesoporous carbons were prepared by a silica-particle-templated sol-gel method[11, 12] in which resorcinol (98%, Aldrich), and formaldehyde (37 wt%, ACS reagent, Aldrich, as a carbon precursor) were polymerized in the presence of colloidal silica particles Ludox HS 40 (wt% silica in water, Aldrich, average silica particle size 12 nm, as a template), followed by subsequent carbonization and removal of silica particles. The schematic synthesis scheme is shown in Figure 4.1. In a typical synthesis, the mole ratio of resorcinol:formaldehyde: SiO_2:H_2O was kept at 1:2:7.5:86. Resorcinol, formaldehyde and additional water according to the above ratio were mixed and stirred in the presence of silica colloidal solution Ludox HS-40. The initial pH of the mixture was adjusted to close to 8, then the mixture was gelled/aged at 50 °C for one day and 90 °C for another day to produce silica-RF gel composites. After that, the silica-RF gel composite was first dried

71

in air for 1 day, and then dried at 100 °C under vacuum for another day, and finally the composite was carbonized at 850 °C for 3 h under flowing nitrogen gas with a heating rate of 5 °C min^{-1}. The resultant silica-carbon composite was crushed into powder and stirred in 40% NaOH solution overnight to dissolve out the silica component. The mesoporous carbon was finally obtained by filtration and was washed with copious water until the filtrate was neutral.
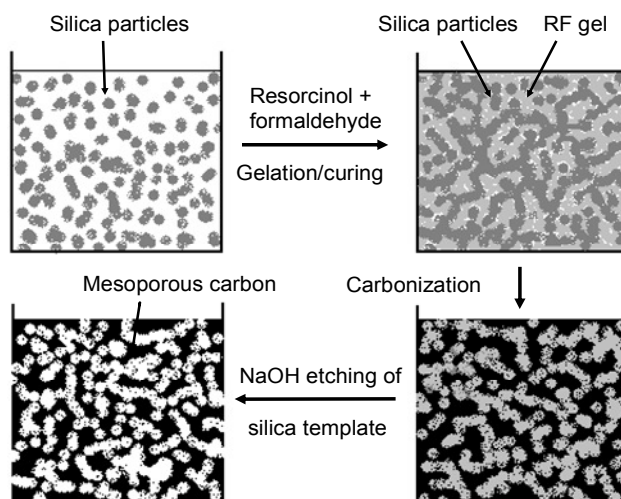
Figure 4.1 Schematic presentation for the synthesis of mesoporous carbons: (1) gelation/curing of resorcinol and formaldehyde (RF) in the presence of silica nanoparticles; (2) carbonization of RF gel-silica composite at 850 °C to get a carbon-silica composite; (3) NaOH etching of silica template to obtain mesoporous carbon

4.2.2 Catalyst deposition onto mesoporous carbon

The MC was ground in an agate mortar down to fine powder, and the resulting powder (around 0.1 g) was suspended in 50 mL dilute H_2PtCl_6 solution and sonicated for 30 min. The mass of platinum salt diluted corresponded to 20 wt% of platinum in the final material. An excess amount (10x) of formaldehyde was diluted in 2 mL distilled water and added dropwise into the carbon suspension to reduce the platinum salt adsorbed on

the carbon surface. The mixture was kept stirring for 15 min at room temperature, and then the temperature was increased to 90°C and kept at the temperature for 2 h, after which the mixture was cooled down and a dilute HCl (4 mol L^{-1}) solution was added to help with deposition of Pt onto MC. Finally, the Pt-deposited carbon powder was filtered, thoroughly washed with water, and dried at 100 °C under vacuum.

4.2.3 Characterization of mesoporous carbon

4.2.3.1 N$_2$ adsorption method

The prepared mesoporous carbon was characterized by the N$_2$ sorption method at 77K using a Micrometrics ASAP 2010 apparatus. The MC sample was degassed at 200 °C for one day before measurement. The specific surface area (S$_{BET}$) of the carbon was extracted from the Brunauer-Emmett-Teller (BET) model[13] and the mesopore (mesoporous volume V$_{meso}$, mesoporous surface area S$_{meso}$) and micropore (microporous volume V$_{micro}$, microporous surface area S$_{micro}$) properties were extracted from the t-plot method.[14, 15] The Barrett-Joyner-Halenda (BJH) model[16] was used to evaluate the pore size and its distribution. The total pore volume (V$_{total}$) was recorded at P/P$_0$ near to saturation.

4.2.3.2 Thermal gravimetric analysis

The silica residue was analyzed by thermal gravimetric analysis (TGA) with Mettler Toledo TGA/STDA 851e analyzer in O$_2$ atmosphere of temperature from 50 °C to 1000 °C at a heating rate of 10 °C min^{-1}. The platinum content in the MC-supported Pt catalyst was also measured by the TGA heating to 850 °C at 15 °C min^{-1} under O$_2$ atmosphere.

4.2.3.3 *Ex-situ* cyclic voltammetry

The electrochemically active surface area (ESA) of the Pt/MC was measured with *ex-situ* cyclic voltammetry (CV) and CO stripping voltammetry using a CH Instruments model 660A electrochemical workstation with a standard three-electrode cell. A home-made Hg/Hg_2SO_4 (0.1 mol L^{-1} H_2SO_4) electrode and a Pt wire served as reference and counter electrodes respectively. The working electrode was a thin-film-coated glassy carbon (GC) plate electrode made by attaching a graphite rod with graphite adhesive to the back of a square GC plate (5 mm each side, geometric surface area 0.025 cm^2). The thin film on the GC was made from an ink mixture of the catalyst of Pt/MC, solubilized Nafion and isopropanol. Further details on formulating the ink and coating a thin film on the GC are provided in reference.[17] ESA values of commercial Pt/XC-72R catalyst samples were measured in a similar way for comparison.

4.2.3.4 Fuel cell testing

The thin film decal transfer method of fabrication of membrane electrode assemblies (MEAs), developed by Wilson and co-workers[3, 18] was employed to make MEAs for both commercial Vulcan XC-72R supported catalyst (20% Pt, Alfa Aesar) and synthesized MC-supported catalyst (Pt/MC, 18% Pt). In brief, an ink was prepared by mixing under stirring of carbon-supported catalyst (20% Pt/CX, or 20% Pt/XC-72R), solubilized Nafion solution (5%, EW 1100), isopropanol, glycerol and tetrabutyl ammonium hydroxide solution (1 mol L^{-1} in methanol) in a small vial with cap. A thin catalyst layer was painted onto a poly(tetrafluoroethylene) (PTFE)-coated template, and then two thin layers were transfer to a Nafion 117 membrane by hot pressing to form a MEA. This

method worked well for the commercial Vulcan XC-72R supported catalyst however an MEA could not be made in this way using the ink of Pt/MC by the decal method with regular ink formulation. The ink film formed after the ink was painted on the templates and heated in oven at 140 °C consistently cracked and peeled from the template (see Figure 4.8 (a)). In contrast, we have previously shown that for Pt deposited onto a carbon xerogel support synthesized without silica template, MEAs could be made using the thin-film method with the regular formulation.[19] So, for MC-supported Pt catalyst, we prepared the ink the same way as in the decal method, and then applied the ink directly onto gas diffusion media to make catalytically active gas diffusion electrodes. Then, an MEA was fabricated by hot pressing two gas diffusion electrodes with a Nafion 117 sandwiched between. For commercial Pt/ XC-72R catalyst, the decal method was still used. The detail about the decal method to make MEAs is seen in references.[3, 18, 19] The MEAs were tested on a Scribner 850 C test station. Cells were broken in at a cell voltage of 0.5 V overnight, after which a series of polarization curves was acquired under different operating conditions. Cell resistance was monitored during acquisition of polarization curves using the current interrupt method.

4.3   Results and discussion

4.3.1   Silica-templated mesoporous carbon

N_2 adsorption–desorption isotherms and pore size distributions (PSDs) of MC compared with carbon black XC-72R are shown in Figures. 4.2 and 4.3, respectively. The MC showed the type IV isotherm with H1 hysteresis loop that is a typical characteristic of mesoporous materials. MC has much higher specific surface area than Vulcan XC-

72R. MC has a broad pore size distribution of 5 to 200 nm with a peak pore size around 60 nm. Silica colloidal particles used in this work as a pore generator have an average particle size of ca. 12 nm. The larger pore size in MC is thought to reflect aggregation of silica particle in the process of synthesis. While Vulcan XC-72R also has a broad pore size distribution, its structure is very different. Oil-furnace carbon black (e.g. Vulcan XC-72/72R) is composed of aggregates that are fused together from primary particles by covalent bonds, with aggregates easily agglomerating together by van der Waals bonds. The large pores in Vulcan XC-72R are mainly from the interstices of aggregates and agglomerates.
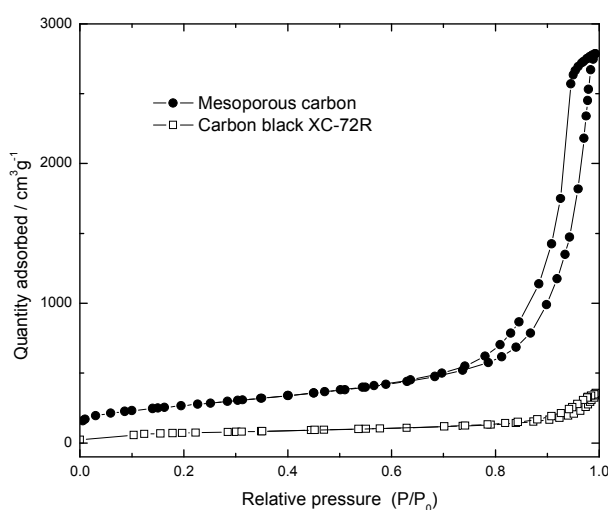
Figure 4.2 N_2 adsorption and desorption isotherm of MC (●) and XC-72R (□)
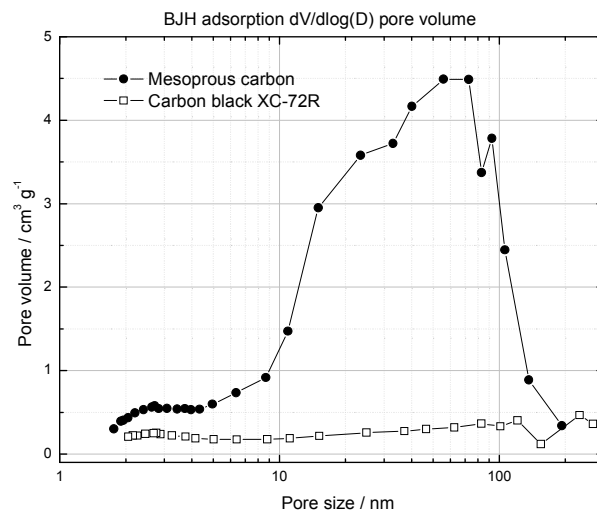
Figure 4.3 BJH pore size distribution of MC (●) and XC-72R (□)

Table 4.1 Textural properties of MC in comparison with Vulcan XC-72R

Carbon	S_{BET}	S_{micro}	V_{total}	V_{micro}	V_{meso}	d_{BET}	d_{BJHads}	d_{BJHdes}
	$m^2\ g^{-1}$	$m^2\ g^{-1}$	$cm^3\ g^{-1}$	$cm^3\ g^{-1}$	$cm^3\ g^{-1}$	nm	nm	nm
XC-72R	237	83	0.62	0.04	0.55	10.4	17.6	22.7
MC	958	128	4.31	0.10	4.33	18.0	18.0	17.6

S_{BET}: BET surface area, S_{micro}:micropore surface area by t-plot, V_{total}:total pore volume at near saturation pressure, V_{meso}:cumulative volume of pores between 1.7 and 300 nm by BJH adsorption branch, d_{BET}, d_{BJHads}, d_{BJHdes}:average pore width by 4V/A

Other textural properties of mesoporous carbon and carbon black XC-72R supports are summarized in Table 4.1. Mesoporous carbon has much larger BET surface area than XC-72R; however, the ratio of meso-macropore area with respect to micropore area of MC support is higher than that of XC-72R, indicating that MC consists mainly of meso-macropores.

The silica residue in MC was analyzed by TGA, indicating 3% silica left after NaOH etching of the RF-silica composite (Figure 4.4). The silica residue content in MC was not

reported in the original paper [12] describing the synthesis of disordered mesoporous carbon by the silica-sol-templated method, but the 3% silica residue is reasonable because the template used in the synthesis was isolated silica nanoparticles or nanoparticle aggregates which were possibly isolated by carbon in the carbon-silica composite and could not be accessible by NaOH solution. Even for using ordered silica as a template, 2-4% silica residue in the resulting carbon was reported.[20]
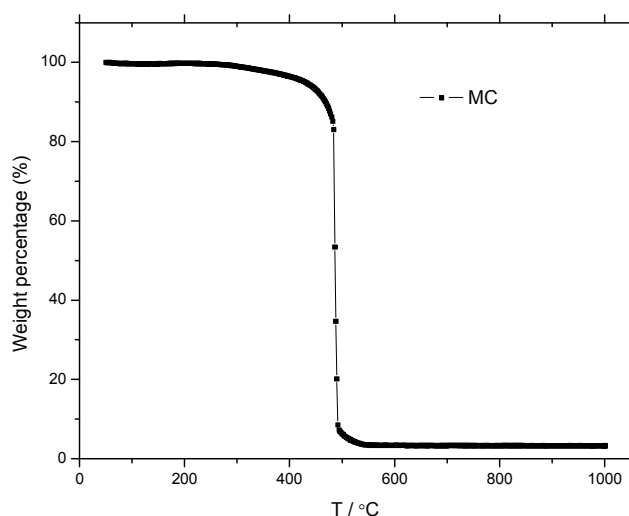
Figure 4.4 TGA graphs of mesoporous carbon, O_2 atmosphere, heating rate 10 ℃ min^{-1}

4.3.2 Pt deposition onto silica-templated mesoporous carbon

The prepared MC-supported Pt catalyst (Pt/MC, 18% Pt by TGA) prepared as described in the experimental section was subjected to transmission electron microscopy (TEM) analysis. The TEM micrographs and histograms of Pt particle size distribution of Pt/MC and Pt/XC-72R catalysts are shown in Fig. 4.5. The Pt particles on XC-72R have smaller particle size (mean diameter 2.8 ± 0.7 nm) and are homogeneously dispersed

78

throughout the support, while the Pt particles on MC have larger particle size (mean diameter 4.4 ± 1.8 nm) and are not as homogeneously dispersed as those on XC-72R. The
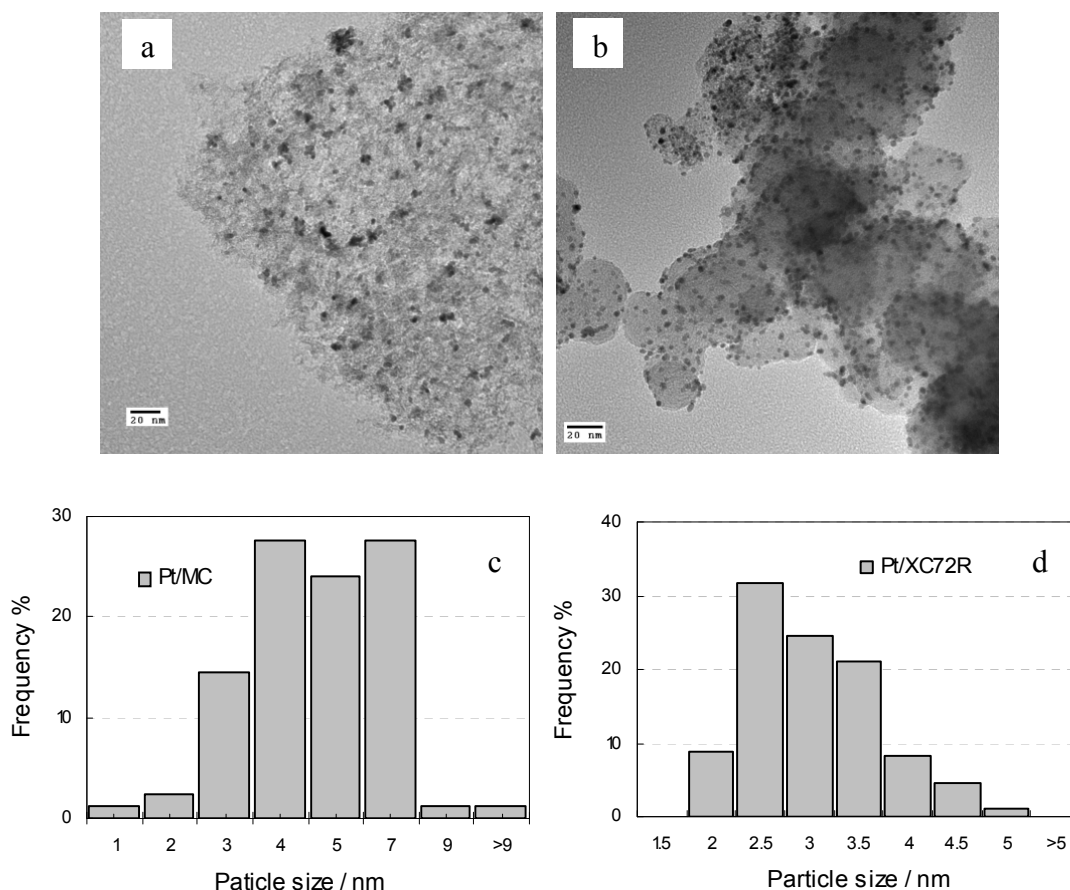
Figure 4.5 TEM micrographs of carbon-supported Pt catalyst (a) Pt/MC (b) Pt/XC-72R and histogram of Pt size distribution in (c) Pt/MC, d mean= 4.4 ± 1.8 nm (SD) and (d) Pt/XC-72R, d mean=2.8 ± 0.7 nm (SD)

Pt particles on the MC support apparently have a greater tendency to agglomerate together. It is known that the support will affect the catalyst particles dispersion. MC has higher surface area, so for approximately the same catalyst loading, e.g. 20%, it might be expected that Pt on MC would have less tendency to agglomerate; however that is not the case. The reason for the Pt particle agglomeration on the MC support is not completely

understand at this time; one possibility is that some aspect of the surface chemistry of the MC support promotes Pt particle agglomeration, and is different from the surface chemistry of carbon black. In any case, the different Pt particle size and spatial distribution on both carbon supports would affect the catalysts' performance which is shown by in-cell performance.

4.3.3 *Ex-situ* **Cyclic Voltammetry**

Ex-situ CV is often used to estimate ESA for dispersed supported Pt catalysts. Figures 4.6 and 4.7 present *ex-situ* CVs by H_2 stripping and CO stripping methods respectively for Pt/MC and Pt/XC-72R samples. The CV shapes of H_2 stripping are as expected for Pt supported on carbon insofar as they exhibit well-defined regions for H adsorption/desorption and Pt oxidation/oxide reduction atop a relatively large capacitive background current for carbon. The capacitive background current for Pt/MC is much larger due to the MC's much higher specific surface area and larger pore size. The broad peaks around potential of -0.15V (vs. Hg/Hg_2SO_4) are from reduction/oxidation of the quinone-like groups on the MC support. Estimated ESA values from hydrogen desorption charge density are given in Table 4.2 in comparison with those obtained from *ex-situ* CV of CO stripping and *in-situ* CV of H_2 stripping (the details about ESA value estimation are provided in reference [17]). ESA values from *ex-situ* CVs are smaller for Pt/MC than for Pt/XC-72R perhaps due to the larger Pt particle size in Pt/MC as already indicated in TEM images, and by the fact that some Pt particles could be buried deep inside the pores in MC where they are not accessible to electrolyte. The negative shift of the adsorbed CO

80

oxidation peak potential for the Pt/MC sample (shown in Figure 4.7) also verifies the larger size Pt particles or agglomerates for that sample.[21, 22]
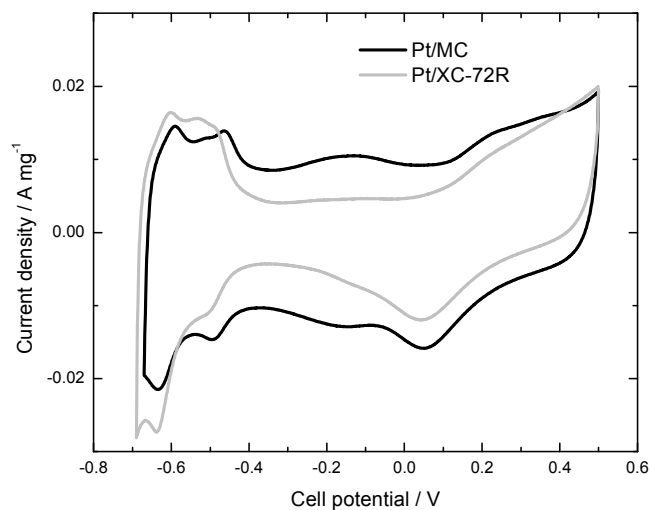
Figure 4.6 Pt/MC catalyst in 0.5 mol L^{-1} H_2SO_4 solutions, potential range -0.67-0.5 V, scan rate 20 mV s^{-1} compared with that of Pt/XC-72R
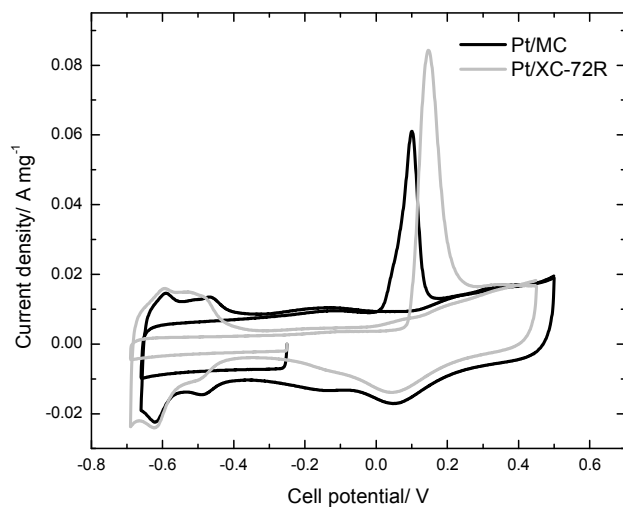
Figure 4.7 Pt/MC catalyst in 0.5 mol L^{-1} H_2SO_4 solutions, CO stripping, potential range from -0.25 to -0.67V, then from 0.45 to -0.67V, scan rate 20 mV s^{-1}, compared with that of Pt/XC-72R

Table 4.2 ESA of catalysts by *ex-situ* CVs of H_2 and CO stripping

Catalyst	S_H	S_{CO}
	$m^2 g^{-1}$	$m^2 g^{-1}$
Pt/MC	32	32
Pt/XC-72R	67	66

Attempts were made to evaluate both carbon-supported Pt catalysts in MEA form using single-cell fuel cell testing methods. However, for MC supported Pt catalyst, an MEA could not be fabricated by the thin-film decal transfer method using the usual amounts of Pt/C and binder (Nafion), which worked very well with Pt/XC-72R catalyst and the catalyst of Pt deposited onto carbon xerogel synthesized without silica template.[17] After painting the regular inks onto the PTFE templates and heating them in the oven at 140 ºC, for the MC supported ink, an even, smooth thin film layer could not be formed. Some parts of the thin film layers came off after heating. The bad thin films on templates for MC-supported catalyst ink are shown in Figure 8 (a).
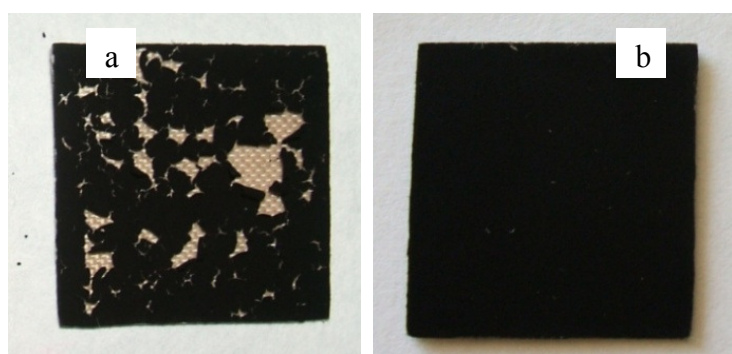
Figure 4.8 Pt/MC/Nafion inks painted on PTFE templates after heating at 140 °C (a) ink Pt/MC with 28% Nafion; (b) ink Pt/MC with 54% Nafion

One significant difference between MC and carbon black XC-72R and also carbon xerogel support is the specific pore volume of the supports. MC has much higher specific pore volume (4.31 cm^3 g^{-1}) with larger pore size and broader pore size distribution (see Figure 4.3 and Table 4.1) than the other supports. It is suspected that the amount of Nafion added in the usual ink formulation for Pt/MC is not enough to bind the MC particles together, because much of the Nafion ends up inside the MC meso-macropores. To test this idea, a larger amount of Nafion, up to 54 weight percent Nafion content, was added to the ink to make a thin-film electrode on the PTFE template. After this adjustment, an even smooth thin film could be made on the PTFE template after heating to 140 °C as shown in Figure 4.8 (b).

Table 4.3 Estimation of carbon support pore volume and Nafion filling in the carbon support pores in dried thin films made from MEA ink formulations

Sample	Pt/C mass	C mass	Pore volume	Pore volume	Nafion mass	Nafion volume	Ratio[a]
	g	g	cm^3 g^{-1}	cm^3	g	cm^3	
Pt/CB[b]	0.0625	0.05	0.62	0.031	0.5	0.013	0.41
Pt/CX[b]	0.0625	0.05	0.81	0.0405	0.5	0.013	0.31
Pt/MC[b]	0.0625	0.05	4.31	0.216	0.5	0.013	0.06
Pt/MC[c]	0.0625	0.05	4.31	0.216	1.5	0.038	0.18

Pt/C catalysts (20% Pt), 5% Nafion EW 1100 solution, and Nafion (dry) density of 1.98 are assumed in use of ink formulations. [a] ratio of Nafion volume to carbon pore volume. [b] ink with 28% Nafion, [c] ink with 54% Nafion

Further analysis of Nafion volume in the ink and pore volume of carbon support in the ink is given in Table 4.3. It is seen that in the usual MEA ink formulation, the ratio of Nafion volume to carbon support volume for Pt/XC-72R and Pt/CX (Pt/CX is carbon

xerogel supported Pt catalyst; see reference[17].) are about 40% and 31% respectively, whereas this ratio for Pt/MC is quite low, only 6%. This calculation shows that there is a much higher excess pore volume in the Pt/MC ink which is consistent with our observation that the Nafion in that ink does not provide adequate binder properties. As the Nafion content increased to 54% in the Pt/MC ink, the ratio of Nafion volume to the MC support volume is increased to 18% and an even and smooth thin film could be made on the PTFE template (see Figure 4.8 (b)). Apparently, after the Nafion content in this ink was increased, there was enough remaining Nafion as binder to bind together the Pt /MC particles and an even thin film electrode could be made. This finding provides an important insight, namely that the optimal support-to-binder ratio will probably be different for supports having pore sizes and volumes that differ greatly from those of more conventional materials, e.g. carbon black.

Because for the regular ink formulation, an MEA could not be fabricated from Pt/MC ink with the decal transfer method, in order to compare the performance of carbon supported Pt catalyst under similar ink formulation, MEAs from MC-supported catalyst were made by applying the ink directly to gas diffusion media, while MEAs from Pt/XC-72R were made with the decal transfer method. The MEAs made by both methods were treated the same way before testing. The single cell testing results of cells fabricated with Pt/MC and Pt/XC-72R catalysts are shown in Figure 4.9. The performance of Pt/MC is much inferior to that of Pt/XC-72R, although the higher surface area, large pore size and broad pore size distribution of the MC support are expected to improve the catalyst dispersion and mass transport of the reactants and products in fuel cells. The inferior

performance might be caused by (1) the different methods used to fabricate MEAs; (2) the larger Pt particle size in Pt/MC; (3) the Nafion buried inside large-size pores of MC not being in good contact with Pt particles. It is likely that not a single parameter among the various parameters such as particle size and distribution of the catalyst, surface area, pore size, pore size distribution, mechanical strength of the catalyst support, and, catalyst and support interaction can determine the electrode performance but a combination (or balance) of the parameters will decide the final performance of the electrode in PEMFCs.
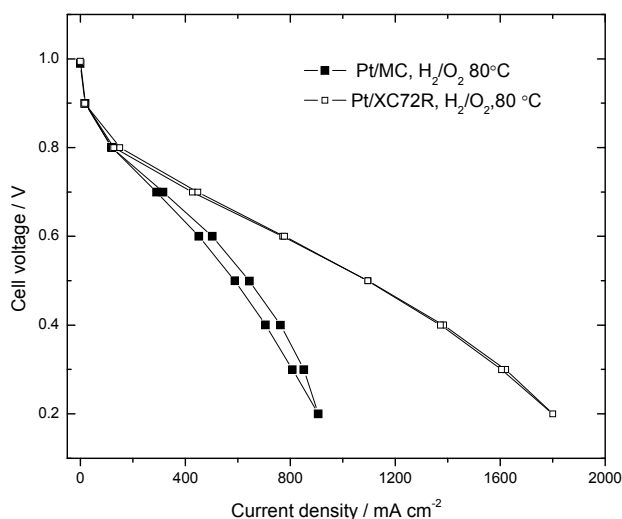
Figure 4.9 Polarization curves of catalyst Pt/MC (■) in comparison with Pt/XC-72R (□), anode/cell/cathode temperature 79/80/76 ℃, H_2 (1.25), O_2 (1.5), atmospheric pressure, Pt loading around 0.25 mg cm^{-2} for electrodes in both cells

The work reported here provides an important insight into the use of MC supports in PEMFC electrodes, namely, that the optimal ratio of ionomer to catalyst/support may be quite different for MC supports, particular supports having high specific pore volume, than for more conventional supports such as carbon black. More ionomer binder may be needed when using supports having high specific pore volume because some ionomer

will be consumed in filling the pores. It is not yet known what affect this fact will have on overall fuel cell performance for electrodes fabricated using MC supports. It was initially expected that the higher free volume inside the MC support would enhance mass transfer rates of gases within electrodes thereby giving higher activity, however it is also possible that the higher amount of Nafion required for the same amount of Pt catalyst will create a higher mass transfer resistance for electrodes fabricated with the MC supports, thereby giving a lower activity. Further study focusing on optimizing ink formulations for MC supports and on the effect of adjusting Pt-to-ionomer ratios in electrodes fabricated using various catalyst supports with different (higher) Pt loading, will be needed to more thoroughly evaluate the possible advantages of mesoporous and other self-supporting structured carbon materials as catalyst supports in fuel cell electrodes

4.4   Conclusions

Mesoporous carbon supports having high specific surface area and pore size and volume were studied as catalyst supports in PEMFC electrodes. Pt particles grown on the MC supports were slightly larger and more agglomerated than on carbon black supports. Composite electrodes with Pt/MC and Nafion ionomer/binder could not be prepared using conventional ink formulations by the decal transfer method, probably due to Nafion being taken up inside MC pores. Further work aimed at optimizing fuel cell electrode structure and composition, focusing on the tradeoffs inherent in the use of structured carbon supports having large pore volumes, is needed.

4.5   References

1.   P. Costamanga and S. Srinivasan, *Journal of Power Sources*, 2001, **102**, 242-252.

2.   P. Costamagna and S. Srinivasan, *Journal of Power Sources*, 2001, **102**, 253-269.

3.   M. S. Wilson and S. Gottesfeld, *Journal of Applied Electrochemistry*, 1992, **22**, 1-7.

4.   S. Litster and G. McLean, *Journal of Power Sources*, 2004, **130**, 61-76.

5.   K. S. W. Sing, D. H. Everett, R. A. W. Haul, L. Moscou, R. A. Pierotti, J. Rouquerol and T. Siemieniewska, *Pure and Applied Chemistry*, 1985, **57**, 603-619.

6.   H. Chang, S. H. Joo and C. Pak, *Journal of Materials Chemistry*, 2007, **17**, 3078-3088.

7.   H. Yang and D. Zhao, *Journal of Materials Chemistry*, 2005, **15**, 1217-1231.

8.   J. B. Joo, P. Kim, W. Kim, J. Kim and J. Yi, *Catalysis Today*, 2006, **111**, 171-175.

9.   P. Kim, H. Kim, J. B. Joo, W. Kim, I. K. Song and J. Yi, *Journal of Power Sources*, 2005, **145**, 139-146.

10.   J. Joo, P. Kim, W. Kim and J. Yi, *Journal of Electroceramics*, 2006, **17**, 713-718.

11.   S. J. Han and T. Hyeon, *Carbon*, 1999, **37**, 1645-1647.

12.   S. J. Han, K. Sohn and T. Hyeon, *Chemistry of Materials*, 2000, **12**, 3337-3341.

13.   S. Brunauer, P. H. Emmett and E. Teller, *Journal of the American Chemical Society*, 1938, **60**, 309-319.

14.   J. H. de Boer, B. C. Lippens, B. G. Linsen, J. C. P. Broekhoff, A. van den Heuvel and T. J. Osinga, *Journal of Colloid and Interface Science*, 1966, **21**, 405-414.

15.   B. C. Lippens and J. H. de Boer, *Journal of Catalysis*, 1965, **4**, 319-323.

16.   E. P. Barrett, L. G. Joyner and P. P. Halenda, *Journal of the American Chemical Society*, 1951, **73**, 373-380.

17.   B. Liu and S. Creager, *Journal of Power Sources*,2009, in press.

18. M. S. Wilson, J. A. Valerio and S. Gottesfeld, *Electrochimica Acta*, 1995, **40**, 355-363.

19. S. C. Savett, J. R. Atkins, C. R. Sides, J. L. Harris, B. H. Thomas, S. E. Creager, W. T. Pennington and D. D. DesMarteau, *Journal of the Electrochemical Society*, 2002, **149**, 1527-1532.

20. M. Kruk, M. Jaroniec, R. Ryoo and S. H. Joo, *Journal of Physical Chemistry B*, 2000, **104**, 7960-7968.

21. F. Maillard, S. Schreier, M. Hanzlik, E. R. Savinova, S. Weinkauf and U. Stimming, *Physical Chemistry Chemical Physics*, 2005, **7**, 385-393.

22. F. Maillard, M. Eikerling, O. V. Cherstiouk, S. Schreier, E. Savinova and U. Stimming, *Faraday Discussions*, 2004, **125**, 357-377.

CHAPTER 5

ELECTROCHEMICAL GRAFTING OF AN ARYL FLUOROSULFONIMIDE SALT ONTO GLASSY CARBON

5.1   Introduction

Intimate integration of electrolyte with electrode is essential to achieving high activity and long life in a polymer-electrolyte-membrane (PEM) fuel-cell electrode.[1, 2] Present methods for making such electrodes involve simple blending of a carbon-supported platinum electrocatalyst with a solubilized form of a perfluorosulfonic acid (PFSA) polymer electrolyte such as Nafion[TM] to form an ink from which thin-film electrodes are formed by solvent casting.[3, 4] Intimate contact between electrodes and electrolyte in such electrodes relies on relatively weak bonding between the fluoropolymer and the carbon support. Poor wetting of the carbon by the fluoropolymer electrolyte could cause low initial activity, and slow changes in structure associated with gradual de-wetting of the carbon by the electrolyte and/or loss of electrolyte by slow dissolution in water could cause a gradual loss of activity. Improvements are needed to ensure a more robust and long-lived contact of electrolyte with catalyst.

One way of achieving intimate integration of electrolyte with electrode is to covalently attach the electrolyte to the electrode via a robust surface bond. A few workers have prepared carbon supports onto which are attached various molecular organic acid groups. For example, Qi and co-workers reported on the use of peracetic acid,[5] 2-aminoethanesulfonic acid,[6] 2-aminoethylphosphonic acid[7] and a sulfonated silane[8] for

modifying carbon supports. Modest improvements in fuel-cell performance with a diminished need for additional fluoropolymer electrolyte in the electrode were reported. A drawback to these approaches is that they utilize acid-to-surface bonds that are potentially unstable with respect to acid-catalyzed hydrolysis. Direct carbon-carbon bonding is preferred in a fuel-cell electrode compared with bonding schemes involving heteroatoms, for example ester and amide bonds, because the latter are more likely to be subject to redox and/or acid-promoted bond scission, e.g. acid-catalyzed hydrolysis. Also, functional groups containing certain heteroatoms can adsorb to electrocatalysts in ways that can diminish catalytic activity.

Several recent reports describe the attachment of a variety of substituted phenyl groups onto carbon electrodes by electroreduction of suitably substituted aryl diazonium salts.[9-20] The grafting mechanism is thought to involve electroreduction of the aryl diazonium group followed by rapid loss of dinitrogen to generate a phenyl radical which immediately attacks carbon to create a robust carbon-carbon bond for surface attachment. Variants of the aryl diazonium grafting method have recently been used to attach aryl sulfonic acid electrolytes to carbon and the resulting materials have been shown to be suitable for use in making fuel-cell electrodes,[13, 21, 22] but attachment of fluorinated acid electrolytes, in monofunctional or polymeric form, has not to our knowledge been previously reported. Fluorinated proton-conducting electrolytes are by far the mostly widely used electrolytes in PEMFC technology, so methods for grafting them on to carbon in a robust manner could be important.

This chapter reports on the covalent attachment of a monofunctional aryl fluorosulfonimide electrolyte onto glassy carbon electrode surfaces via electroreduction of a fluorosulfonimide-substituted aryl diazonium zwitterion. Figure 5.1 illustrates the structures and the approach. Fluorosulfonimide electrolytes possess many attractive attributes for fuel-cell applications[23-26] including very strong acidity when in acid form and excellent chemical and electrochemical inertness especially at high temperatures, e.g., fluorosulfonimide ionomers are stable to 400 ^{o}C in acid form. Fluorosulfonimide acid electrolytes are less susceptible than fluorosulfonic acid electrolytes to dehydration and oxidative degradation reactions which can affect protonic conductivity, which means that fuel cell electrodes prepared using fluorosulfonimide electrolytes in place of fluorosulfonates might possess greater durability and thereby provide longer service life. The fluorosulfonimide acid group also possesses two sites for functionalization, unlike fluorosulfonates which possess just one. This attribute provides much flexibility for designing new oligomeric/polymeric electrolytes that might have structures and properties quite different from those of conventional PFSA electrolytes, both in surface-grafted electrolyte layers and also in bulk polyelectrolyte membranes.
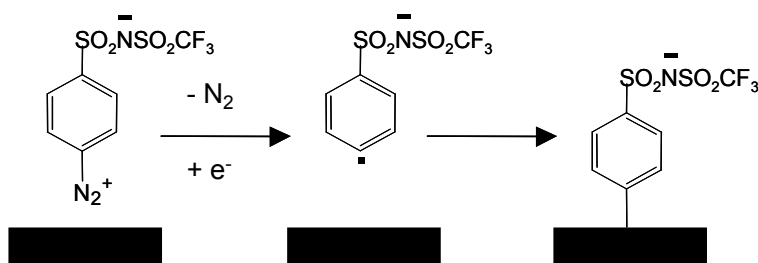
Figure 5.1 Reductive electrochemical grafting of an aryl fluorosulfonimide diazonium zwitterion onto glassy carbon to produce a robust bonded fluorosulfonimide electrolyte

5.2 Experimental

5.2.1 Materials

The aryl diazonium fluorosulfonimide zwitterion, which we will hereafter refer to by the abbreviation "$^+N_2$-Ar-$SO_2N^-SO_2CF_3$" was synthesized from 4-Chlorosulfonylnitrobenzene in excellent yield. Details on the synthesis of this compound are provided in reference.[27] Acetonitrile solvent (99.9%, HPLC grade, Fisher), tetraethylammonium tetrafluoroborate (TEABF$_4$, 99+%, Alfa Aesar) and tetrabutylammonium tetrafluoroborate (TEABF$_4$, 99+%, Alfa Aesar) electrolyte, potassium hexacyanoferrate (K$_3$Fe(CN)$_6$, 100%, J. T. Baker), hexamineruthenium trichloride (Ru(NH$_3$)$_6$Cl$_3$, Aldich,) and other chemical reagents were of reagent grade or better and were used as received from the suppliers. De-ionized (DI) water was purified using a Milli-Q system to a conductivity of approximately 5.5×10^{-6} S m^{-1} prior to use.

5.2.2 Instrumentation

Electrochemical measurements were made using a CH Instruments model 660A electrochemical workstation with picoamp booster and Faraday cage. X-ray photoelectron spectra were acquired using a Kratos Axis 165 system with an aluminum Kα source run at 15 KV and 15 mA, and a hemispherical analyzer run with a pass energy of 80 eV on survey scans and 20 eV on high resolution scans. Spectra were acquired with the X-ray beam and electron collection optics oriented normal to the surface.

5.2.3 Electrodes and electrochemical measurements

Glassy carbon disk electrodes sealed in PEEK were obtained from commercial suppliers. They had a diameter of 3 mm corresponding to a geometric exposed area of 0.071 cm^2. Glassy carbon plate electrodes were originally obtained from Atomergic (grade v-10) as 25 x 25 x 3 mm plates that were subsequently cut into nine squares, each of which was approximately 8 mm on a side. Plate electrodes were prepared for use in electrochemical experiments by temporarily attaching them to the end of a graphite rod using a paste made from graphite powder and beeswax.[28] All glassy carbon electrodes were cleaned prior to use by polishing on polishing cloth by hand with 1.0, 0.3, and 0.05 micron polishing alumina suspensions (Buehler) in water for 10 min each. After polishing, electrodes were ultrasonically cleaned three times in DI water after which they were rinsed with DI water and blown dry with nitrogen gas. Glassy carbon plate electrodes were partially immersed in solutions for electrochemical study. This arrangement allowed for convenient removal of electrodes from the rod for mounting on a UHV sample holder for XPS analysis following electrochemical experiments.

In one instance, electrode coating was attempted using a non-electrochemical method. A polished carbon plate was immersed in 5 mL (2 mL H_2O + 3 mL CH_3CN) of a $1.0E10^{-3}$ mol L^{-1} solution of $^+N_2$-Ar-$SO_2N^-SO_2CF_3$. The vessel containing the solution with the carbon plate in it was immersed in warm water (approximately 30 ^{o}C) and shaken for three hours on a mechanical shaker, then the carbon plate was removed from the solution, sonicated in DI water 3 times (3 min, 3 min, 2 min), and mounted for XPS analysis.

Electrochemical experiments were carried out in a three-electrode cell with Ag/AgCl/sat'd KCl as reference electrode and Pt wire as counter electrode. Coating experiments were carried out in acetonitrile solutions containing approximately milli-molar diazonium salt and 0.1 mol L^{-1} tetra-alkylammonium salt as supporting electrolyte. Details for individual experiments are provided in the figure captions or the text. After coating, electrodes were rinsed with water and acetonitrile and sonicated in DI water prior to use in subsequent experiments. In some cases additional treatments were applied; these are described in the text as appropriate. Electrochemical characterization experiments involving blocking of redox reactions for redox probe molecules were performed in aqueous solutions containing approximately millimolar quantities of redox probe and 0.1 mol L^{-1} of a pH 7 buffer prepared from sodium phosphate salts.

5.3   Results and Discussion

Figure 5.2 presents a series of cyclic voltammograms acquired at a glassy carbon disk electrode in an acetonitrile solution containing 1.5 mmol L^{-1} of $^+N_2$-Ar-$SO_2N^-SO_2CF_3$ and 0.1 mol L^{-1} TBABF$_4$. The voltammetry shows a chemically irreversible reduction peak that diminishes in size and shifts negative with continued scanning. This behavior is consistent with gradual formation of a barrier layer on the electrode that partially suppresses further diazonium reduction. Similar behavior has been widely reported for electroreduction of other aromatic diazonium salts on carbon and other electrodes.
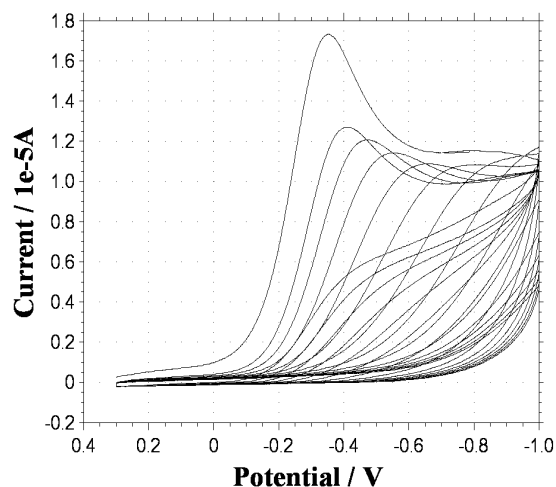
Figure 5.2 Series of sequential cyclic voltammograms (100 mV s^{-1}) acquired at a freshly polished glassy carbon disk electrode in a 1.5 mmol L^{-1} solution of $^{+}$N$_2$-Ph-SO$_2$N^{-} SO$_2$CF$_3$ in acetonitrile containing 0.1 mol L^{-1} TEABF$_4$. Potentials applied vs. Ag/AgCl/sat'd KCl. Coating was accomplished by fifteen sequential scans between +0.3 and -1.0 V

It is hypothesized that the voltammetry in Figure 5.2 reflects formation of an anionic aryl fluorosulfonimide film on the electrode by a process similar to that illustrated in Figure 5.1. Much of the remainder of this chapter is dedicated to presenting data which confirm this hypothesis. One way to test the electrostatic character of the surface of a modified electrode is to examine the electrode reactions of various redox probe molecules at the electrode. The general idea behind this approach is that if a redox probe molecule has a net charge which is the same as that on the electrode surface, then oxidation/reduction of that probe molecule will be suppressed. Similarly, if the redox probe and the electrode surface have the opposite charge, then oxidation/reduction of the probe molecule will be facilitated, or at least, unaffected. This approach is commonly used to characterize chemically modified electrodes, and it has been used in many prior

studies of carbon electrodes that have been modified with other aryl diazonium salts having charged substituents.
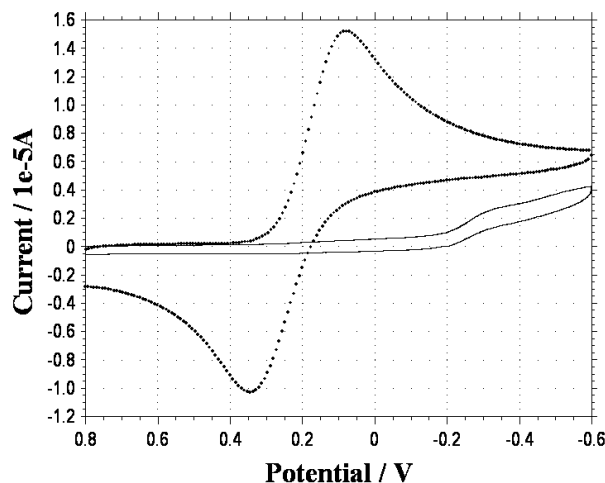
Figure 5.3 Cyclic voltammetry illustrating the effect of the electrochemically grafted layer on hexacyanoferrate oxidation/reduction. Solution contains 1 mmol L^{-1} K$_4$Fe(CN)$_6$ in 0.1 mol L^{-1} of sodium phosphate buffer, pH 7 in water. Potentials are applied vs. Ag/AgCl/sat'd KCl. Potential scan rate is 100 mV s^{-1}. Dotted line; uncoated glassy carbon disk electrode. Solid line same electrode following electroreductive coating with aryl fluorosulfonimide using the procedure illustrated in Figure 5.2

Figures 5.3 and 5.4 present cyclic voltammograms for two redox probe species, hexacyanoferrate (abbreviated Fe(CN)$_6^{3-}$) and hexamineruthenium(3+) (abbreviated Ru(NH$_3$)$_6^{3+}$) at glassy carbon disk electrodes that had been previously modified by a treatment similar to that illustrated in Figure 5.2. Oxidation/reduction of the probe molecules occurs easily at the bare electrodes as indicated by the voltammetric peak shapes of the volotammograms at bare carbon, e.g. nearly equal oxidative and reductive peak currents and peak splitting near 60 mV. (Notice that the voltammogram for Fe(CN)$_6^{3-}$ redox shows a peak splitting at bare carbon that is somewhat larger than 60 mV, indicating quasi-reversible redox behavior. This is not unexpected since it is well

96

known that ferricyanide redox kinetics at glassy carbon are highly variable and depend strongly on subtle details of the surface structure and treatment.[29])
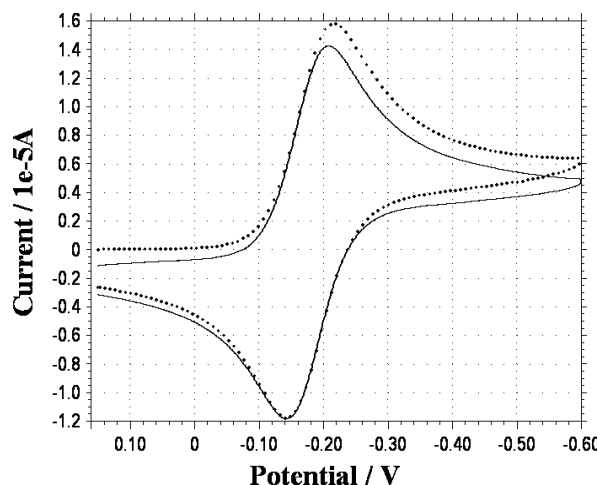
Figure 5.4 Cyclic voltammetry illustrating the effect of the electrochemically grafted layer on hexamine-ruthenium oxidation/reduction. Solution contains 1 mmol L^{-1} Ru(NH$_3$)$_6$Cl$_3$ in 0.1 mol L^{-1} of sodium phosphate buffer, pH 7 in water. Potentials are applied vs. Ag/AgCl/sat'd KCl. Potential scan rate is 100 mV s^{-1}. Solid line; uncoated glassy carbon disk electrode. Dotted line; same electrode following electroreductive coating with aryl fluorosulfonimide using the procedure illustrated in Figure 5.2. Coating was accomplished by twenty-five sequential scans between +0.3 and -0.8V at a scan rate of 0.1V s^{-1}

The key feature of the voltammograms in Figures 5.3 and 5.4 is the effect of the diazonium electroreductive treatment on the voltammetry. The obvious effect is that Ru(NH3)$_6$$^{3+}$ redox is almost completely unaffected whereas Fe(CN)$_6$$^{3-}$ redox is almost completely suppressed at the treated electrodes. Figure 5.3 shows a voltammetric feature near -0.2 V that we do not yet fully understand; it could reflect Fe(CN)$_6$$^{3-}$ reduction at a strongly shifted potential due to a double-layer effect, or it could reflect a cationic redox-active impurity that has become trapped on the electrode surfaces. It is not seen in all voltammograms of Fe(CN)$_6$$^{3-}$ reduction at coated electrodes. The shape of the wave (no

peak, approximately sigmoidal) could be indicative of an array of pinhole in microelectrodes; however this possibility would be difficult to examine in detail since the feature is present only intermittently. The key attribute of all voltammograms of coated electrodes is that current for $Fe(CN)_6^{3-}$ reduction/re-oxidation is suppressed near the midpoint potential for this redox process(approximately +0.2 V vs. reference). This suppression is always observed. The combination of $Fe(CN)_6^{3-}$ redox being strongly suppressed and $Ru(NH_3)_6^{3+}$ redox being unaffected by the coating is strongly consistent with the presence on the electrode surface of a coating with a high negative charge density, as would exist if the process in Figure 5.1 had occurred.
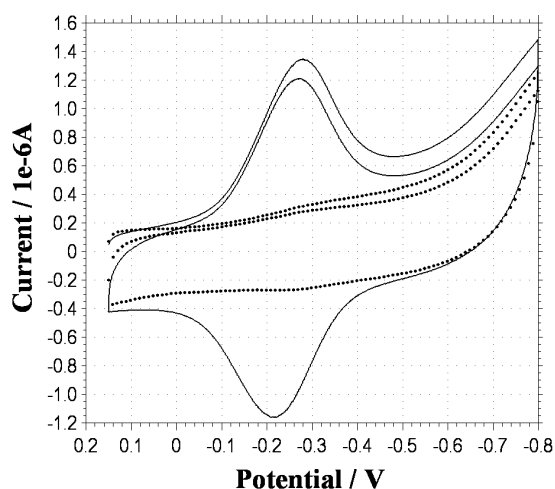
Figure 5.5 Cyclic voltammetry illustrating capture of $Ru(NH_3)6^{3+}$ trications at a glassy carbon disk electrode coated with an electrochemically grafted layer of aryl fluorosulfonimide. Solution contains 5 mmol L^{-1} of sodium phosphate buffer, pH 7 in water. Potentials are applied vs. Ag/AgCl/sat'd KCl. Potential scan rate is 100 mV s^{-1}. Solid line; carbon disk electrode following electroreductive coating with aryl fluorosulfonimide using the procedure illustrated in Figure 5.2, with subsequent exposure to a 5 mmol L-1 solution of $Ru(NH_3)_6Cl_3$ as described in the text. Dotted line; same electrode following a 10 min exposure to a 1.0 mol L^{-1} solution of NaCl in water. Coating was accomplished by fifteen sequential scans between +0.3 and -1.0 V at a scan rate of 0.1V s^{-1}

Figure 5.5 presents the results of a related experiment that also addresses the electrostatic character of electrodes treated as in Figure 5.2. In this case, following electroreductive treatment with a solution of $^+N_2$-Ar-$SO_2N^-SO_2CF_3$, the electrode was exposed for 5 min to a 5 mmol L^{-1} aqueous solution of hexamineruthenium trichloride. The purpose of this treatment is to irreversibly bind $Ru(NH_3)_6^{3+}$ trications at the electrode surface by ion exchange. Following this treatment, cyclic voltammetry in a 5 mmol L^{-1} phosphate buffer (chosen to have a lower ionic strength than the buffers used to acquire the data in Figure 5.3 and Figure 5.4) reveals a persistent feature at a potential expected for $Ru(NH_3)_6^{3+}$ redox. The shape of this wave (equal charges on oxidative and reductive scans, peak splitting near zero) is consistent with a surface-confined redox event. Control experiments with freshly polished glassy carbon electrodes not subjected to treatment with $^+N_2$-Ar-$SO_2N^-SO_2CF_3$ never show any feature for $Ru(NH_3)_6^{3+}$ redox. The integrated charge under the redox waves in Figure 5.5 is approximately 1.7 microcoulombs which after accounting for the charge on $Ru(NH_3)_6^{3+}$ and the electrode area corresponds to a molar density of surface negative charge of approximately $7.4E10^{-10}$ mole cm^{-2}. Removal of the electrode from the buffer solution followed by a 10 min exposure to an aqueous 1.0 mol L^{-1} NaCl solution, followed by a repeated voltammetric analysis in dilute phosphate buffer, results in loss of the voltammetric feature for $Ru(NH_3)_6^{3+}$ redox.

The behavior illustrated in Figure 5.5 is strongly consistent with the presence of a surface film on the electrode having a high negative charge density following electroreductive treatment with $^+N_2$-Ar-$SO_2N^-SO_2CF_3$. The amount of surface negative charge is in the range expected for a monolayer and is inconsistent with the presence of a

thick polymer layer. It is difficult to say anything more definitive about the surface coverage due to uncertainties regarding the exact amount of charge on the surface (e.g. is it appropriate to use 3+ or 2+ for the charge on the redox probe, is the ion-exchange process proceeding to completion, and are there other cations present in the film?). As be shown later, it is believed that some residual tetra-alkylammonium cations do remain trapped in the films, so the molar surface coverage given above should be considered as a lower limit of the true fluorosulfonimide surface coverage.
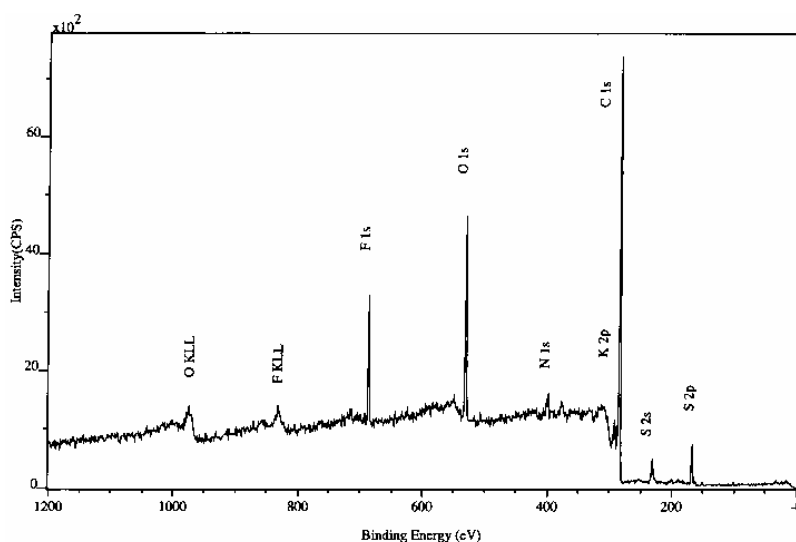
Figure 5.6 Low-resolution X-ray photoelectron spectrum in survey scan mode for a glassy carbon plate electrode coated with an aryl fluorosulfonimide layer as described in the text, with subsequent soaking in a 1.0 mol L^{-1} aqueous KCl solution prior to analysis. Photoelectron emission peaks are observed at binding energies characteristic of C, F, O, S, N and K. Control experiments using electrodes that have not been coated with the aryl fluorosulfonimide layer show peaks for only C and O (data not shown)

X-ray photoelectron spectroscopy (XPS) was also used to characterize the surface layers that form on glassy carbon following treatment similar to that illustrated in Figure 5.2. The electrodes used for these experiments were glassy carbon plates to facilitate

subsequent mounting of the electrodes in the sample chamber for XPS analysis. Figure 5.6 presents a survey spectrum that was obtained for a glassy carbon plate electrode that was treated as described in Figure 5.2 using 20 sequential reductive scans, followed by aggressive rinsing with acetonitrile and sonication in acetonitrile then DI water. Following this treatment the electrode was soaked in an aqueous 1.0 mol L^{-1} KCl in an attempt to provide potassium counterions for the surface fluorosulfonimide sites. The survey spectrum reveals that carbon, oxygen, fluorine, nitrogen, sulfur and potassium are all clearly present on the surface of the coated electrode. All of these elements except carbon and oxygen are absent in a spectrum of a carbon plate electrode that had been identically treated except not subjected to the diazonium reduction treatment. Extended and aggressive rinsing of the coated electrode by water and acetonitrile had no effect on the XPS response. These data provide complementary evidence to that in Figure 5.3, Figure 5.4 and Figure 5.5 for electroreductive grafting of an aryl fluorosulfonimide electrolyte onto carbon to create a bonded layer that is very robust.

The binding energies and assignments of the principal peaks in Figure 5.6 are as follows: 168 eV (S 2p); 285 eV (C 1s); 293 eV (K 2p); 399 eV (N 1s); 532 eV (O 1s); and 688 eV (F 1s). The binding energies are fully consistent with the presence of an aryl fluorosulfonimide layer on the surface.[30] Especially, the sulfur binding energy is consistent with high-valent sulfur and the nitrogen binding energy is consistent with an imide nitrogen. The presence of a signal for potassium provides evidence for electrostatic capture of cations that is complementary to and fully consistent with the evidence presented in Figure 5.5 for electrostatic capture of $Ru(NH_3)_6^{3+}$ trications.

Close examination of the high-resolution spectra for selected elements provides further insight. For example, Figure 5.7 presents a high-resolution spectrum for the C 1s region for an electrode that had been coated as described above for Figure 5.6, but had not been treated with KCl prior to analysis. Hence, this spectrum lacks the K 2p features near 293 eV. Even so, the spectrum still shows a single small peak near 292 eV. The binding energy of this peak is that expected for the trifluoromethyl group in the bis(trifluoromethyl)sulfonimide anion.[30] The presence of a peak at this position in Figure 5.7 is consistent with the structure given in Figure 5.1.
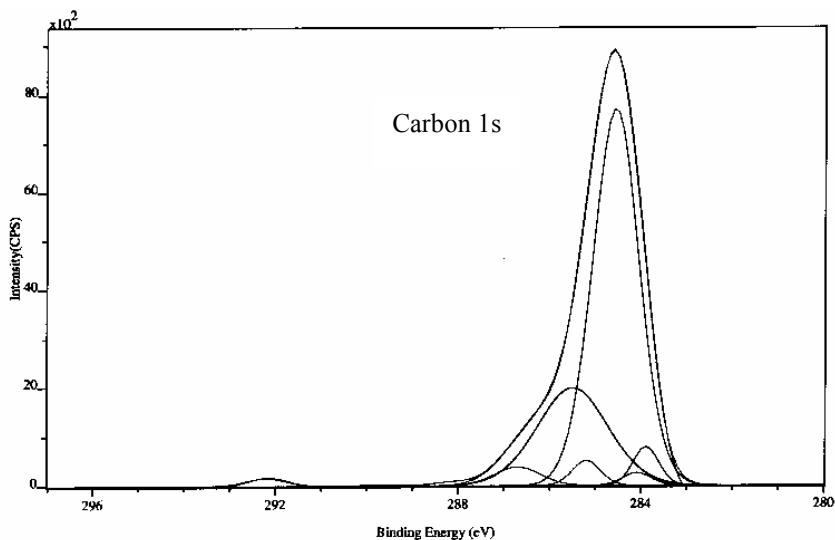
Figure 5.7 High-resolution X-ray photoelectron spectra of the carbon 1s region for an electrode coated using a procedure similar to that used to prepare the electrode from Figure 5.6, except that the KCl treatment step was omitted. The small photoelectron emission peak at 292 eV is indicative of carbon bonded to three fluorines

Figure 5.8 presents a high-resolution spectrum for the N 1s region of the same electrode used to generate the data in Figure 5.6. Two peaks are clearly evident in this spectrum, one at a binding energy near 399 eV and another at a binding energy near 402 eV. It is believed that the latter peak reflects the presence of tetrabutylammonium ions in

the film that were not removed by treatment with aqueous KCl. Prior work has shown that positively-charged nitrogen from quaternary ammonium salts (and also imidazolium salts) exhibit binding energies that are shift to higher values relative to nitrogen that is not cationic.[30, 31] It is significant that the intensity of the higher binding energy peak for quaternary nitrogen is smaller than that of the lower binding energy peak for imide nitrogen. This observation is consistent with the fact that some of the tetrabutylammonium ions have been replaced by potassium. From the relative intensities of the two peaks we estimate that there are approximately one-third as many quaternary ammomium nitrogens present as there are imine nitrogens. it is postulated that "missing" quaternary ammonium ions were replaced by potassium during the KCl treatment.
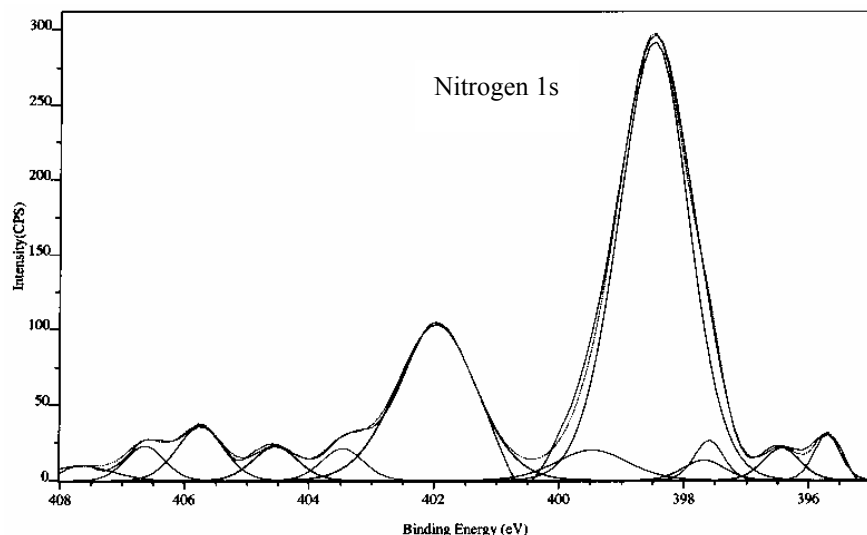
Figure 5.8 High-resolution X-ray photoelectron spectrum of the electrode from Figure 5.6 showing the regions near the N 1s photoelectron emission energies. The photoelectron emission peak near 399 eV indicative of the imide nitrogen, and the peak near 402 eV is indicative of quaternary ammonium nitrogen

Tables 5.1 and 5.2 present a compositional analysis of the surfaces of several glassy carbon plate electrodes that had been subjected to various treatments prior to XPS analysis. Surface composition is described in terms of atom percent compositions that were obtained from XPS peak integrations normalized using relative sensitivity factors, transmission functions, and electron escape depth corrections as provided with the instrument software. The principal peaks were fit manually to a Gaussian function; in cases where the peaks were not obviously Gaussian, up to three Gaussian functions were used and their individual integrated intensities summed to give the total for a given peak. Note that the elemental compositions were normalized to force them to sum to 100 percent to remove contributions from fitting of noise peaks. Note also that the tables include two entries for the N 1s signal for those samples which exhibited two peaks in the high resolution spectra. The peaks correspond to imide and quaternary ammonium nitrogens, as discussed above.

Some important points regarding the fluorosulfonimide films may be gleaned from the data in Tables 5.1 and 5.2. First, the carbon signal is quite high for all samples relative to the signal expected if the only source of C 1s photoelectron emission was the film. The fact that the carbon signal remains high after coating suggests that the coating is thin enough that photoelectron escape from the carbon substrate is not fully inhibited. Photoelectron escape depths vary with energy and material but are expected to be on the order of a few nanometers for C 1s photoelectrons, so these data are consistent with a relatively thin film and inconsistent with the presence of a very thick polymer film. Second, a control experiment on an uncoated electrode shows only carbon and oxygen,

with no nitrogen, sulfur or fluorine or potassium following brief exposure to a KCl solution. Thus, these elements are present only when electrodes have been intentionally subjected to an appropriate coating treatment, and there are no anionic sites present prior to coating that is capable of capturing potassium cations. Third, in some samples (including the uncoated carbon sample), small signals for silicon were observed. We believe that these signals reflect the presence of small silica particles that had become attached to the sample surfaces during handling. They are unlikely to reflect the presence of any special silicon containing components in the films themselves. Fourth, calculated values of several key elemental ratios involving fluorine, sulfur, and imide nitrogen (Table 5.2) are in general agreement (within approximately 30% for samples for which high-resolution spectra were available) with values expected from the elemental composition of the fluorosulfonimide-containing structure illustrated in Figure 5.1 (i.e., expected values from Figure 5.1 are F/S)1.5, F/N(imide))3.0, and S/N(imide)/S)2.0). The agreement is good but not excellent; this fact may reflect imprecision in the peak integrations, and/or possibly some contribution from layering of different elements in the coatings (e.g., some elements might be on average buried deeper than others such that their signals are slightly attenuated). In some cases, the atom percents were obtained from survey spectra since high-resolution spectra were not available for all samples. This fact also contributes some error to the elemental compositions reported in the Tables.

Table 5.1 Elemental composition of the surface of glassy carbon plate electrodes subjected to various surface treatments

Treatment	XPS, atom percent composition							
	C 1s	O 1s	N 1s (quat)	N 1s (imide)	F 1s	S 2p	K 2p	Si 2p
Bare carbon, no fluorosulfonimide coating, KCl treated	91.1	7.8						1.1
Fluorosulfonimide-coated carbon, KCl treated	73.4	14.6	0.6	1.4	6.2	3.2	0.6	
Fluorosulfonimide-coated carbon, not KCl treated	75.3	14.0	0.6	1.2	4.4	2.3		2.2
Fluorosulfonimide-coated carbon, heat treated 8h with 50 % aqueous triflic acid	74.2	14.9	0.4	1.2	6.6	2.7		
Fluorosulfonimide-coated carbon, then dry heat treated, 120 C[a]	78.7	11.6		2.0	5.5	2.2		
Fluorosulfonimide-coated carbon, then heat treated in neat triflic acid	71.7	17.9		1.8	5.8	2.8		
Fluorosulfonimide-coated carbon, treated by multiple oxidative voltammetric scans to +1.5 V vs reference	85.0	15.0						
Fluorosulfonimide-coated carbon, chemically coated	89.0	7.3		2.1	0.6	0.6		0.4

[a] The electrolyte used for coating these samples was 0.1 M TEABF4. Peak areas for these samples were obtained from low-resolution survey scans. Nitrogen signals for these samples are for all nitrogen not just imide nitrogen

Table 5.2 Elemental ratios for surface of glassy carbon plate electrodes subjected to various surface treatments

Treatment	F/S	F/imide N	S/imide N
Fluorosulfonimide-coated carbon, KCl treated	1.9	4.4	2.3
Fluorosulfonimide-coated carbon, not KCl treated	1.9	3.7	1.9
Fluorosulfonimide-coated carbon, heat treated 8h with 50 % aqueous triflic acid	2.4	5.5	2.3
Fluorosulfonimide-coated carbon, TEABF$_4$ electrolyte then dry heat treated 8h, 120 C[a]	2.5	2.8	1.1
Fluorosulfonimide-coated carbon, then heat treated 8h in neat triflic acid.[a]	2.1	3.2	1.6
Fluorosulfonimide-coated carbon, chemically coated[a]	1.0	0.29	0.29

[a] The electrolyte used for coating these samples was 0.1 M TEABF4. Peak areas for these samples were obtained from low-resolution survey scans. Nitrogen signals for these samples are for all nitrogen not just imide nitrogen

Several entries in Tables 5.1 and 5.2 refer to samples which had been subjected to some type of aggressive chemical or electrochemical treatment prior to XPS analysis. These experiments were performed to learn about the robustness of the grafted films when subjected to conditions that approximate, in a general way, conditions that might be expected inside an operating PEM fuel cell. The general trend is that treatment with hot trifluoromethanesulfonic acid (both neat and as a 50% w/w solution in water) or with dry heat (120 ºC) in an oven followed by extensive rinsing with DI water did not result in any substantial diminution of F, S, or N signal in the photoelectron spectra. The element ratios in Table 5.2 are different from the values obtained for electrodes that had not been

subjected to heat treatments, however the differences are within the error expected for values obtained from the low-resolution survey spectra that were acquired for the treated samples. Of particular interest is a sample that was subjected to a series of cyclic voltammetric scans to very oxidizing potentials. This particular film was subjected to CV treatment in two steps. The first step consisted of 15 sequential scans from -0.4 V to +1.4 V vs Ag/AgCl/KCl(sat'd) in a solution containing 0.1 mol L^{-1} KCl, 0.1 mol L^{-1} phosphate buffer (pH 7), and approximately 1 mmol L^{-1} potassium ferricyanide. The second step consisted of 20 more scans, this time to a positive limit of +1.5 V in the same solution. XPS analysis following this treatment reveals that the fluorosulfonimide coating was gone. Subsequent characterization of this electrode by the redox probe molecule method of Figures 5.3 and 5.4 reveals that the electrode is no longer capable of blocking oxidation/reduction of hexacyanoferrate following the electrooxidative treatment. These findings, which are consistent with a prior report from D'Amours and Belanger[18] on a related system, suggest that carbon corrosion in a PEM fuel cell could cleave the bond that holds a grafted electrolyte onto a carbon electrode. If this were to happen, it could be a contributing factor to age-related performance loss in the fuel cell.

Finally, we note the last entries in Tables 5.1 and 5.2 which correspond to a glassy carbon plate electrode that had been immersed in a warm solution of $+N_2$-Ar-SO_2N-SO_2CF_3 and then shaken for 3 h with no electrochemical treatment. This approach to coating was tried because there is evidence from published reports that aryl diazonium modification of carbon surfaces can be accomplished thermally, without applying reducing potentials.[13, 14, 32] Signals for S, F, and N are all present on the

resulting surface but are smaller than for the electrodes coated by reductive CV cycling, especially for S and F. Compositional analysis reveals some unexpected results for element ratios (Table 5.2); however, this finding may simply reflect the poor precision on the elemental determinations due to the low surface coverage. These data suggest that fluorosulfonimide coatings can be formed on glassy carbon by nonelectrochemical methods; however, further study, perhaps using different conditions to provide larger amounts of material on the carbon surface, will be required to say anything more definitive about the structure of films formed by this nonelectrochemical method.

5.4   Conclusion

The results described herein represent to our knowledge the first example of attachment of a fluorinated acid electrolyte onto a carbon surface via a covalent chemical bond that is sufficiently robust to withstand the aggressive conditions (high temperature, strong acidity, low humidity) expected inside an operating fuel cell. Further work addressing aryl sulfonimide electrolyte grafting by chemical method to mesoporous carbons will be introduced in Chapter 6.

5.5   References

1.   S. Litster and B. McLean, *Journal of Power Sources*, 2004, **130**, 61-76.

2.   V. Mehta and J. S. Cooper, *Journal of Power Sources*, 2003, **114**, 32-53.

3.   P. Costamanga and S. Srinivasan, *Journal of Power Sources*, 2001, **102**, 242-252.

4.   M. S. Wilson and S. Gottesfeld, *Journal of Applied Electrochemistry*, 1992, **22**, 1-7.

5.   Z. Xu, Z. Qi and A. Kaufman, *Journal of Power Sources*, 2003, **115**, 49-53.

6.   Z. Xu, Z. Qi and A. Kaufman, *Electrochemical and Solid State Letters*, 2003, **6**, A171-A173.

7.   Z. Xu, Z. Qi and A. Kaufman, *Chemical Communications*, 2003, 878-879.

8.   E. B. Easton, Z. Qi, A. Kaufman and P. G. Pickup, *Electrochemical and Solid State Letters*, 2001, **4**, A59-A61.

9.   M. Delamar, R. Hitmi, J. Pinson and J. M. Saveant, *Journal of the American Chemical Society*, 1992, **114**, 5883-5884.

10.   P. Allongue, M. Delamar, B. Desbat, O. Fagebbaume, R. Hitmi, J. Pinson and J. M. Saveant, *Journal of the American Chemical Society*, 1997, **119**, 201-207.

11.   C. Saby, B. Ortiz, G. Y. Champagne and D. Belanger, *Langmuir*, 1997, **13**, 6805-6813.

12.   B. Ortiz, C. Saby, G. Y. Champagne and D. Belanger, *Journal of Electroanalytical Chemistry*, 1998, **455**, 75-81.

13.   J. A. Belmont, US 5554739, 1996.

14.   J. L. Bahr and J. M. Tour, *Chemistry of Materials*, 2001, **13**, 3823-3824.

15.   F. Anariba, S. H. DuVall and R. L. McCreery, *Analytical Chemistry*, 2003, **75**, 3837-3844.

16.   A. Downard, *Electroanalysis*, 2000, **12**, 1085-1096.

17.   J. K. Kariuki and M. T. McDermott, *Langmuir*, 2001, **17**, 5947-5951.

18.   M. D'Amours and D. Belanger, *Journal of Physical Chemistry B*, 2003, **107**, 4811-4817.

19.   Y.-C. Liu and R. L. McCreery, *Journal of the American Chemical Society*, 1995, **117**, 11254-11259.

20.   Y. C. Liu and R. L. McCreery, *Analytical Chemistry*, 1997, **69**, 2091-2097.

21.   A. P. Saab, F. H. Garzon and T. A. Zawodzinski, *Journal of the Electrochemical Society*, 2003, **150**, A214-A218.

22.   M. J. Waje, X. Wang, W. Li and Y. Yan, *Nanotechnology*, 2006, **16**, S395-S400.

23.   S. E. Creager, J. J. Sumner, R. D. Bailey, J. J. Ma, W. T. Pennington and D. D. Desmarteau, *Electrochemical and Solid-State Letters*, 1999, **2**, 434-436.

24.   S. C. Savett, J. R. Atkins, C. R. Sides, J. L. Harris, B. H. Thomas, S. E. Creager, W. T. Pennington and D. D. DesMarteau, *Journal of the Electrochemical Society*, 2002, **149**, A1527-1532.

25.   J. R. Atkins, C. R. Sides, S. E. Creager, J. L. Harris, W. T. Pennington, B. H. Thomas and D. D. DesMarteau, *Journal of New Materials for Electrochemical Systems*, 2003, **6**, 9-16.

26.   D. D. DesMarteau, *Journal of Fluorine Chemistry*, 1995, **72**, 203-208.

27.   S. E. Creager, B. Liu, H. Mei and D. DesMarteau, *Langmuir*, 2006, **22**, 10747-10753.

28.   J. W. Long, K. E. Ayuers and D. R. Rolison, *Journal of Electroanalytical Chemistry*, 2002, **522**, 58-65.

29.   K. R. Kneten and R. L. Mccreery, *Analytical Chemistry*, 1992, **64**, 2518-2524.

30.   S. Caporali, U. Bardi and A. Lavacchi, *Journal of Electron Spectroscopy and Related Phenomena*, 2006, **151**, 4-8.

31.   J. Thome, A. Hollander, W. Jaeger, I. Trick and C. Oehr, *Surface and Coatings Technology*, 2003, **174-175**, 584-587.

32.   M. Pandurangappa, N. S. Lawrence and R. G. Compton, *The Analyst*, 2002, **127**, 1568-1571.

CHAPTER 6

CHEMICAL GRAFTING OF AN ARYL FLUOROSULFONIMIDE

ELECTROLYTE ONTO CARBON XEROGEL AND CARBON BLACK

6.1 Introduction

Three-phase zones where the gas, electron and proton are in intimate contact are essential for polymer-electrolyte-membrane fuel cell (PEMFC) electrodes to achieve high activity and long life operation in application.[1, 2] A commonly used method for making PEMFC electrodes involves simple mixing of a carbon-supported platinum electrocatalyst with a polymeric protonic conductor such as Nafion® to form an ink from which thin-film electrodes are formed by solvent casting.[3, 4] The binding between electrodes and electrolyte in such electrodes is relatively weak and catalyst utilization can be low (about 45%).[1] Improvements are needed to ensure a more robust and long-lived contact of electrolyte with catalyst and higher catalyst utilization.

One way to achieve intimate integration of electrolyte with electrode is to attach the electrolyte to the electrode via a robust covalent surface bond. Several workers have prepared carbon supports or carbon supported catalysts onto which are attached various molecular organic acid groups. For example, Qi and co-workers reported on the use of 2-aminoethanesulfonic acid,[5] 2-aminoethylphosphonic acid,[6] a sulfonated silane[7] and a sulfate salt[8] for modifying carbon or catalyst-supported carbon. Modest improvements in fuel-cell performance with a diminished addition of fluoropolymer electrolyte (*e.g.* Nafion) in the electrode were demonstrated. A drawback to these approaches is that they

utilize surface bonds that are potentially unstable with respect to acid-catalyzed hydrolysis. Direct carbon-carbon bonding is preferred in a fuel-cell electrode for better performance.

Chapter 5 reported a technique for electrochemically grafting a perfluorosulfonimide (SI) superacid onto glassy carbon electrodes.[9] A robust layer of sulfonimide acid was confirmed by XPS and electrochemical probes; however, electrochemical grafting of electrolyte onto powdery, high-surface-area carbon supports is not practical for a real fuel cell application; and even for monolithic samples (e.g. carbon aerogel/xerogel monolith), the scale-up of electrochemical grafting is problematic.

This chapter presents the continued work on the covalent attachment of monofunctional aryl fluorosulfonimide acid electrolytes onto high-surface-area carbon black (CB) and carbon xerogel (CX) supports via chemical grafting of a parent diazonium zwitterion without the help of electrochemical reduction. Figure 6.1 schematically illustrates the approach. Recently, there is more interest on chemical grafting of different organic functional groups (such as nitrophenyl) onto carbon black[10], ordered mesoporous carbon[11, 12], graphite powder[13], carbon nanotube[14], and diamond[15], even metallic substrates[16] via diazonium chemistry by either spontaneous reduction[10, 11, 14-16] or using reducing agent.[10, 13, 17] Even the mechanism of chemical grafting via diazonium chemistry was investigated.[10]

Carbon blacks (such as Vulcan XC-72/72R from Cabot) are the most commonly used catalyst support in PEMFC applications. Carbon xerogels are also promising electrode materials due to their high electrical conductivity, high surface area and skeletonized self-

supporting nanoporous structure. Several researchers have already used carbon xerogels in the study of fuel cell electrodes.[18-21] Fluorosulfonimide electrolytes also possess many attractive attributes for fuel-cell applications[22-25] including very strong acidity when in acid form and excellent chemical and electrochemical stability especially at high temperatures. Fuel cell electrodes prepared using fluorosulfonimide–grafted carbon black or carbon xerogel as catalysts supports might possess better performance and greater durability than existing materials, thereby providing longer service life. The fluorosulfonimide acid group also possesses two sites for functionalization, different from fluorosulfonates which possess just one. This attribute provides much flexibility for designing new oligomeric/polymeric electrolytes that might have structures and properties quite different from those of conventional perfluorosulfonic acid electrolytes, both in surface-grafted electrolyte layers and also in bulk polymer electrolyte membranes. By integration of the particular fluorosulfonimide electrolyte as described above onto the most commonly used CB and CX supports, and by using these materials to fabricate PEMFC electrodes, a better cell performance is expected. Somewhat surprisingly, the single-cell testing results for MEAs made from platinum supported on SI-grafted CX samples did not verified this expectations. Some possible reasons for this lower cell performance are discussed.
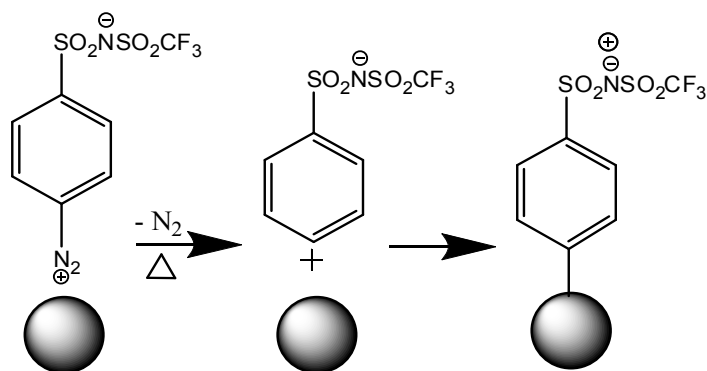
Figure 6.1 Schematic grafting of fluorosulfonimide superacid onto carbon xerogel or carbon black

6.2 Experimental

6.2.1 Materials

The aryl fluorosulfonimide diazonium salt ($^{+}N_2C_6H_4SO_2N^{-}SO_2CF_3$) was prepared as described previously.[9] Carbon black Vulcan XC-72 (CB, Cabot, free sample), resorcinol (98%, Aldrich), formaldehyde (37 wt%, ACS Reagent, Aldrich), and acetonitrile (extra dry, Acros Organics), were used as received from the suppliers. De-ionized (DI) water was purified using a Milli-Q system to a resistivity no less than 18.2 MΩ cm prior to use.

6.2.2 Synthesis of carbon xerogel

The resorcinol(R)-formaldehyde (F) sol-gel method using sodium carbonate as catalyst (C) with ambient-pressure drying as described in literature[26, 27] was modified to synthesize the CX samples used for chemical grafting experiments. In brief, resorcinol, formaldehyde, water, and catalyst sodium carbonate were mixed then gelled/cured to produce a hydrogel which was dried directly in air to produce a RF gel which was

116

subsequently carbonized in N_2 atmosphere to obtain a carbon xerogel. Further details on the CX synthesis are given in reference.[28]

6.2.3 Chemical grafting of aryl fluorosulfonimide onto carbon black and carbon xerogel

Carbon black Vulcan XC-72 is in small bead form and was used for grafting as received. The CX sample prepared as described above was first ground to a fine powder by mortar and pestle prior to use in grafting experiments. The CB or fine CX powder sample (about 0.5 g) was suspended in 10-15 mL of a $^+N_2C_6H_4SO_2N^-SO_2CF_3$ diazonium salt solution in acetonitrile (approx. 1.5-2.0 w/v%) and the mixture was kept stirring overnight at room temperature. Following this treatment the grafted CB or CX powder was collected by filtration with 0.2 μm Nylon filter, washed with acetonitrile and DI water several times, then Soxhlet extracted with acetonitrile/THF overnight and dried in a vacuum oven overnight under dynamic vacuum at 120 °C.

6.2.4 Deposition of Pt catalyst onto sulfonimide-grafted carbon xerogel

SI-grafted (SI-CX) powder samples (about 0.1 g) were sonicated in 30 mL DI water for 15 min. Then, a diluted H_2PtCl_6 (Acros Organics, 40% Pt) solution was added to the SI-grafted CX powder suspension and the resulting suspension was sonicated for another 30 min. The mass of platinum in the H_2PtCl_6 salt added to the CX suspension was sufficient to correspond to 20 wt% of platinum metal in the final material, should all the Pt be deposited onto the carbon support. After sonication, the pH of the mixture was adjusted to 11 using a 4 mol L^{-1} NaOH solution and an excess amount (10x) of formaldehyde was diluted in DI water (2 mL) and added drop by drop into the grafted carbon suspension

under stirring. The mixture was kept stirring for another 15 min at room temperature, then the reaction temperature was raised to 90 ºC and kept at 90 ºC for 2 h under stirring. Then the reaction mixture was cooled to room temperature and diluted HCl (2 mol L^{-1}) was added to promote Pt catalyst precipitation onto the carbon supports. The Pt-deposited SI-grafted CX powder (Pt/SI-CX) was then collected by filtration, thoroughly washed with DI water, and dried at 100 °C under vacuum. As a comparison, Pt catalyst was also deposited onto CX samples without any grafted electrolyte (S_{BET}, 462 m^{2}g^{-1}, peak pore diameter around 14 nm, detailed characterization is given in reference [28]) following the same procedures as described above (denoted as Pt/CX). For all Pt/CX samples subjected to further analysis, the final Pt content was approximately 20% weight percent (samples with Pt content outside the range between 18 and 22 percent were not used) as measured by thermogravimetric analysis (TGA) under O_2 atmosphere.

6.2.5 Materials characterization

The CB and synthesized CX samples were characterized by the N_2 sorption method at 77K using a Micrometrics model ASAP 2010 apparatus. The specific surface area (S_{BET}) of the CB and CX samples was extracted from the Brunauer-Emmett-Teller (BET) model and the mesopore (mesoporous volume V_{meso}, mesoporous surface area S_{meso}) and micropore (microporous volume V_{micro}, microporous surface area S_{micro}) properties were extracted from the t-plot method and the Barrett-Joyner-Halenda (BJH) model was used to evaluate the pore size and its distribution. The total pore volume (V_{total}) was recorded at P/P_0 near to 1. The CB and CX samples were degassed at 200 ºC for one day before

measurement. TGA analysis for sulfonimide-grafted CX samples was performed using a Mettler Toledo TGA 851 thermal analyzer under N_2 atmosphere.

The acid content (also called herein the ion exchange capacity, IEC) of the sulfonimide-grafted carbon powder (CB and CX) samples was measured using an acid-base back-titration method. Before titration, the grafted samples were converted to acid form using diluted HCl and dried under vacuum and heat. For SI-grafted carbon black samples, a known amount of grafted carbon black sample (about 0.2 g) was placed in 5.00 mL of a $1.115E10^{-2}$ mol L^{-1} standardized NaOH solution, and the resulting solution was sealed and kept stirring overnight in a glass bottle. The suspension was then centrifuged, and after centrifugation, 3.00 mL of the top clear solution was taken out and titrated with a $7.956E10^{-3}$ mol L^{-1} standard HCl solution. A pH meter (Acumet AB 15, Fisher) was used to record the pH change during the titration to identify the end point. For sulfonimide-grafted CX samples, a similar procedure was followed except that the SI/CX sample was removed from the standard base solution by filtration prior to titrating the remaining base. The sulfonimide-grafted CX sample was also characterized by EDX (Energy dispersive X-ray spectroscopy) attached to scanning electronic microscope (SEM). In this measurement the grafted CX sample was mounted inside the SEM on a conductive adhesive tape for EDX analysis. The Pt/SI-CX samples were characterized in comparison with uncoated CX-supported Pt (Pt/CX) by XRD with a Scintag XDS2000 powder X-ray diffractometer using Cu Kα radiation of wavelength 0.1540 nm, and by TEM with a Hitachi H7600T transmission electron microscope. The electrochemically active surface area (ESA) of the Pt/SI-CX was measured with *ex-situ* cyclic voltammetry

(CV) and CO stripping voltammetry using a CH Instruments model 660A electrochemical workstation with picoamp booster and Faraday cage with a standard three-electrode cell. A home-made Hg/Hg_2SO_4 (0.1 mol L^{-1} H_2SO_4) electrode and a Pt wire served as reference and counter electrodes respectively. The working electrode was a thin-film-coated glassy carbon (GC) plate electrode made by attaching a graphite rod with graphite adhesive to the back of a square GC plate (5 mm each side, geometric surface area 0.025 cm^2). The thin film on the GC was made from an ink mixture of the catalyst of Pt/SI-CX, solubilized Nafion and isopropanol. Further details on formulating the ink and coating a thin film on the GC are provided in reference.[28] ESA values of Pt/CX samples without grafted SI layers were measured in a similar way for comparison.

Membrane electrode assemblies (MEAs) were fabricated from the ink of Pt/SI-CX or Pt/CX catalyst by the thin-film method using Nafion 117 membranes. A detailed description of the MEA fabrication method is provided in reference.[28] The active electrode area is 5 cm^2, and the Pt loading on both anode and cathode is about 0.25 mg Pt/cm^2. The single-cell testing of MEAs was performed on a model 850C test station from Scribner Associates Company. Cells were broken in at a cell voltage of 0.5 V overnight before polarization curve measurement.

The *in-situ* CV measurements were performed in the MEAs in the fuel-cell test fixture[29] operating in a two-electrode configuration in which the anode served as both pseudo-reference and counter electrodes, and the cathode served as the working electrode. Details are provided in reference.[28]

6.3   Results and Discussion

6.3.1   Carbon support characterization
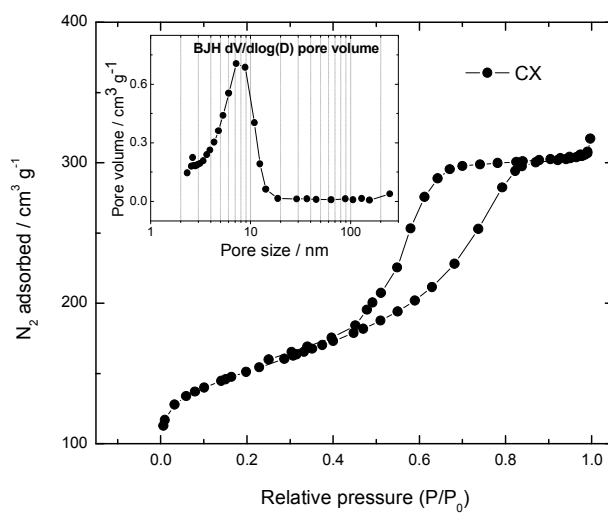
Figure 6.2 N_2 adsorptoion/desportion isotherm and pore size distribution (inset) of carbon xerogel
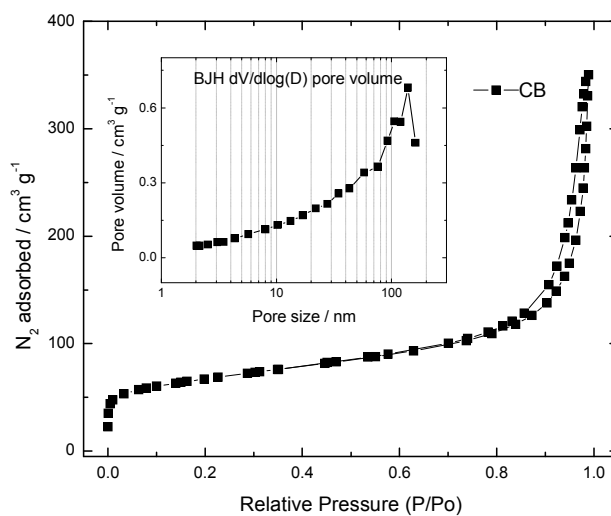
Figure 6.3 N_2 adsorptoion/desportion isotherm and pore size distribution (inset) of carbon black

The method in references[26, 27] was followed to synthesize the CX samples used in this work to study chemical grafting of fluorosulfonimide electrolytes onto carbon. The N_2 adsorption/desorption isotherm and pore size distribution of the resulting CX samples are presented in Figure 6.2. According to IUPAC definition, the isotherm is a type IV isotherm with H2 hysteresis loop which indicates the presence of mesopores.[30] From the inset in Figure 6.2, the carbon xerogel has a sharp pore distribution from 3 to 20 nm with peak width of 8 nm in the mesopore range. The CB sample was also subjected to the N_2 physisorption analysis, and the isotherm and pore size distribution of CB sample are shown in Figure 6.3. The CB N_2 adsorption/desorption isotherm also has the hysteresis loop which indicates that mesopores exist in the CB sample, however the shape and position of the hysteresis loop are very different from that for the CX sample. The BJH pore size/volume analysis for the CB sample shows a very broad pore size distribution spanning a range from 2 to about 300 nm meter which is the maximum size that can be probed by this method. This behavior likely reflects the agglomerate nature of the CB samples. Other textural properties for CX and CB samples from the N_2 gas adsorption analysis are listed in Table 6.1. From the data in Table 6.1 we can see that the BET surface area for the CX sample is larger but the mesopore volume of CX is lower than that of CB, and accordingly the micropore volume from the CX sample is larger, while the micropore volume from CB is small but the microporous surface area is not small which may indicate the presence of some very small micropores inside the CB sample.

Table 6.1 Textural properties of carbon xerogel (CX) and carbon black XC-72(CB)

Carbon	S_{BET}	S_{micro}	$S_{micro}/$	V_{total}	V_{micro}	V_{meso}	$V_{meso}/$	d_{BET}	d_{BJHads}	d_{BJHdes}
	m^2g^{-1}	m^2g^{-1}	S_{BET}	cm^3g^{-1}	cm^3g^{-1}	cm^3g^{-1}	V_{total}	nm	nm	nm
CX	532	277	0.52	0.49	0.12	0.34	0.72	3.7	6.3	5.0
CB	235	89	0.38	0.54	0.04	0.45	0.83	9.2	20.7	19.1

S_{BET}: BET surface area, S_{micro}:micropore surface area by t-plot, V_{total}:total pore volume at near saturation pressure, V_{meso}:cumulative volume of pores between 1.7 and 300 nm by BJH adsorption branch, d_{BET}, d_{BJHads}, d_{BJHdes}:average pore width by 4V/A

6.3.2 Chemical grafting of fluorosulfonimide electrolytes onto carbon supports

The CX and CB supports described above were subjected to a series of steps that sought to immobilize fluorosulfonimide electrolytes onto the supports via covalent chemical bonding of aryl fluorosulfonimide groups onto carbon. This approach is similar to the well-studied electrochemical approach for modifying carbon surfaces with substituted aryl groups via electrochemical reduction of aryl diazonium salts (or zwitterions) at carbon. Electroreduction of the aryl diazonium group is followed by rapid C-N bond cleavage to produce a phenyl radical which can covalently bind to carbon. Several recent papers have described work which indicates that under certain conditions, similar chemistry can occur on high-surface-area carbon supports that are simply suspended in a solution of the relevant aryl diazonium salt, without electrochemical potential control of the carbon. The results described below are for carbon samples that were modified using this approach, details of which are given in the experimental section.

Table 6.2 presents elemental analysis results obtained by SEM/EDX analysis on two different CX samples. No S and F was detected in the uncoated CX sample, while S, F and N elements were found in the grafted CX sample. This finding strongly suggests that

the fluorosulfonimide grafting onto CX samples was successful. From the F element content in the SI-grafted sample (F element is specific to the grafted acid group), the sulfonimide acid group content on the sample was estimated to be 0.35 mmol g^{-1}. This value is compared with values obtained by other means in Table 6.3, as discussed below.

Table 6.2 Elemental analysis (EDX) of sulfonimide-grafted CX samples

Sample	C %	O %	N %	S %	F %
Uncoated CX	88.16	11.84	0	0	0
SI-Grafted CX	84.93	7.55	2.86	2.66	1.99

[a.] Elemental analysis was also performed using XPS, for which data were acquired as described in ref 28. The elemental composition in the table was confirmed however there was much scatter in the data such that reliable quantification could not be performed.

The sulfonimide-grafted samples were further characterized by acid-base back titration to determine the amount of titratable acid in the samples. Titration provides a direct measure of acid content for the bulk CX and CB samples whereas other methods provide elemental composition information that is often from a spatially localized region which may or may not be representative of the entire sample. Knowing how much grafted sulfonimide acid group is present within the support will help in planning fabrication of fuel cell electrodes using these materials.

Acid-base back titration curves for the SI-grafted CX and CB powder samples using a standard HCl solution to titrate the remaining base following addition of acidified SI/CX or SI/CB samples to a known volume of standard NaOH solution are shown in Figures 6.4 and 6.5 respectively. From the titration curves in Figure 6.4, the sulfonimide acid

content of the SI-grafted CX powder was calculated to be 0.18 mmol g^{-1}. We note that the acid content from the carbon substrate alone, before SI grafting, was already subtracted to obtain this value. By combining this value for acid content with the specific surface area obtained from nitrogen physisorption analysis prior to fluorosulfonimide grafting, we estimate an equivalent sulfonimide acid surface coverage on carbon of 0.34E10^{-10} mol cm^{-2}. Similarly, from the curves shown in Figure 6.5, the sulfonimide acid content of the grafted CB powder is calculated to be 0.13 mmol g^{-1}, which equates to a sulfonimide acid surface coverage on carbon of 0.55E10^{-10} mol cm^{-2}. The difference between the titration curves without any carbon added to the standard base and those with uncoated carbons added prior to titration reflects the intrinsic acid content on the carbon support prior to fluorosulfonimide grafting. This acid amount also includes the systematic measurement error due to solution transfer, filtration, and the porous nature of the carbon substrates, etc. These data are summarized in Table 6.3.

The surface coverage of sulfonimide acid groups on the CX and CB samples is between 10 and 20 times lower than that (7.4 E10^{-10} mol cm^{-2}) reported in our previous paper on flat glassy carbon (GC) electrodes which were modified using the electrochemical aryl diazonium reduction grafting technique. There are several possible reasons for the coverage difference between the two sample types. Two principal reasons are as follows: (1) The electrochemical grafting was performed by cyclic voltammetry over many cycles each of which forced sulfonimide diazonium salt reduction to occur very near to the GC substrate possibly leading to high surface coverage; and (2) the CX and CB substrates used for chemical grafting here has mesoporous and microporous structures which have

very small pore sizes, smaller than the molecular size of the fluorosulfonimide agent. In such a case, the growth (grafting) of the sulfonimide group inside the pores, especially the very small micropores, might be sterically restricted. On the flat, smooth surface of the GC substrate, no such steric restrictions would be present.

It is instructive to compare our findings with those of others who have prepared acid-grafted carbon supports using other acid groups and grafting techniques. Qi and coworkers reported a surface coverage of $2.0E10^{-10}$ mol cm^{-2} of grafted sulfonated silane groups[7] (equivalent to 0.39 mmol g^{-1} Pt/C after conversion using data provided in the paper) on Pt-supported carbon black (XC-72). Elemental analysis was performed in this work via electron microprobe analysis. These same workers reported 0.23 mmol g^{-1} grafted ethanesulfonic acid[5] on Pt-supported carbon black (XC-72) using a TGA method to measure acid content. This estimate of acid content corresponds to a surface coverage of $1.2E10^{-10}$ mol cm^{-2} assuming a carbon surface area of 195 m^2 g^{-1}.[7] Wang et.al.[12] reported a much higher surface loading of 1.93 mmol g^{-1} grafted sulfonic acid group per gram of an ordered mesoporous carbon CMK-5 (equivalent to surface coverage of $1.3E10^{-10}$ mol cm^{-2} sulfonic acid on CMK-5 after conversion from the data provided by the authors). They used a potentiometric titration method to measure acid content. Our sulfonimide acid group surface coverages on the SI-grafted CX and CB samples are close to each other but lower than to these results reported by the Qi or Wang groups. For the grafting work in Qi's group, the substrates for grafting were mostly carbon-supported Pt catalyst, for which the Pt catalyst on the carbon might promote acid group grafting leading to higher surface coverage. For the work reported by Wang, an additional

reducing agent hypophosphorous acid was used for reduction of the diazonium salt, which might help achieve a higher surface coverage.
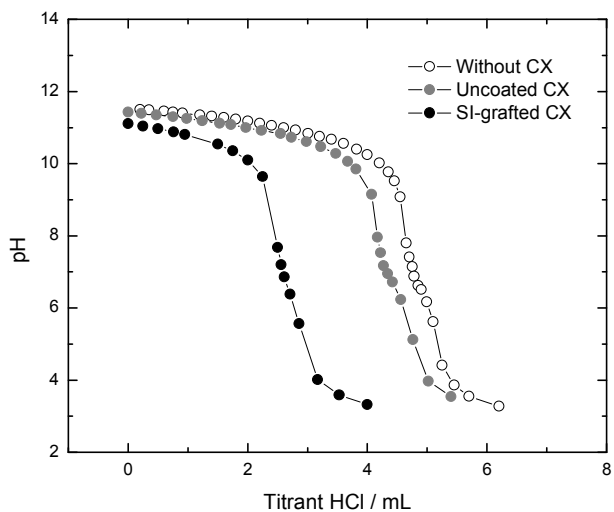
Figure 6.4 Back titration curves of sulfonimide-grafted carbon CX (●), uncoated CX (●) and without CX (○)
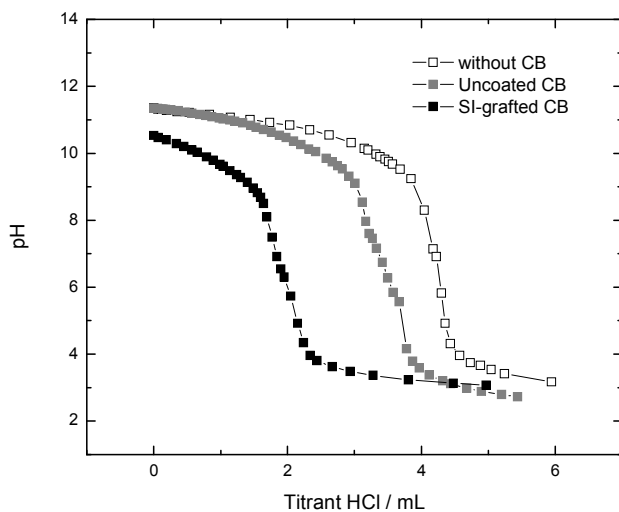
Figure 6.5 Back titration curves of sulfonimide-grafted carbon black CB (■), uncoated CB (■) and without CB (□)

127

Table 6.3 Acid group content on the SI-grafted CX and CB samples determined by different methods

Samples	Acid content on carbon (mmol g^{-1})		
	Back titration	EDX	TGA
Uncoated CX	0.05		
SI-grafted CX	0.23	0.35	0.14
Uncoated CB	0.05		
SI-grafted CB	0.18		

It is also instructive to compare the acid contents given above for various electrolyte-grafted carbon supports with that of a typical fuel cell electrode made by the thin-film fabrication method.[4, 31] A commonly used electrode ink formulation includes 70% Pt/carbon and 30% ionomer, usually dispersed in a solvent to form an ink prior to electrode preparation. The sulfonic acid content (from the ionomer) in an electrode prepared in this way is approximately 0.45 mmol g^{-1} carbon. The acid content in our SI-grafted CX or CB samples is lower than this so it does not meet the acid level needed for the fuel cell electrodes made by thin-film method. Therefore, if these grafted CX and CB samples were to be used to fabricate electrodes, it is likely that additional Nafion ionomer would need to be added to the electrode formulation to make electrodes useful for fuel cell applications, as in fact has been reported in the literature for some other acid-grafted carbon supports.[5, 7, 8, 32, 33] Yet another reason for the need of additional ionomer in the electrodes is that is can serve as a binder necessary for holding together electrodes made by the thin-film method.

The sulfonimide-grafted CX powder samples were also subjected to a thermogravimetric analysis (TGA). Representative TGA curves are shown in Fig.6.6. The weight loss from sulfonimide-grafted CX at temperatures from 250 to 500 ºC is about 3.8%, and is thought to reflect cleavage of the carbon-carbon bond binding the acid group onto carbon. In contrast, for an uncoated CX sample the weight loss over the same temperature range is almost negligible. From this mass loss a sulfonimide acid content of 0.14 mmol g^{-1} carbon is estimated by assuming that the weight loss from 250 to 500 ºC is attributable solely to the grafted functional group having a molar mass of 288.25 g mol^{-1} (see Table 6.3). This finding also indirectly confirms the successful grafting of sulfonimide electrolyte onto CX samples.
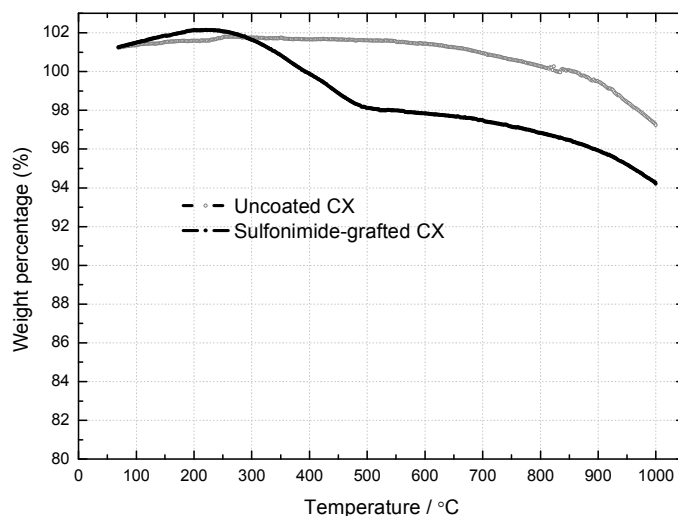
Figure 6.6 TGA curves of sulfonimide-grafted CX (●) and uncoated CX (○) samples

6.3.3 Pt catalyst deposition and characterization

The SI-grafted carbon samples described herein are being prepared in part for use as catalyst supports for PEM fuel cell applications. Therefore, it is instructive to prepare and

characterize Pt catalysts deposited onto SI-grafted CX samples (Pt/SI-CX). Platinum deposition was accomplished from hexachloroplatinic acid solution using formaldehyde as reducing agent, and platinum content for Pt/SI-CX samples was determined by TGA to be approximately 20 weight percent. The resulting materials were characterized with XRD TEM, and *ex-situ* CV. In addition, membrane-electrode assemblies (MEAs) were made from the Pt/SI-CX catalyst samples and were characterized by *in-situ* CV (*i.e.* CV in the MEA form), and by polarization curves in a fuel cell test station. We recently reported a similar study on Pt deposition onto CX supports without grafted electrolytes (ref 28), and that work provides background to the present work on SI-grafted CX supports.

The XRD diffractograms for the samples of Pt/SI-CX and Pt/CX are shown in Figure 6.7. The diffractogram shows features expected for Pt as labeled on the graph. From the line broadening, Pt nanoparticle sizes may be quantified using the Scherer equation (Equation 6.1) [34] using the Pt (220) line for calculation.

$$d(\mathrm{nm}) = \frac{0.9\lambda}{B\cos(\theta)} \qquad\qquad (6.1)$$

In this equation d is the Pt crystal size (diameter), λ is the X-ray wavelength (0.1540 nm), B is the full width at half height for the diffraction peak in radians and θ is half of the diffraction angle. Particle size values obtained in this way for Pt/SI-CX and Pt/CX are given in Table 6.4. Pt particle diameters are higher for the Pt/SI-CX sample (5.6 nm) than the Pt/CX (4.5 nm). From the particle size obtained as described above, the Pt specific surface area may be calculated using Equation 6.2:

$$S(\text{m}^2 \ \text{g}^{-1}) = \frac{6000}{\rho d} \qquad\qquad (6.2)$$

In this equation d is the Pt particle diameter (nm), and ρ is the Pt density (21.4 g cm^{-3}). Pt specific surface areas calculated in this way are listed in Table 4 for Pt/SI-CX and Pt/CX samples. As expected, specific surface areas are lower for the Pt/SI-CX sample which has the large Pt particles.
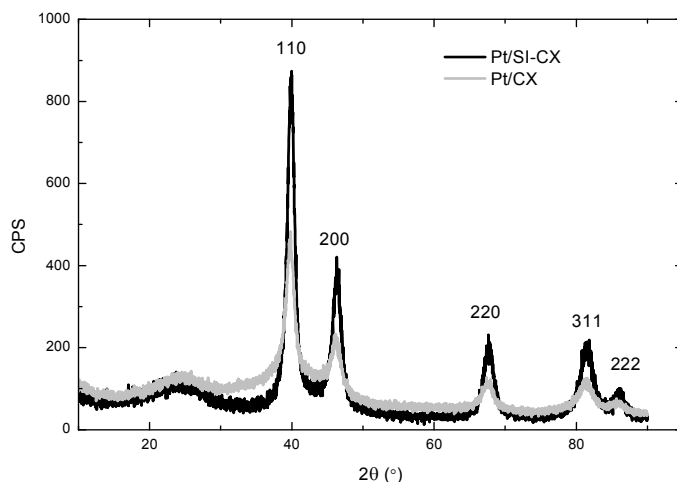
Figure 6.7 XRD diffractrograms of Pt/SI-CX and Pt/CX

Table 6.4 Pt nanoparticle size and specific surface area by different methods (XRD, TEM, *ex-situ* CV (H), *ex-situ* CV (CO) and *in-situ* CV (H)

Sample	d_{XRD} nm	S_{XRD} m^2g^{-1}	d_{TEM} nm	S_{TEM} m^2g^{-1}	S_H m^2g^{-1}	S_{CO} m^2g^{-1}	$S_{in\text{-}situ}$ m^2g^{-1}
Pt/SI-CX	5.6	50.1	5.2	53.9	23	19	15
Pt/CX	4.5	62.3	3.3	85	67	63	55

d_{XRD}: particle size by XRD, d_{TEM}: particle size by TEM, S_{XRD}, S_{TEM}: the specific surface area calculated from the equation (2) from XRD and TEM respectively, S_H: specific surface area from *ex-situ* CV(H desorption charge), S_{CO}: surface area from *ex-situ* CO stripping CV, $S_{in\text{-}situ}$: surface area from *in-situ* CV(in MEA)

Transmission electron microscopy (TEM) was also used to characterize SI-grafted carbon supported Pt catalysts and provide an alternate estimate of Pt particle size. TEM micrographs and histogram graphs of Pt particle size for the Pt/SI-CX and Pt/CX samples are shown in Figures 6.8 and 6.9 respectively. Both TEM micrographs clearly show well-distributed Pt nanoparticles supported on grafted carbons, though the particles are obviously larger on Pt/SI-CX than on Pt/CX. The mean Pt diameter for Pt/SI-CX and Pt/CX samples is estimated to be 5.2 ± 1.5 nm and 3.3 ± 1.1 nm respectively by counting more than 200 particles from each TEM image using ImageJ software [35]. Error estimates are standard deviations of the means from which a slightly broader Pt particle size distribution for Pt/SI-CX than for Pt/CX is seen.

The specific surface area (SA) of Pt could be calculated according to Equation (6.2) from the Pt particle size measured by TEM or XRD on the Pt/SI-CX and Pt/CX samples. Values calculated in this manner are listed in Table 6.4. Pt specific SA of Pt/SI-CX is smaller than that of Pt/CX due to larger Pt particle size on Pt/SI-CX. Usually the Pt catalyst specific surface area from TEM and XRD are larger than that measured by *ex-situ* or *in-situ* CV because TEM or XRD measurements include electrochemically-inaccessible Pt particle. Also, in the case of TEM, the images capture only a localized area of the sample so other sample regions which might contain larger Pt particles which would not be adequately accounted for. Also the ESA measured *ex-situ* (in a half cell) is commonly higher than that measured *in-situ* (in MEA form) due to better ion conduction by help from free acid (H_2SO_4) in the half-cell measurement. These points are further developed in the following discussion.
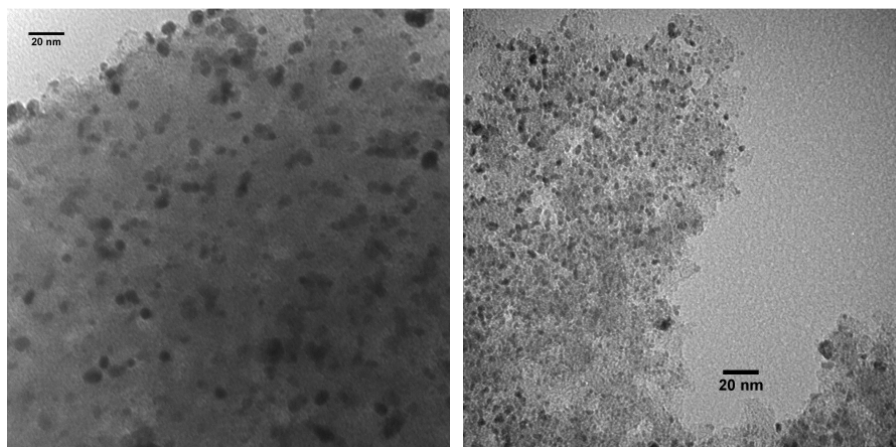
Figure 6.8 TEM micrographs of Pt/SI-CX (left) and Pt/CX (right)
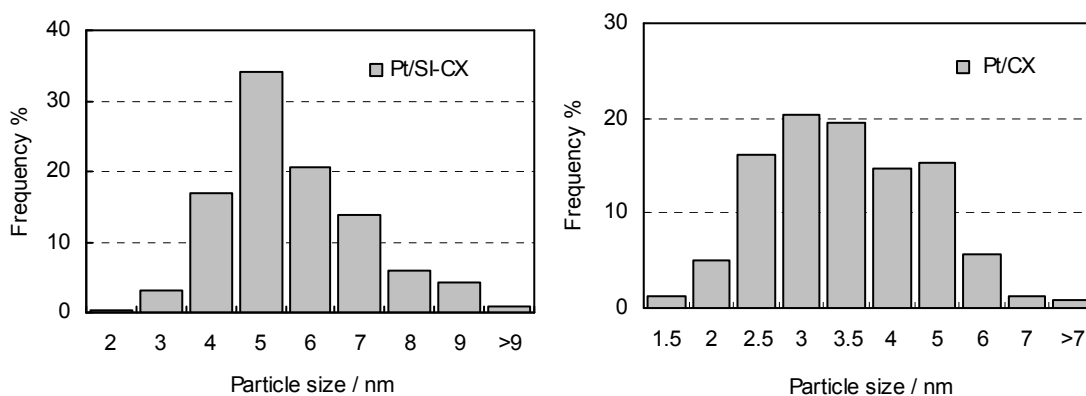
Figure 6.9 Histograms of Pt particle size of Pt/SI-CX (d_{mean}= 5.2 ±1.5 (SD) nm) and Pt/CX (d_{mean}= 3.3±1.1 (SD) nm)

Ex-situ CV is commonly used to estimate electrochemically active Pt surface area (ESA) for dispersed supported Pt catalysts, for comparison with areas calculated from Pt particle sizes. Details on how such measurements are made were provided in our recent paper on Pt/CX materials (ref 28) and in other references. Figure 6.10 (top) presents *ex-situ* CVs for Pt/SI-CX and Pt/CX samples for the H adsorption/desorption region. The CV shapes are as expected for Pt on carbon insofar as they exhibit well-defined regions

for H adsorption/desorption and Pt oxidation/oxide reduction atop a relatively large capacitive background current for carbon. Estimates of the hydrogen adsorption or desorption charge density were made as described in references [36, 37], and ESA values calculated using these values combined with the known Pt loading on the electrodes (as described in reference [28]) are given in Table 6.4. As expected, ESA values are smaller for Pt/SI-CX due to larger Pt particle size in the sample.
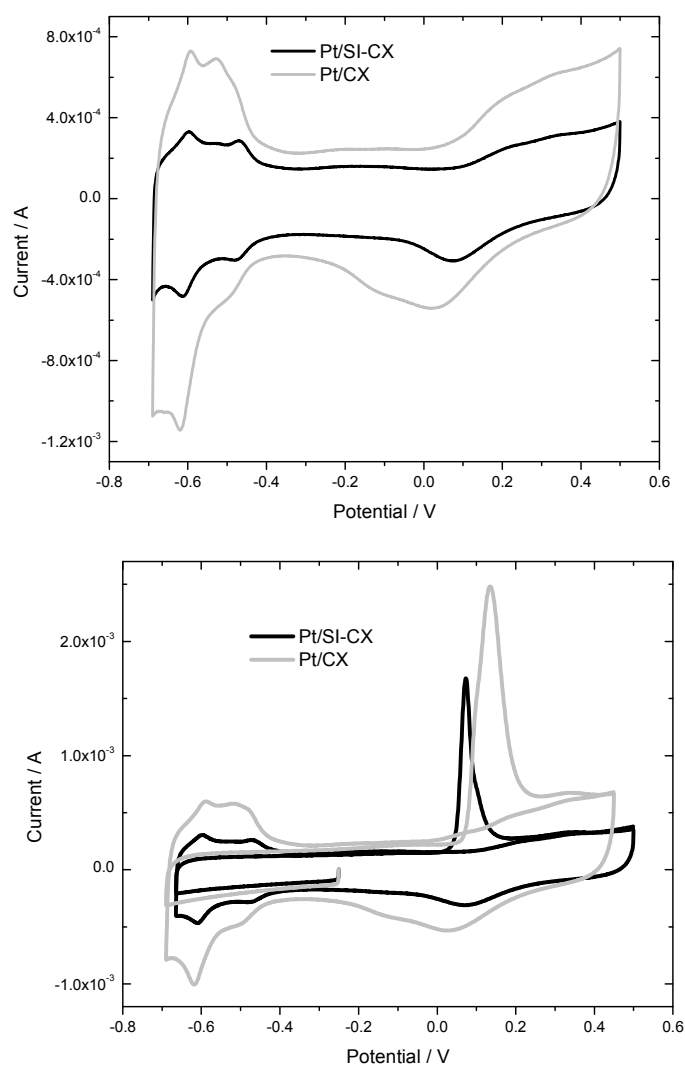
Figure 6.10 *Ex-situ* CVs (top) and CO stripping CVs (bottom) of Pt/SI-CX and Pt/CX

Figure 6.10 (bottom) shows CO stripping voltammograms for Pt/SI-CX and Pt/CX samples, and ESA values obtained as described in reference [28] are reported in Table 6.4. ESA values from CO stripping are in good agreement with those from hydrogen adsorption or desorption, which serves to validate both methods.

When comparing the specific surface area values for the Pt/SI-CX and Pt/CX samples as obtained from XRD or TEM particle size data with the ESA valued obtained by electrochemical methods, It is noted that the ESA value for Pt/SI-CX is especially low, much more so than would be expected based just upon the larger Pt particle sizes for that sample. This finding could be caused by some especially large Pt particles that might exist in the Pt/SI-CX sample but which are not accounted for in the imaging experiments because they are out of the field of view. Such particles would also not be properly accounted for in the XRD measurement for which use of the Scherer equation requires one to assume a fixed particle size. We speculate that the negatively charged groups onto the grafted CX surface may affect the process of Pt deposition by the impregnation-reduction method, by inhibiting nucleation and causing slower growth which promotes formation of large particles.

In-situ CV may be used to estimate the Pt ESA in electrodes in MEAs. Comparison of ESAs for such samples with those obtained by *ex-situ* CV provides information on catalyst utilization in the MEA. ESA values measured *in-situ* for both Pt/SI-CX and Pt/CX samples (cathodes only; see Figure 6.11 and Table 6.4) are very close to those measured *ex-situ* using both H adsorption/desorption and CO stripping. The good agreement between *in-situ* and *ex-situ* ESA measurements indicates a high catalyst

utilization in MEAs fabricated by the thin-film method in our lab. The *in-situ* ESA of Pt/SI-CX is also lower than that of Pt/CX which may have consequences for the fuel-cell performance.
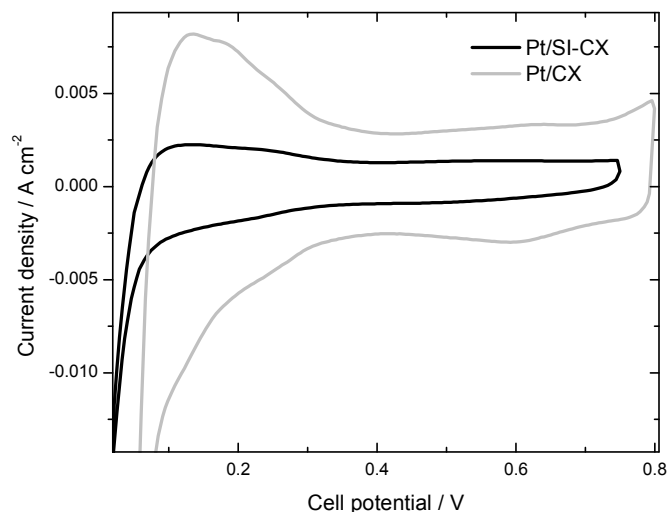
Figure 6.11 *In-situ* CVs of Pt/SI-CX and Pt/CX

Single-cell performance testing was attempted on the MEAs fabricated by the thin-film method from the inks made from both Pt/SI-CX and Pt/CX catalysts. Relatively good performance was observed for the Pt/CX catalyst as is described separately in Chapter 3, however the performance testing of the Pt/SI-CX MEA failed because an adequate set-point current could not be achieved. For example, after the cell was broken in at 0.5 V, the current density for the Pt/SI-CX cell was found to be just around 60 mA cm^{-2}, while, in contrast, the current density for the Pt/CX cell was close to 1000 mA cm^{-2}, much higher than that of Pt/SI-CX). From the ESA value (15 m^2 g^{-1}) obtained from *in-situ* CV, there should be some low to medium performance for the MEA made of Pt/SI-CX, but the measured performance was unexpectedly very low. It is believed that there are several

factors which could be responsible for this finding. (1) After sulfonimide electrolyte grafting onto the carbons (CX or CB), the surface properties of the CX or CB changed and the impregnation-reduction Pt catalyst deposition method produced larger size Pt particles on the CX support leading to lower cell performance for the Pt/SI-CX. (2) After electrolyte grafting the pore size of the CX support is expected to be smaller. This effect plus the more hydrophilic character of the CX support after sulfonimide grafting may increase the mass transport resistance in the Pt/SI-CX electrode, thereby resulting in lower performance for the cell made using this material. Similarly, the more hydrophilic nature of the Pt/SI-CX support could promote cathode flooding which would also negatively impact cell performance. Future work on grafting of sulfonimide electrolytes onto/into larger-pore-size carbon substrates (such as silica-templated mesoporous carbon) and finding a better Pt catalyst deposition method which can synthesize smaller size Pt particle catalysts on electrolyte-grafted carbon supports are under way.

6.4   Conclusions

From the above discussion, we can conclude that a monoprotic aryl fluorosulfonimide acid electrolyte was successfully grafted onto high surface area CX and CB supports without aid of electrochemical induction. The sulfonimide electrolyte grafted onto CX or CB support was confirmed by back acid-base titration, EDX and TGA. The sulfonimide acid contents on the grafted CX and CB were calculated to be about 0.18 and 0.13 mmol g^{-1} carbon respectively according to acid-base titration. These findings are almost consistent with other analytical results from TGA and EDX.

Pt catalyst particles were deposited onto the sulfonimide-grafted CX samples and the resulting materials were characterized by XRD and TEM for Pt particle size and dispersion in comparison with Pt catalyst deposited onto uncoated CX samples. Pt particle size was consistently larger on the Pt/SI-CX samples. The ESA of the Pt/SI-CX was measured with *ex-situ* CV, CO stripping, and *in-situ* CV methods and compared with that of Pt/CX. The ESA for Pt/SI-CX was much smaller than that of Pt/CX, leading to much lower single cell performance of the MEAs made from the Pt/SI-CX catalyst, while cell performance of the MEA made from Pt/CX was close to that obtained from the commercial Pt/CX-72R (20% Pt) catalyst.

6.5   References

1.   S. Litster and G. McLean, *Journal of Power Sources*, 2004, **130**, 61-76.

2.   V. Mehta and J. S. Cooper, *Journal of Power Sources*, 2003, **114**, 32-53.

3.   P. Costamagna and S. Srinivasan, *Journal of Power Sources*, 2001, **102**, 242-252.

4.   M. S. Wilson and S. Gottesfeld, *Journal of Applied Electrochemistry*, 1992, **22**, 1-7.

5.   Z. Xu, Z. Qi and A. Kaufman, *Electrochemical and Solid-State Letters*, 2003, **6**, A171-A173.

6.   Z. Q. Xu, Z. G. Qi and A. Kaufman, *Chemical Communications*, 2003, 878-879.

7.   E. B. Easton, Z. Qi, A. Kaufman and P. G. Pickup, *Electrochemical and Solid-State Letters*, 2001, **4**, A59-A61.

8.   Z. Xu, Z. Qi and A. Kaufman, *Electrochemical and Solid-State Letters*, 2005, **8**, A313-A315.

9.   S. E. Creager, B. Liu, H. Mei and D. DesMarteau, *Langmuir*, 2006, **22**, 10747-10753.

10.   M. Toupin and D. Belanger, *Langmuir*, 2008, **24**, 1910-1917.

11.	Z. Li and S. Dai, *Chemistry of Materials*, 2005, **17**, 1717-1721.

12.	X. Wang, R. Liu, M. M. Waje, Z. Chen, Y. Yan, K. N. Bozhilov and P. Feng, *Chemistry of Materials*, 2007, **19**, 2395-2397.

13.	M. Pandurangappa, T. Ramakrishnappa and R. G. Compton, *International Journal of Electrochemical Science*, 2008, **3**, 1218-1235.

14.	J. L. Bahr and J. M. Tour, *Chemistry of Materials*, 2001, **13**, 3823-3824.

15.	C. Mangeney, Z. Qin, S. A. Dahoumane, A. Adenier, F. Herbst, J.-P. Boudou, J. Pinson and M. M. Chehimi, *Diamond and Related Materials*, 2008, **17**, 1881-1887.

16.	A. Adenier, E. Cabet-Deliry, A. Chausse, S. Griveau, F. Mercier, J. Pinson and C. Vautrin-Ul, *Chemistry of Materials*, 2005, **17**, 491-501.

17.	M. Pandurangappa, N. S. Lawrence and R. G. Compton, *Analyst*, 2002, **127**, 1568-1571.

18.	H. Du, B. Li, F. Kang, R. Fu and Y. Zeng, *Carbon*, 2007, **45**, 429-435.

19.	M. Glora, M. Wiener, R. Petricevic, H. Pröbstle and J. Fricke, *Journal of Non-Crystalline Solids*, 2001, **285**, 283-287.

20.	R. Petricevic, M. Glora and J. Fricke, *Carbon*, 2001, **39**, 857-867.

21.	A. Smirnova, X. Dong, H. Hara, A. Vasiliev and N. Sammes, *International Journal of Hydrogen Energy*, 2005, **30**, 149-158.

22.	S. E. Creager, J. J. Sumner, R. D. Bailey, J. J. Ma, W. T. Pennington and D. D. Desmarteau, *Electrochemical and Solid-State Letters*, 1999, **2**, 434-436.

23.	S. C. Savett, J. R. Atkins, C. R. Sides, J. L. Harris, B. H. Thomas, S. E. Creager, W. T. Pennington and D. D. DesMarteau, *Journal of the Electrochemical Society*, 2002, **149**, A1527-1532.

24.	J. R. Atkins, C. R. Sides, S. E. Creager, J. L. Harris, W. T. Pennington, B. H. Thomas and D. D. DesMarteau, *Journal of New Materials for Electrochemical Systems*, 2003, **6**, 9-16.

25.	D. D. DesMarteau, *Journal of Fluorine Chemistry*, 1995, **72**, 203-208.

26.	R. Petricevic, G. Reichenauer, V. Bock, A. Emmerling and J. Fricke, *Journal of Non-Crystalline Solids*, 1998, **225**, 41-45.

27. R. Saliger, V. Bock, R. Petricevic, T. Tillotson, S. Geis and J. Fricke, *Journal of Non-Crystalline Solids*, 1997, **221**, 144-150.

28. B. Liu and S. Creager, *Journal of Power Sources*, 2009, in press.

29. K. R. Cooper, V. Ramani, J. M. Fenton and H. R. Kunz, *Experimental methods and data analyses for polymer electrolyte fuel cells*, 1.5 edn., Scribner Associates, Inc., 2007.

30. K. S. W. Sing, D. H. Everett, R. A. W. Haul, L. Moscou, R. A. Pierotti, J. Rouquerol and T. Siemieniewska, *Pure and Applied Chemistry*, 1985, **57**, 603-619.

31. M. S. Wilson, J. A. Valerio and S. Gottesfeld, *Electrochimica Acta*, 1995, **40**, 355-363.

32. Z. Xu, Z. Qi and A. Kaufman, *Journal of Power Sources*, 2003, **115**, 49-53.

33. Z. Xu, Z. Qi and A. Kaufman, *Electrochemical and Solid State Letters*, 2003, **6**, A171-A173.

34. J. I. Langford and A. J. C. Wilson, *Journal of Applied Crystallography*, 1978, **11**, 102-113.

35. http://rsb.info.nih.gov/ij/, accessed on August 4, 2009.

36. A. Pozio, M. De Francesco, A. Cemmi, F. Cardellini and L. Giorgi, *Journal of Power Sources*, 2002, **105**, 13-19.

37. T. Vidakovic, M. Christov and K. Sundmacher, *Electrochimica Acta*, 2007, **52**, 5606-5613.

CHAPTER 7

GRAFTING POLYMER ELECTROLYTE ONTO CARBON BLACK AND ITS

APPLICATION IN PEM FUEL CELL

7.1   Introduction

Currently, the most commonly employed method to fabricate electrodes for polymer-electrolyte-membrane fuel cells (PEMFCs) is the thin film method developed by Wilson and coworkers[1, 2] in Los Alamos National Laboratory. In the method, electrodes were made by solution casting from an ink in which carbon supported Pt catalyst was simply mixed with solubilized proton conductor such as Nafion and solvents. Only catalyst with intimate contact with both electronic conductor (such as carbon) and protonic conductor (such as Nafion), and gas reactants is active in electrode. Adding Nafion in the electrodes instead of PTFE (polytetrafluoroethlyene) significantly increases proton conduction, therefore the three-phase zone (where the proton conductor, electronic conductor, and reagent gas are in intimate contact) in the electrodes. The catalyst utilization is increased from about 20% to about 45% after addition of Nafion instead of PTFE[3]. From the catalyst utilization, there is much chance of improvement of the electrode fabrication.

One way to improve the electrodes in PEMFCs is to covalently bind a proton conductor directly to the electrodes therefore to increase the three-phase zone in the electrodes and to improve the electrode performance and stability. Qi and coworkers[4-9] have reported several ways to incorporate the monofunctional electrolyte into the carbon supported Pt catalysts, from which fuel cell electrodes are fabricated. Fuel cell testing indicates

medium performance increase or diminished Nafion addition was achieved from these grafted electrodes. Chapter 6 also reported chemical grafting of monofunctional sulfonimide superacid electrolyte onto the electrode, but low cell performance than expected was obtained due to grafted sulfonimide effects on the electrodes.[10]

Usually monofunctional electrolyte grafted into the electrode doesn't provide enough electrolytes needed for optimal performance of the electrode as reported in literature.[10] Therefore, in this chapter attempt is made to covalently bond polymer electrolyte onto the electrode directly by using step-growth polymerization method to grow the sulfonated poly(arylene ether sulfone) electrolyte. Sulfonated poly(arylene ether sulfone) polymer or copolymer was intensively studied as membrane material for PEMFCs by McGrath group[11-18] in Virginia Tech. Sulfonated poly(arylene ether sulfone) polymer or copolymer display excellent properties such as high thermal stability, mechanical stability and proton conductivity. It is hoped by incorporation of sulfonated poly(arylene ether sulfone) polymer into the electrodes, the cell performance and stability will be significantly increased.

The grafting of sulfonated poly(arylene ether sulfone) polymer into carbon black was executed by first grafting of fluorophenyl group onto carbon black via diazonium chemistry, then followed by the step group polymerization of sulfonated dichlorodiphenyl sulfone (SDCDPS) with bisphenol AF at higher temperature and dry, basic condition. The whole grafting scheme is shown in Scheme 7.1. After polymer electrolyte grafting onto the carbon black sample, Pt catalyst was deposited onto with the common impregnation-reduction method, next, MEAs were fabricated with the Pt-

deposited, polymer-electrolyte-grafted carbon black, and finally these MEAs were tested on fuel cell test station and performance was evaluated with the MEAs made with Pt catalyst without grafting.
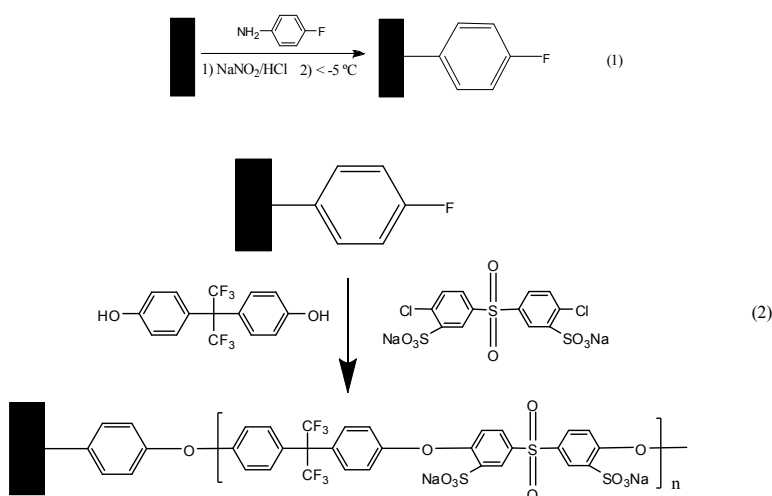
Scheme 7.1 Grafting of polymer electrolyte onto carbon black

7.2   Experimental

7.2.1   Synthesis of sulfonated dichlorodiphenyl sulfone

Synthesis of disodium sulfonated dichlorodiphenyl sulfone was followed from literature.[12, 19] In brief, a mixture of 4, 4'- dichlorodiphenyl sulfone (5.76 g) and 20% fuming sulfuric acid (14 mL) was heated under stirring and N_2 protection at 110 $^\circ$C for 6 h. The solution was cooled and poured into ice water. Then, 36 g NaCl was added into the solution to salt out the sodium form SDCDPS, the white precipitates was filtered out with filter paper. The sodium SDCDPS was re-dissolved into 80 mL DI water and the pH was adjusted to 6-7 with 20% NaOH solution. Next, the product was salted out by addition of 36 g NaCl again and filtered with filter paper. The crude product is

recrystallized from a mixture of isopropanol/water (7/3 v/v). The yield was 5.6 g. The ^{1}H NMR spectrum of the compound was similar to that reported in literature.[12]

7.2.2 Grafting of fluorophenyl group onto carbon black

Diazotization of $NH_2C_6H_4F$ was reported in several papers.[20, 21] A fluorophenyl group was grafted onto carbon black with the in-situ generated diazonium salt of $NH_2C_6H_4F$. For the grafting, about 1.0 g $NH_2C_6H_4F$ was added into a round bottom flask with a stir bar in a ice-salt bath, then 0.75 ml conc. HCl diluted in water was added into the flask under magnetic stirring. After the flask was cooled down, then 0.63 g $NaNO_2$ dissolved in 1 ml water was added dropwise into the flask under stirring, the reaction was kept low (<0~5 °C) for about 10 min. Then 1.0 g carbon black XC-72 was suspended in the *in-situ* generated diazonium salt in the flask, the ice-salt bath was removed, and the suspension was kept stirring for another 2 h. After that, the suspension was vacuum filtered with nylon filter, wash with DI water. The washing/filtration process was repeated for another 4 times. The grafted carbon black product was first air dried under hood, then vacuum dried at 100 °C overnight.

7.2.3 Grafting sulfonated poly(arylene ether sulfone) onto carbon black

Polymer electrolyte (sulfonated poly(arylene ether sulfone)) grafting onto carbon black (Scheme 1) was conducted in a flame-dried, three-necked flask. The flask was fitted with a nitrogen inlet, thermometer, stir bar, and Dean–Stark trap fitted with a condenser. The flask was charged with fluorophenyl-grafted carbon black (1.00 g), SDCDPS (1.47 g), bisphenol AF (0.57g), potassium carbonate (0.46 g), NMP (18 mL), and toluene (9 mL). The reaction flask was heated in an oil bath to 150 °C, and the toluene was refluxed for 4

h to remove any water. The toluene was then removed, and the reaction was allowed to continue for 16 h at 190 °C. Then, the reaction mixture was cooled down to room temperature and the suspension was vacuum filtered with 0.2 μm nylon membrane and washed with acetonitrile/H_2O mixture, the filtration/washing was repeated for another 4 times. Then, the grafted carbon black was air-dried in the hood, later then dried in vacuum at 105 °C for overnight.

7.2.4   Catalyst deposition onto polymer electrolyte grafted carbon black

Pt was deposited on polymer sulfone-grafted carbon black XC-72R (PE-CB) with the impregnation-reduction method described in previous chapters (for example, see Chapter 2) following the similar procedures in the catalyst deposition section. The Pt content was determined with thermogravimetric analysis (TGA) to be approximately 20% weight percent for the Pt-deposited, PE-grafted carbon black samples (Pt/PE-CB)

7.2.5   Characterization of the materials

The textural properties of carbon black XC-72R were characterized by N_2 adsorption method detailed in Chapter 2. The fluorophenyl-grafted carbon black, and the sulfonated poly(arylene ether sulfone)-grafted carbon black(PE-CB) samples were characterized with EDS, WDS (energy-dispersive, wavelength-dispersive spectroscopy attached to SEM) and the sulfonic acid content on the PE-CB samples was measured with acid-base back titration as described in Chapter 6. The Pt/PE-CB samples were characterized with XRD, TEM, *ex-situ* and *in-situ* cyclic voltammetry (CV) as described in previous chapters. Finally, MEAs were made with Pt/PE-CB and commercial Pt/XC-72R (Pt/CB) samples and tested similarly as described in previous chapters in detail.

7.3   Results and discussion

7.3.1   Characterization of fluorophenyl-grafted carbon with TGA and WDX

The fluorophenyl-grafted CB sample was characterized with TGA and wavelength-dispersive X-ray spectroscopy (WDX). The TGA curve of fluorophenyl-grafted CB is shown in Figure 7.2 in comparison with uncoated CB and CB mixed with 4-fluoroaniline (then washed with solvent to remove 4-fluoroaniline). From Figure 7.2, CB shows less than 1% weight loss at temperature at 500 °C, CB mixed with 4-fluoroaniline (after solvent washing to remove 4-fluoroaniline) has about 1% weight loss at 500 °C, which indicates 4-fluoroaniline has small amount leftover on CB due to its adsorptive property, while fluorophenlyl-grafted CB has about 3% weight loss at 500 °C (from the graph, it is assumed that from 200 to 500 °C, the weight loss from grafted CB is due to grafted fluorophenyl loss). Then, about 2.4% fluorophenlyl was grafted onto CB sample; this corresponds to 0.26 mmol/g fluorophenyl group on CB.
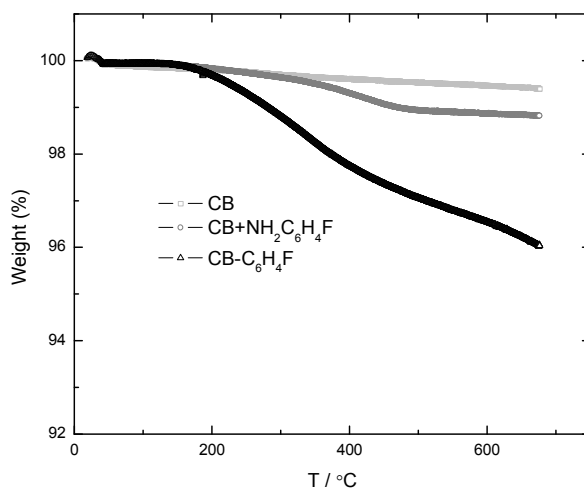
Figure 7.1 TGA curve of fluorophenyl grafted carbon black

The elemental analysis of the 4-fluorophenyl-grafted CB by WDS is shown on Table 7.1. The 4-fluorophenyl group on the carbon can be estimated from the fluorine content (F is specific) in the grafted sample, and the fluorophenyl is about 0.26 mmol g^{-1} grafted carbon. This result is very close to the TGA result. From specific surface area of carbon black XC-72R of 237 m^2 g^{-1}, the surface coverage of 4-fluorophenyl group on CB is 1E-10 mol cm^{-2}, indicative of monolayer grafting.

Table 7.1 WDS of fluorophenyl-grafted carbon black (weight percent)

Sample #	C	O	F	S
Un-grafted CB	86.47	13.38		0.15
CB+NH$_2$PhF[a]	86.88	13.12		
FPh-CB[b]	86.97	12.30	0.50	0.22

[a] 4-fluoroaniline mixed with CB and solvent extracted, [b] fluorophenyl –grafted CB

7.3.2   Characterization of polymer-grafted carbon black by titration and EDX

After *in-situ* polymerization of fluorophenyl-grafted CB with bishphenol AF and sulfonated dichlorodiphenyl sulfone, the polymer-electrolyte-grafted CB was subjected to EDX and acid-base back titration. The EDX results are shown in Table 7.2.

Table 7.2 Element analysis results by EDX for PE-CB sample

Sample	C wt%	O wt%	F wt%	S wt%	Cl wt%	K wt%	Si wt%
PECB	89.99	7.99	0.99	0.65	0.05	0.11	0.22

From the Table 7.2, it is seen that fluorine element content is increased after polymerization. The potassium element existed may indicate some salt leftover on the grafted CB even after extensive washing and filtration.

The acid content on polymer-grafted CB is an important parameter. The acid content estimated from the back titration method is shown on Table 7.3. CB has small amount of intrinsic acid content due to acid functional groups on it. The acid content from the polymer electrolyte on grafted CB is also very low (about 0.05 mmol/g grafted carbon) which may tell the polymer electrolyte is not efficient. The typical titration curve is shown in Figure 7.3.
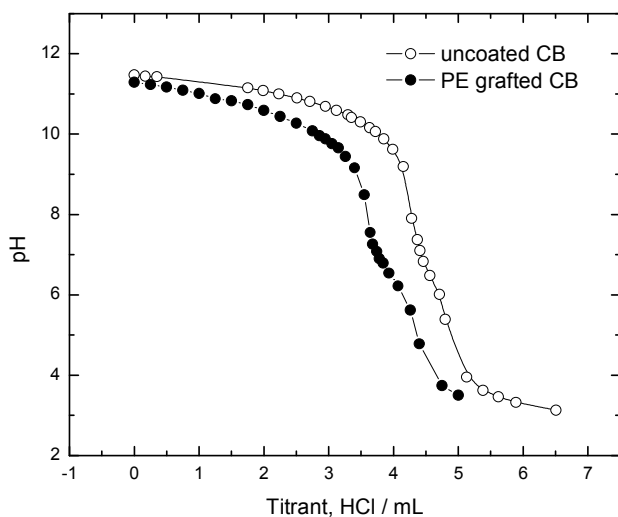
Figure 7.2 Back titration of polymer-electrolyte-grafted carbon black

Table 7.3 Acid group content on the polymer-grafted carbon black by titration

Sample	Uncoated CB	Grafted CB
Acid group (mmol/g)	0.048	0.10

7.3.3 Characterization of polymer-electrolyte-grafted carbon-black-supported Pt catalyst

The polymer electrolyte grafting on carbon black was intended to employ it in PEMFC application. So, Pt catalyst was deposited on the PE-CB samples by the common impregnation-reduction method and the resultant Pt/PE-CB samples were characterized with XRD, TEM and was fabricated to an MEA and tested in single cell test station in comparison with un-grafted commercial Pt/XC-72R catalyst as discussed in the following sections.

7.3.3.1 XRD analysis

The XRD diffractograms for the samples of Pt/PE-CB and Pt/XC-72R are shown in Figure 7.3. The diffractogram shows features expected for carbon supported Pt as labeled on the graph. Pt nanoparticle sizes may be estimated from the line broadening of the Pt (220) line using the Scherer equation as described in previous chapters. Particle size values obtained in this way for Pt/PE-CB and Pt/XC-72R are given in Table 7.4 Pt particle diameters are slightly higher for the Pt/ PE-CB sample (2.9 nm) than the Pt/XC-72R (2.2 nm). From the particle size, the Pt specific surface area may be calculated (See section in Chapter 2) and shown in Table 7.4.
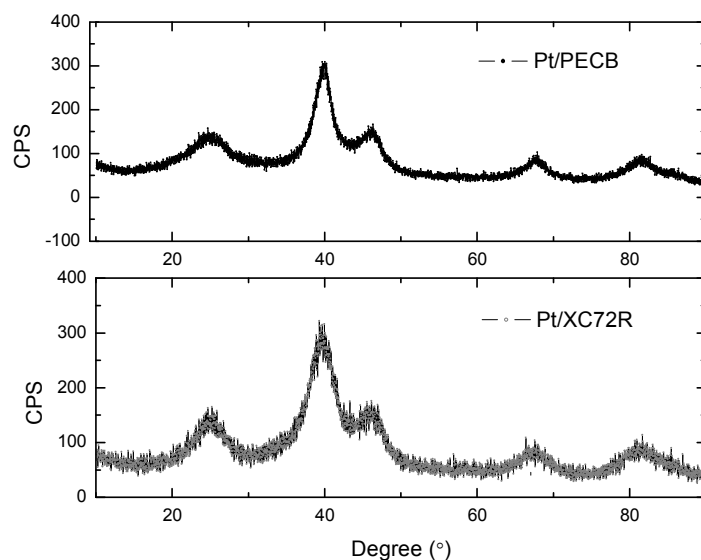
Figure 7.3 XRD graphs of Pt/PE-CB and Pt/XC-72R

Table 7.4 Pt Particle size determined by different methods

Sample	d_{XRD} nm	S_{XRD} $m^2 g^{-1}$	d_{TEM} nm	S_{TEM} $m^2 g^{-1}$	S_H $m^2 g^{-1}$	S_{CO} $m^2 g^{-1}$	$S_{in\text{-}situ}$ $m^2 g^{-1}$
Pt/PE-CB	2.9	96.7	3.4	82.5	65	52	45
Pt/XC72R	2.2	127.4	2.8	100.1	67	66	65

d_{XRD}: particle size by XRD, d_{TEM}: particle size by TEM, S_{XRD},S_{TEM}: the specific surface area calculated from the equation (2.2) from XRD and TEM respectively, S_H: specific surface area from *ex-situ* CV (H desorption charge), S_{CO}: surface area from *ex-situ* CO stripping CV, $S_{in\text{-}situ}$: surface area from *in-situ* CV (in MEA)

7.3.3.2 TEM analysis

TEM micrographs and histogram graphs of Pt particle size for the Pt/PE-CB and Pt/XC-72R samples are shown in Figures 7.4 and 7.5 respectively. Both TEM micrographs clearly show well-distributed Pt nanoparticles supported on grafted carbons. The mean Pt diameter for Pt/PE-CB and Pt/XC-72R samples is estimated to be 3.4 ± 1.1

nm and 2.8 ± 0.7 nm respectively Error estimates are standard deviations Pt particle size on PE-CB sample is slightly larger and its distribution is slightly broader. The specific surface area (SA) of Pt of both Pt/PE-CB and Pt/XC-72R according to TEM measurement is also calculated and given in Table 7.4. Pt specific SA of Pt/PE-CB is smaller than that of Pt/XC-72R due to larger Pt particle size on Pt/PE-CB. Usually the Pt catalyst specific surface area from TEM and XRD are larger than that measured by *ex-situ* or *in-situ* CV because TEM or XRD measurements include electrochemically-inaccessible Pt particle. Also the ESA measured *ex-situ* (in a half cell) is commonly higher than that measured *in-situ* (in MEA form) due to better ion conduction by help from free acid (H_2SO_4) in the half-cell measurement. These points are further developed in the following discussion.
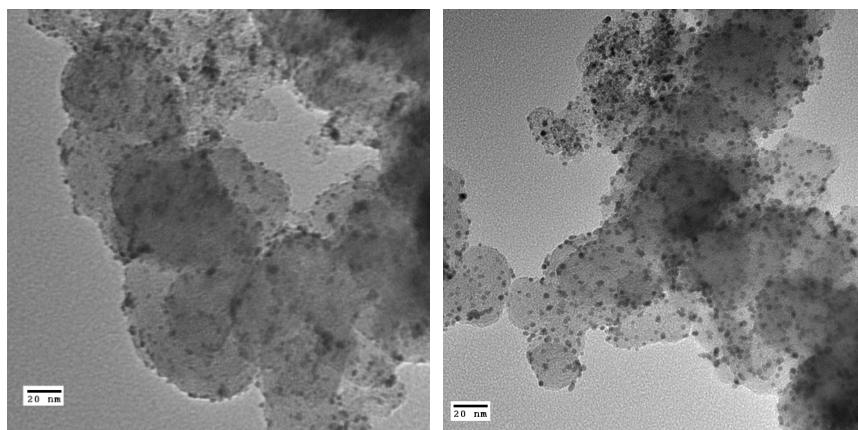
Figure 7.4 TEM graphs of Pt/PE-CB (left) and Pt/XC-72R catalyst (right)
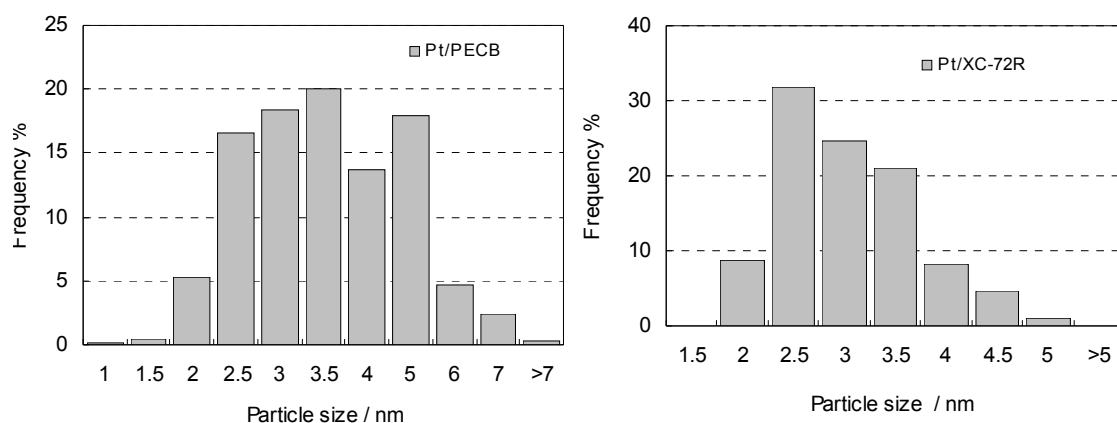
Figure 7.5 TEM graphs and histograms of the Pt/PE-CB (d mean= 3.4 ± 1.1 nm) and commercial Pt/XC-72R, (d mean=2.8 ± 0.7 (SD) nm)

7.3.3.3 *Ex-situ* cyclic voltammetry and *in-situ* voltammetry

Figure 6 and 7 present *ex-situ* CVs of H_2 stripping and CO stripping methods for Pt/PE-CB and Pt/XC-72R samples. In Figure 7.6, the CV exhibits well-defined characteristic of carbon supported Pt catalyst, for example, H adsorption/desorption and Pt oxidation/oxide reduction atop a relatively large capacitive background current for carbon. Figure 7.7 shows well-defined adsorbed CO oxidation peak. The negative shift of adsorbed CO oxidation peak potential for Pt/PE-CB sample also verifies slightly larger Pt particle size observed with TEM.[22, 23] Estimates ESA values from hydrogen desorption charge density are given in Table 7.4 in comparison with those obtained from *ex-situ* CV of CO stripping and *in-situ* CV of H_2 stripping (shown in Figure 7.8). ESA value for Pt/PE-CB from *ex-situ* CV of H_2 stripping is close to that of Pt/XC-72R. ESA values of Pt/PE-CB from *ex-situ* CO stripping and *in-situ* CVs are smaller than that of Pt/XC-72R perhaps due to larger Pt particle size in the Pt/PE-CB, and might also be caused by the Pt particles buried inside electrolyte in grafted carbon, not electronically accessible.
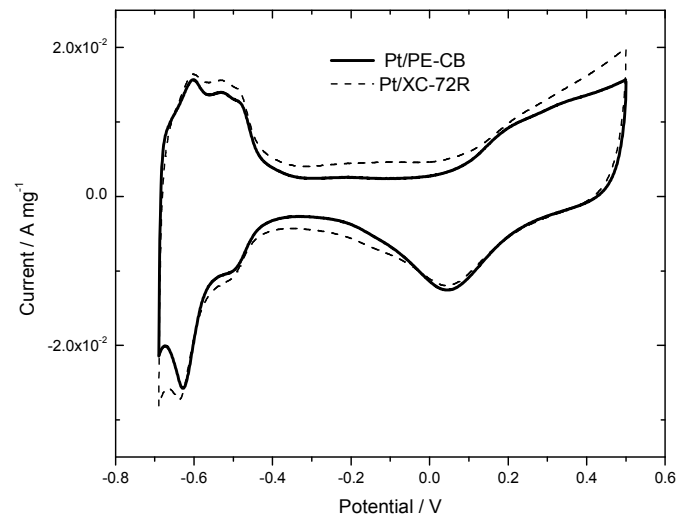
Figure 7.6 *Ex-situ* CVs of Pt/PE-CB and Pt/XC-72R catalysts
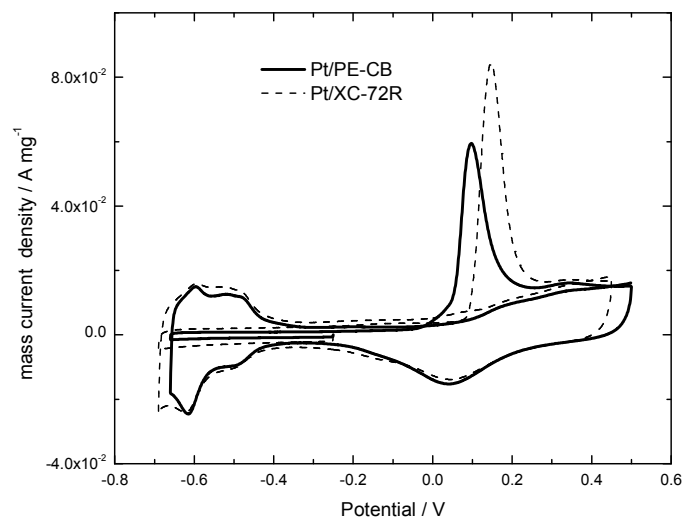
Figure 7.7 *Ex-situ* CVs of Pt/PE-CB and Pt/XC-72R catalysts
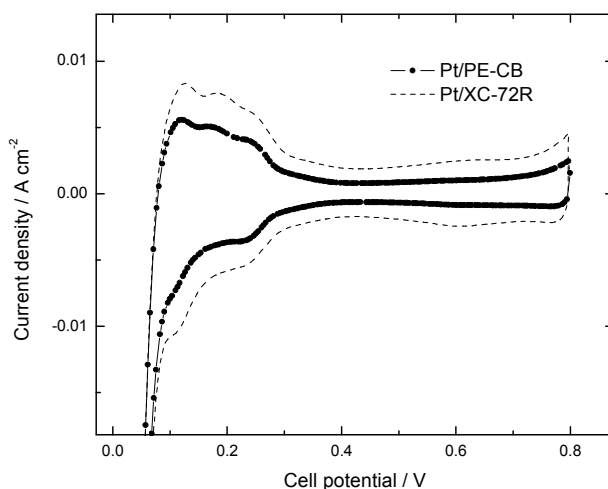
Figure 7.8 *In-situ* CVs of the MEAs made of Pt/PE-CB and Pt/XC-72R catalysts

7.3.3.4 Fuel cell testing

The MEAs fabricated with both catalyst Pt/PE-CB and Pt/XC-72R were tested in H_2/O_2 and H_2/air cells at both 80 ℃ and 50 ℃ under atmospheric pressure conditions. The polarization and resistance curves are shown in Figures 7.9, 7.10 and 7.11, 7.12 respectively. The performance of Pt/PE-CB is slightly lower than that of Pt/XC-72R in H_2/O_2 or H_2/air cells at 80 and 50 ℃. The resistance curves of MEAs made with Pt/CX and Pt/XC-72R shows similar trends for both H_2/O_2 and H_2/air cells under either 80 ℃ or 50 ℃. The two findings may therefore indicate a small amount of polymer-electrolyte grafted on carbon black has little effect on its performance in fuel cells. Further work of increasing the grafted sulfonated poly(arlyene ether sulfone) on carbon black is needed to evaluate the polymer electrolyte grafting effect on the fuel cell electrodes.
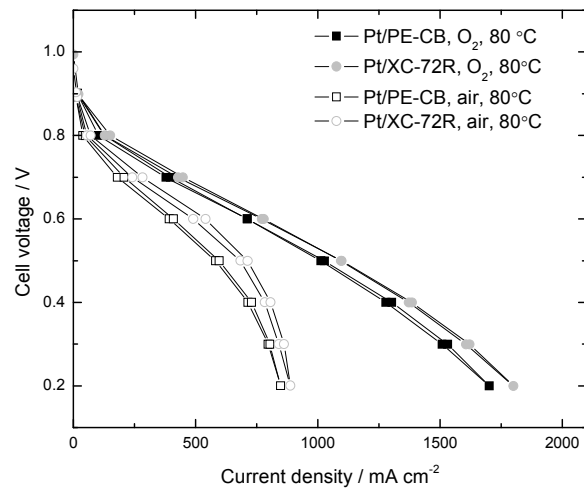
Figure 7.9 Performance curves of the Pt/PE-CB and Pt/XC-72R, H_2/O_2, H_2/Air, both at 80 ºC, 100% relative humidity, atmospheric pressure
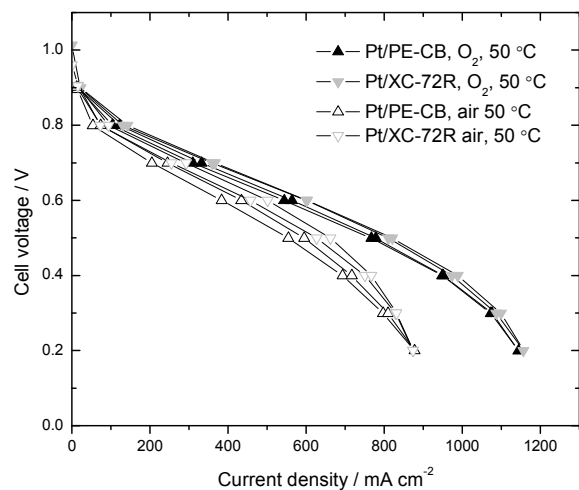
Figure 7.10 Performance curves of the Pt/PE-CB and Pt/XC-72R, H_2/O_2, H_2/Air, both at 50 ºC, 100%, relative humidity, atmospheric pressure
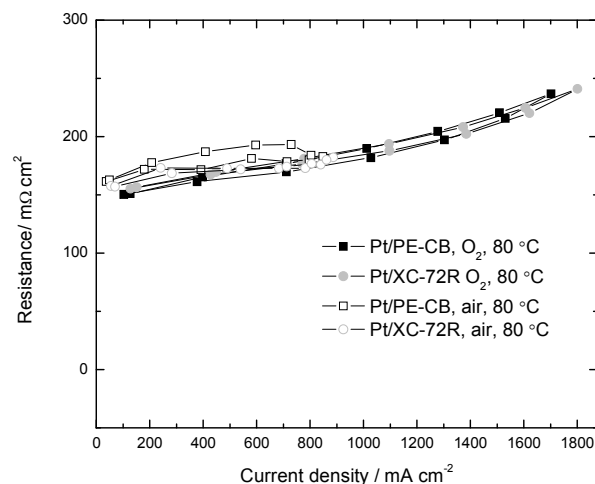
Figure 7.11 Resistance of the carbon supported catalysts by CI, H_2/O_2 and H_2/air at 80 °C
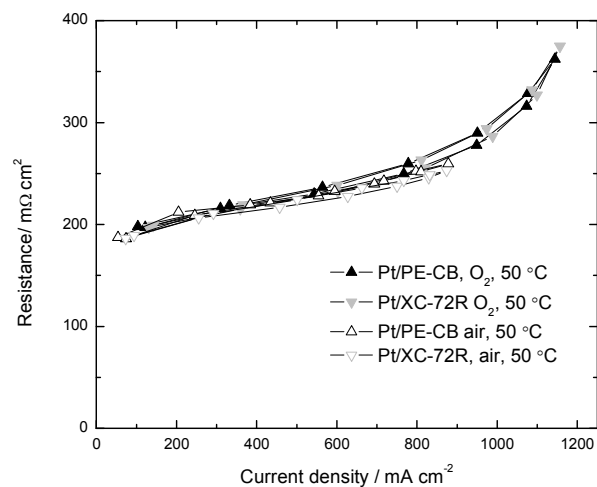
Figure 7.12 Resistance of the carbon supported catalysts by CI, H_2/O_2 and H_2/air at 50 °C

7.4 Conclusions

In-situ step-growth polymerization of sulfonated poly(arlyene ether sulfone) was performed on commercial carbon black samples of XC-72R. The polymer electrolyte grafting is not effective, only about 0.05 mmol/g acid content was found on the grafted carbon by acid-base titration method. In order to study the effect of the grafted polymer electrolyte on the carbon black support, Pt catalyst was deposited on the grafted carbon

black, and the polymer-grafted carbon supported catalyst (Pt/PE-CB) was characterized with XRD, TEM, *ex-situ* CV of H_2 stripping and CO stripping and *in-situ* CV in comparison with commercial available Pt/XC-72R catalyst. The Pt particle size was slightly larger than that of Pt/XC-72R. The ESA value for Pt/PE-CB from the *ex-situ* CV of H_2 stripping is close to that of Pt/XC-72R., while the ESA values from CO stripping and *in-situ* CV for Pt/PE-CB were smaller than that of Pt/XC-72R. Consequently the performance of Pt/PE-CB in MEA format was slightly lower than that of Pt/XC-72R in both H_2/O_2 and H_2/air at both 80 and 50 °C. The resistances monitored by current interrupts methods for both Pt/PE-CB and Pt/XC-72R were similar for H_2/O_2 cells at both 80°C and 50°C, H_2/air cells at both 80 °C and 50 °C. These findings indicate the small amount of polymer electrolyte grafted on carbon black has little effect on its fuel cell performance. Further work to increase the polymer-grafting content is needed for evaluation its effect on performance.

7.5   Reference

1.   M. S. Wilson and S. Gottesfeld, *Journal of Applied Electrochemistry*, 1992, **22**, 1-7.

2.   M. S. Wilson, J. A. Valerio and S. Gottesfeld, *Electrochimica Acta*, 1995, **40**, 355-363.

3.   S. Litster and G. McLean, *Journal of Power Sources*, 2004, **130**, 61-76.

4.   E. B. Easton, Z. Qi, A. Kaufman and P. G. Pickup, *Electrochemical and Solid-State Letters*, 2001, **4**, A59-A61.

5.   N. Jia, R. B. Martin, Z. Qi, M. C. Lefebvre and P. G. Pickup, *Electrochimica Acta*, 2001, **46**, 2863-2869.

6.   Z. Xu, Z. Qi and A. Kaufman, *Journal of Power Sources*, 2003, **115**, 49-53.

7. Z. Xu, Z. Qi and A. Kaufman, *Electrochemical and Solid-State Letters*, 2003, **6**, A171-A173.

8. Z. Q. Xu, Z. G. Qi and A. Kaufman, *Chemical Communications*, 2003, 878-879.

9. Z. Xu, Z. Qi and A. Kaufman, *Electrochemical and Solid-State Letters*, 2005, **8**, A313-A315.

10. B. Liu, D. DesMarteau and S. Creager, *Journal of Materials Chemistry*, submitted

11. F. Wang, M. Hickner, Y. S. Kim, T. A. Zawodzinski and J. E. McGrath, *Journal of Membrane Science*, 2002, **197**, 231-242.

12. L. H. William, W. Feng, B. M. Jeffery, A. B. Vinayak, H. Melinda, K. Yu Seung and E. M. James, *Journal of Polymer Science Part A: Polymer Chemistry*, 2003, **41**, 2264-2276.

13. Y. S. Kim, M. A. Hickner, L. Dong, B. S. Pivovar and J. E. McGrath, *Journal of Membrane Science*, 2004, **243**, 317-326.

14. Y. Li, F. Wang, J. Yang, D. Liu, A. Roy, S. Case, J. Lesko and J. E. McGrath, *Polymer*, 2006, **47**, 4210-4217.

15. K. B. Wiles, C. M. de Diego, J. de Abajo and J. E. McGrath, *Journal of Membrane Science*, 2007, **294**, 22-29.

16. H.-S. Lee, A. Roy, O. Lane, S. Dunn and J. E. McGrath, *Polymer*, 2008, **49**, 715-723.

17. J. Yang, Y. Li, A. Roy and J. E. McGrath, *Polymer*, 2008, **49**, 5300-5306.

18. A. S. Badami, O. Lane, H.-S. Lee, A. Roy and J. E. McGrath, *Journal of Membrane Science*, 2009, **333**, 1-11.

19. U. Mitsuru, T. Hidetsugu, O. Takao, S. Jun-Ichi, Y. Koichiro, M. Toru and T. Takero, *Journal of Polymer Science Part A: Polymer Chemistry*, 1993, **31**, 853-858.

20. L. F. Anthony, *Journal of Labelled Compounds and Radiopharmaceuticals*, 1988, **25**, 1245-1254.

21. J. T. Patt and M. Patt, *Journal of Labelled Compounds and Radiopharmaceuticals*, 2002, **45**, 1229-1238.

22. F. Maillard, S. Schreier, M. Hanzlik, E. R. Savinova, S. Weinkauf and U. Stimming, *Phys. Chem. Chem. Phys.*, 2005, **7**, 385-393.

23. F. Maillard, M. Eikerling, O. V. Cherstiouk, S. Schreier, E. Savinova and U. Stimming, *Faraday Discuss.*, 2004, **125**, 357-377.

CHAPTER 8

BLEND AND CROSS-LINKED SULFONIMIDE MEMBRANE FOR POLYMER ELECTROLYTE FUEL CELL APPLICATION

8.1 Introduction

Polymer electrolyte membrane (PEM) is a key component in PEM fuel cells. Perfluorinated polymer such as Nafion® from DuPont and other closely related perfluorosulfonic acid (PFSA) ionomer are widely employed as membrane materials in PEM fuel cells (PEMFCs). These PFSA ionomers possess many desirable properties appropriate for PEMFC applications, such as high protonic conductivity, good mechanical properties, and excellent long-term chemical stability. However, they also possess some undesirable properties, among which are diminished protonic conductivity at low relative humidity, poor mechanical properties above about 130 °C, and the high production cost.[1, 2]

One way to improve proton-conducting fluoropolymer electrolytes is to change the acidic group from fluorosulfonic acid (in Nafion) to an alternate sulfonimide superacid group. Perfluorosulfonimide (PFSI) electrolytes, that have been developed by DesMarteau[3-8] and co-workers at Clemson, possess many attractive attributes for fuel-cell applications including very strong acidity and excellent chemical and electrochemical inertness especially at high temperatures (PFSIs are stable to 400 °C in acid form). The fluorosulfonimide acid group also possesses two sites for functionalization, unlike fluorosulfonates which possess just one. This attribute provides much flexibility for

designing new polymers having structures and properties quite different from those of conventional PFSA electrolytes. Plain sulfonimide polymers with equivalent weight (EW) of 1200 and 1075 as membrane materials in PEMFC have been studied by Savett et al[6] in comparison with Nafion. In the range of membrane thicknesses and ionomer EWs considered, plain sulfonimide membranes behaved similarly with Nafion in respect to both ionic conductivity and fuel cell performance. This chapter reports our further work on blended and cross-linked sulfonimide polymers as membrane electrolytes for PEMFC application in comparison with Nafion 117, 105 and 112.

8.1.1   Blended sulfonimide polymer

Polymer blending gives a more versatile method for new membrane material development. Relative to a single-component polymer, a polymer blend has more freedom to be tailed to meet the required properties for PEMFC application. For example, Polymers with higher EW usually have lower conductivity but better mechanical properties, whereas polymers with lower EW have higher conductivity but poor mechanical properties. Blending of the one with lower and the other with higher EW may give a polymer blend with higher conductivity and also better mechanical properties than either of the constituent polymers. The resultant polymer may be useful at higher temperature in a fuel cell. The blending of different polymers for membrane materials in fuel cell application has been greatly reported in literature.[9-11] In our lab, a new method to blend the same sulfonimide polymer with different EW was explored. The blending of polymers was accomplished by dissolving them in a mixture of solvents and making their membrane. One sulfonimide blend with EW 1504 (Blend 1504) blended by a plain

sulfonimide polymer with EW 1600 and another one with EW 1300 was explored as membrane electrolyte in PEMFC with a single cell testing and performance were compared with Nafion 117, 105, and 112. The testing results show that the blend sulfonimide's performance was pretty good considering its high EW value.

8.1.2 Cross-linked sulfonimide polymer

Low EW polymer usually has low mechanical properties and even could be dissolved in water, which are undesirable properties for PEMFC application and a freestanding membrane is difficult to prepare from. By cross-linking the low EW polymer with cross-linking agents, resultant polymer with higher mechanical property and better water compatibility could be prepared in a membrane form. This approach has been reported to make membrane materials for PEMFC in literature.[12-14] In our lab, cross-linked sulfonimide ionomers were prepared by ter-polymerization of perfluorovinylethersulfonimide (PFVESI) and tetrafluoroethylene (TFE) co-monomers with small amounts of divinyl ether monomers (Figure 8.1). These cross-linked ionomers show higher conductivity at 80°C and 120°C as compared to non-cross-linked polymers and Nafion. One cross-linked sulfonimide polymer of EW 1000 (Xlinked 1000) was tested as membrane material in PEMFC, and the results show its performance was better than Nafion 112.
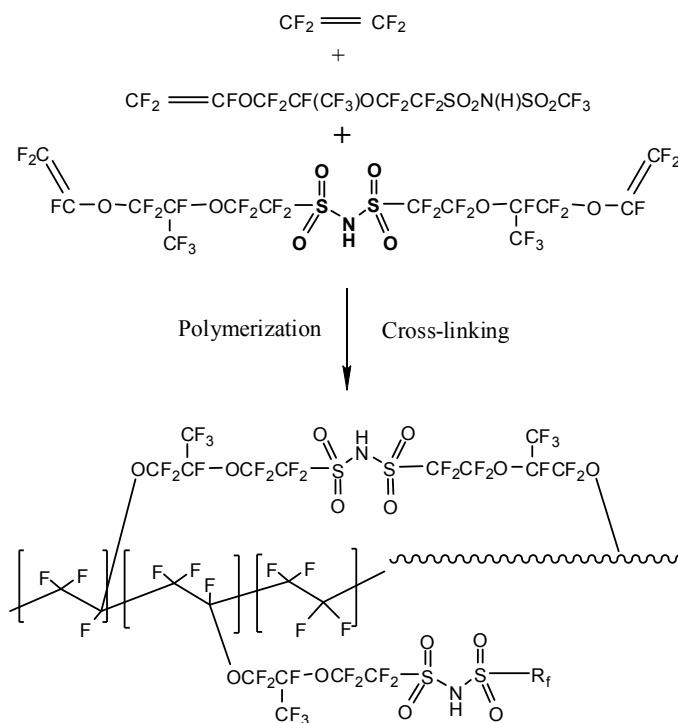
Figure 8.1 Schematics of cross-linking sulfonimide polymer structure

8.2 Experimental

8.2.1 MEA fabrication

For both blended and cross-linked sulfonimide membrane samples, membrane electrode assemblies (MEAs) were prepared using the decal transfer method developed by Wilson and co-workers [15, 16] at Los Alamos National Laboratory. Detail of the method is given in published papers [1-3] and previous chapters. The commercial Pt/XC-72R (Alfa Aesar, 20% Pt) and soluble Nafion 1100 were used to prepare the inks to cast MEAs. All membranes were converted to Na^+ form for hot pressing. After hot pressing, the MEAs was boiled in dilute sulfuric acid to convert polymer electrolyte membranes and Nafion in catalyst layer to acid form. The membranes used for MEA fabrication are listed on

Table 8.1 and two MEAs fabricated from Xlinked 1000 and Blend 1504 are shown in Figure 8.2.

Table 8.1 Basic properties of membranes tested in MEAs

Membrane	EW g mol^{-1}	Thickness μm
X-linked 1000	1000[a]	46
Blend 1504	1504[a]	55
Nafion 112	1100[b]	50
Nafion 105	1000[b]	127
Nafion 117	1100[b]	178

[a] EW measured by Dr Sharif with acid-base back titration method of relevant polymers, [b] nominal EW given by manufacturer
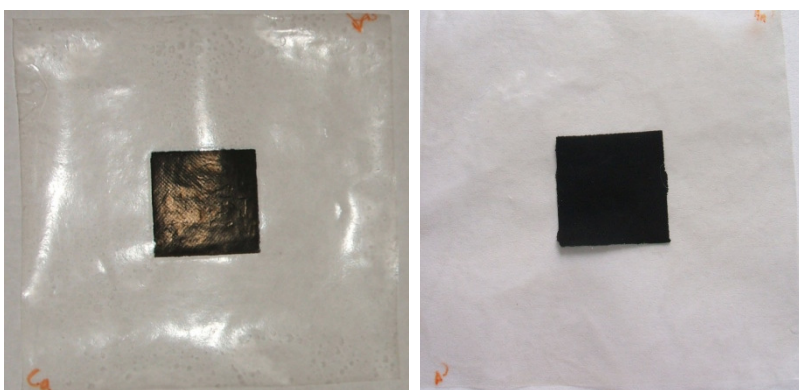

Figure 8.2 MEAs made by decal transfer method, blend 1504 (left) Xlinked 1000 (right)

8.2.2 Single fuel-cell testing

The single-cell testing of MEAs was performed on a model 850C test station from Scribner Associates Company. The details of assembly of the cells were described in

previous chapters. Cells were broken in at a cell voltage of 0.5 V overnight, then the membrane H_2 cross-over was performed, after that, a series of polarization curves was acquired in controlled voltage mode under different operating conditions. The cell open circuit voltage was close to or above 1.0 V for all MEAs. The cell resistance was monitored during acquisition of the polarization curves using the current interrupt method (CI) and by high frequency impedance spectroscopy (HFR) at 1 kHz frequency. [17]

8.2.3 H_2 crossover by linear sweep voltammetry

H_2 crossover was measured by linear sweep voltammetry (LSV) using a fuel cell setup with 5 cm^2 active area MEAs. The anode severed as both pseudo-reference and counter electrodes, and the cathode served as the working electrode. The anode was fed with high purity H_2 gas (humidified) and the cathode is fed with high purity N_2 gas (humidified). The gas flow of both N_2 and H_2 was kept at 50 mL min^{-1} during the measurements. A Solartron 1280B electrochemical workstation was used as the potentiostat. The potential was scanned from 0 to 0.8 V with a scan rate of 2 mV s^{-1} to obtain the limiting crossover currents.

8.3   Results and discussion

8.3.1   Blended sulfonimide membrane EW 1504

8.3.1.1   Ionic conductivities

Membrane ionic conductivity is an important parameter for evaluating of a membrane, and is usually used for screening of better membrane. The ionic conductivities of the blend 1504 were measured at BekkTech with a four point probe direct current (DC)

method at different relative humidity (RH) at 80 °C under atmospheric pressure in comparison with that of Nafion 112. The detailed test protocol is seen on BekkTech (website). The ionic conductivities vs RH curves are shown in Figure 8.3. From the Figure 8.3, it is seen that the conductivities of Blend 1504 was lower than that of Nafion 112 at the whole RH range at 80 °C.
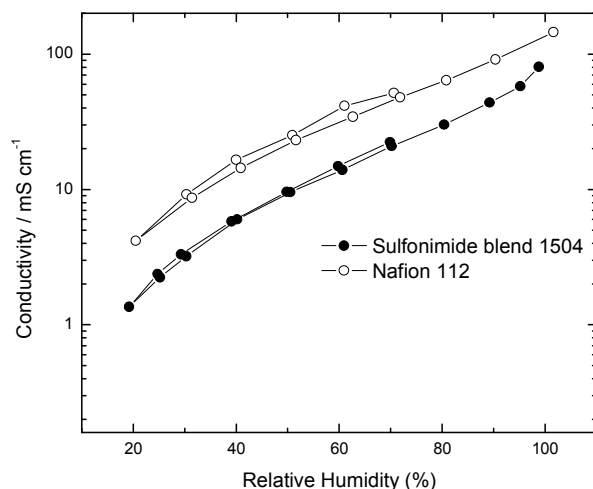
Figure 8.3 Ion conductivity of sulfonimide blend 1504 in different humidity compared with Nafion 112, measured by BekkTek with four point probe DC method

8.3.1.2   H$_2$ cross over membranes by LSV

In addition to proton conductivity, fuel (H$_2$) and oxidant (O$_2$) permeability through membrane is also a critical property of a membrane. Many techniques have been used to measure the gas permeation rate of the membrane.[18] *In-situ* electrochemical method (such as LSV) is the most direct one, in which, gas permeation rate is measured as a mass transfer limited current. The H$_2$ crossover of the Blend 1504 measured with LSV at 30 °C under atmospheric pressure is shown in Figure 8.4 compared with H$_2$ crossover of Nafion 112, 105 and 117. Many factors can affect the H$_2$ crossover of a membrane; the most

167

significant ones among them are membrane itself (membrane materials, thickness, water content in membrane, etc), MEA fabrication (MEA compaction, gas diffusion materials, catalyst, etc), temperature, gas pressure. For our measurement, all other conditions are assumed as the same, the H_2 crossover difference was thought to be caused only by membrane. From Figure 8.4, Nafion 112 has highest H_2 crossover rate, Nafion 117 has lowest crossover rate (because Nafion 117 is the thickest membrane used in the measurement), although, the Blend 1504 has close thickness to that of Nafion 112, its H_2 crossover rate is much lower than that of Nafion 112, This finding may indicate blending strengthen the membrane; which may be due to the more TFE component in the blend membrane with high EW or blending itself may decrease the H_2 crossover due to structure change by blending. The H_2 crossover rate can be calculated according to following equation:[19]

$$N_{H_2} = \frac{j_{\lim}}{nF}$$ (8.1)

N_{H2} is the H_2 crossover flux (mole s^{-1} cm^{-2}), $j_{\lim}$ is the H_2 crossover limiting current (A cm^{-2}), n is electrons transferred in hydrogen oxidation the reaction, F is the Faraday constant (96485 C eq^{-1}). The H_2 crossover flux of Blend 1504 is calculated out and listed on Table 8.2 in comparison with Nafion 112, 105 and 117.

Table 8.2 H_2 crossover rate of different membranes by LSV

Membranes	Blend 1504	Nafion 112	Nafion 105	Nafion 117
N_{H2} / mole s^{-1} cm^{-2}	1.4E-9	2.9E-9	1.2E-9	8.6E-10

O$_2$ permeation rate can also be measured by electrochemical method. But due to lack of appropriate reference electrode for the measurement and harmful high potential range to the electrode used in measurement, no measurement was executed in the lab and the O$_2$ crossover of the membranes is not discussed here.
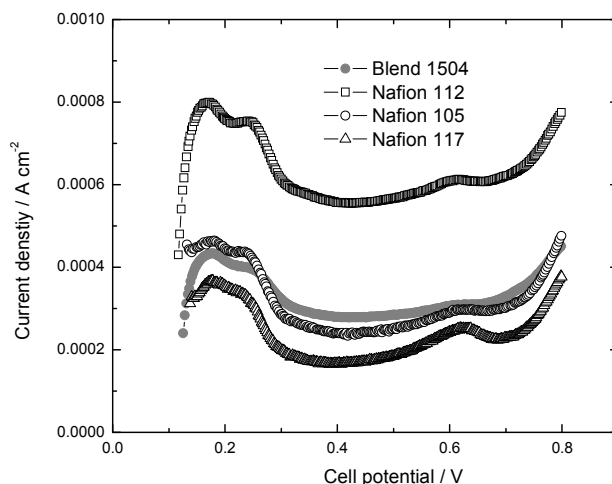
Figure 8.4 H$_2$ crossover of Blend 1504 membranes with Nafion 112, 105 and 117 by LSV at 30 °C cell temperatures, fully humidified.

8.3.1.3 Single-cell testing performance of Blend 1504

Proton conductivity is a good measure to evaluate a membrane material. But not always high proton conductivity gives high cell performance of the membrane, not always low proton conductivity gives low cell performance of the membrane. A determinate judgment of a membrane for PEMFC application is to single-cell test the membrane (in MEA form) under different operation condition in a fuel cell test station. The single cell testing performance of the Blend 1504 under H$_2$/O$_2$ or H$_2$/air at 80 °C and 50 °C (cell temperatures) are shown in Figure 8.5 to 8.8 in comparison with Nafion 112, 105 and 117. Form Figure 8.5 and 8.6, it is seen that the cell performance of Blend 1504 is higher

than that of Nafion 117, but lower than that of Nafion 105 and 112 at 80 °C under H_2/O_2 condition; while it is higher than both Nafion 117 and 105 at 50 °C under H_2/O_2 condition. Considering its much higher EW value, the Blend 1504 performed pretty well in fuel cells.
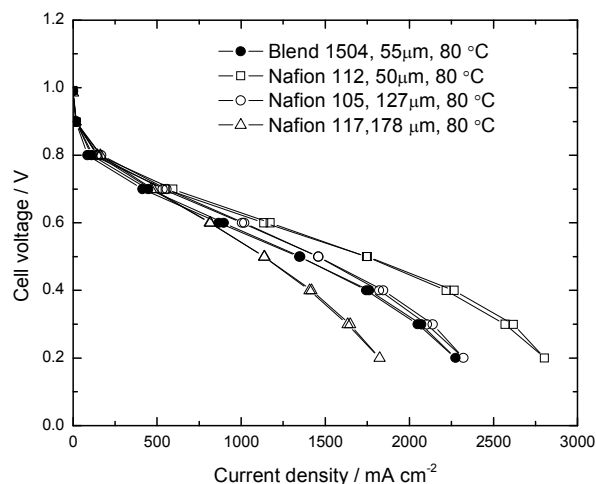

Figure 8.5 Polarization curves of blend 1504 compared with Nafion 112, 105 and 117 at 80 °C, H_2/O_2
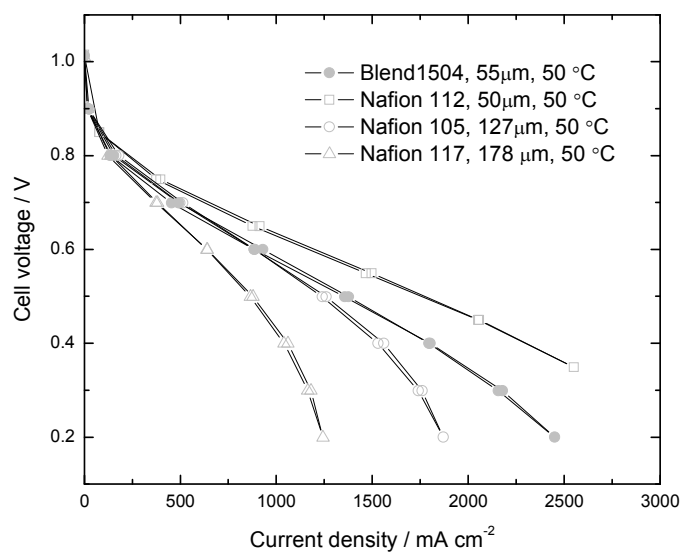

Figure 8.6 Polarization curves of blend sulfonimide1504 compared with Nafion 112, 105 and 117 at 50 °C, H_2/O_2

While in laboratory setting, H_2/O_2 condition is frequently used for fuel cell testing, using pure H_2/O_2 in fuel cells is an ideal situation. In reality, H_2/air condition is usually encountered. For this reason, the Blend 1504 was also tested in H_2/air conditions. The cell performance of Blend 1504 with all Nafion membranes, Nafion 112, 105 and 177 under H_2/air condition are all much lower than those at H_2/O_2 both at 80 °C and 50 °C (compare Figure 8.5, 8.6 with Figure 8.7 and 8.8). For Blend 1504, it has lowest performance among these membranes tested at 80 °C, H_2/air condition; while its performance is higher than that of the Nafion 117, but lower than that of all the other membrane at 50 °C. Higher EW membrane usually performs poor in PEMFCs. In regard to the high EW for Blend 1504, our sulfonimide blend's performance is pretty high which may indicate blending even the same plain polymer with different EWs helps the membrane structure and properties improvement.
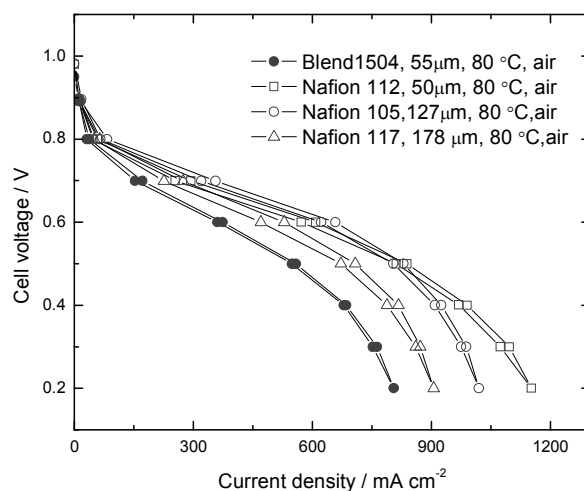

Figure 8.7 Polarization curves of blend 1504 compared with Nafion 112, 105 and 117 at 80 °C, H_2/air
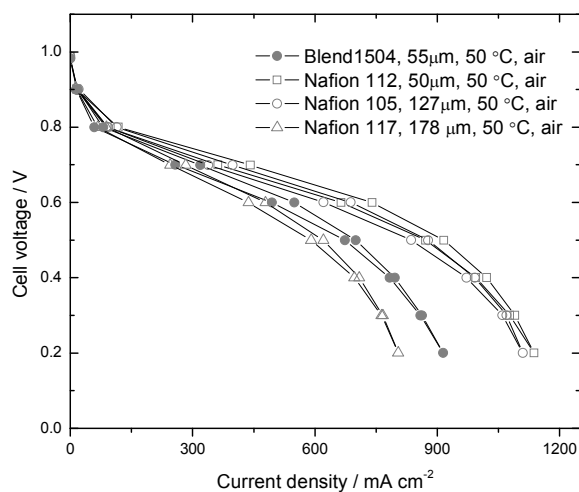
171

Figure 8.8 Polarization curves of blend 1504 compared with Nafion 112, 105 and 117 at 50 °C, H$_2$/air

Membrane conductivity is a good indicator of its performance in fuel cells, but it is its conductance that directly decides the membrane's cell performance in fuel cells. A membrane's conductance is both affected by its conductivity and thickness. Thinner membrane has higher conductance and thinner membrane also decreases the materials cost. That's the reason why thinner membrane is popular currently in fuel cell fields. But thin membrane usually has higher gas crossover and less strong mechanical strength.

Because of the importance of membrane conductance in fuel cell setting, the resistance (the inverse of conductance) of Blend 1504 was also monitored by CI technique and HFR method in the process of polarization curve measurements in comparison with Nafion 112, 105 and 117. The areal resistance of the Blend 1504 operating at both H$_2$/O$_2$ and H$_2$/air at either 80 °C or 50 °C is shown in Figures 8.9 to 8.12 also in comparison with that of Nafion 112, 105 and 117. From these figures, Blend 1504 has slightly higher areal resistance (also displayed lower performance, see Figure 8.7). Nafion 112 has lowest

areal resistance, and next is Blend 1504; then, the final twos are Nafion 105 and 117. Nafion 117 is the thickest membrane therefore with highest resistance. It can also be seen from these figures, due to higher performance at H_2/O_2 conditions, more water was produced in cathodes; therefore it might bring about flooding in the cathode and dryness in anode due to the electro-osmosis drag, the areal resistance increases as the current density increases. While for H_2/air, these membranes performance is much lower, therefore less water, the membrane resistance was almost not changed with the current density change especially for thinner membranes (blend 1504, and Nafion 112).

The HFR resistance of these membranes monitored shows the similar trend as discussed above, but with higher areal resistance values (the figures are not shown). Because at monitoring of frequency 1 kHz of HFR measurement, the impedance phase angle is not zero, therefore, cell resistance other than of membrane resistance and contact resistance such as charge transfer resistance or maybe mass transport resistance has contribution to the measured value.
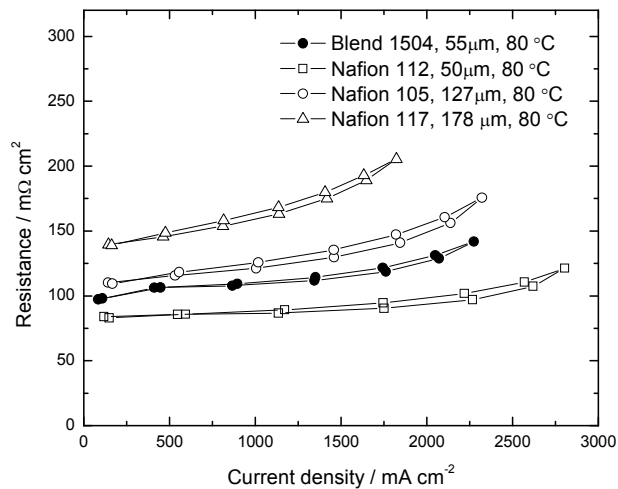
Figure 8.9 Areal resistance curves of different membranes, blend 1504, Nafion 112, 105 and 117 H_2/O^2 at 80 °C
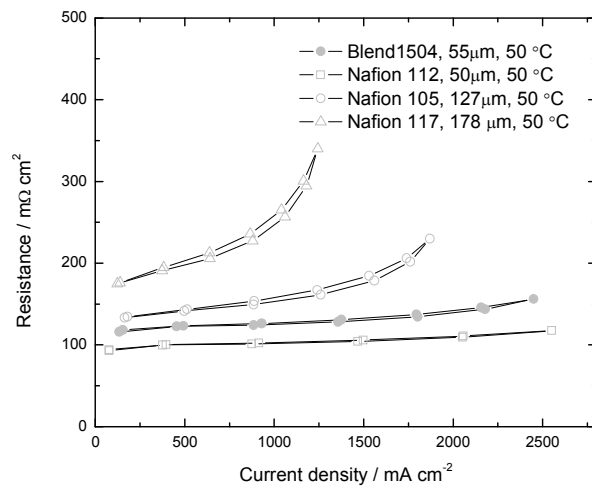
Figure 8.10 Areal resistance curves of different membranes, blend 1504, Nafion 112, 105 and 117 H_2/O_2 at 50 °C

174

Figure 8.11 Areal resistance curves of different membranes, blend 1504, Nafion 112, 105 and 117 H$_2$/air at 80 °C

Figure 8.12 Areal resistance curves of different membranes, blend 1504, Nafion 112, 105 and 117 H$_2$/air at 50 °C

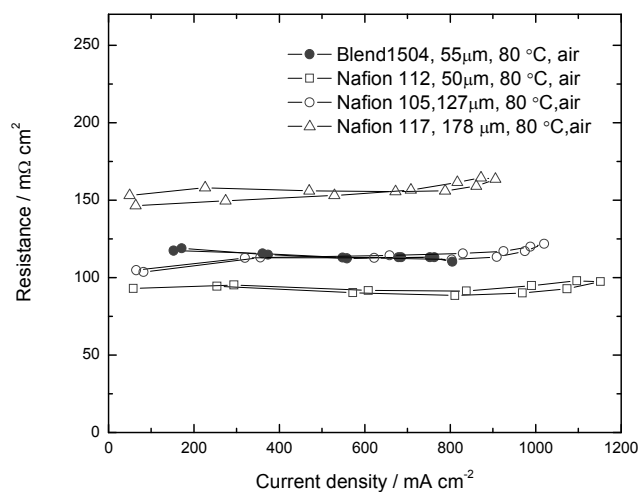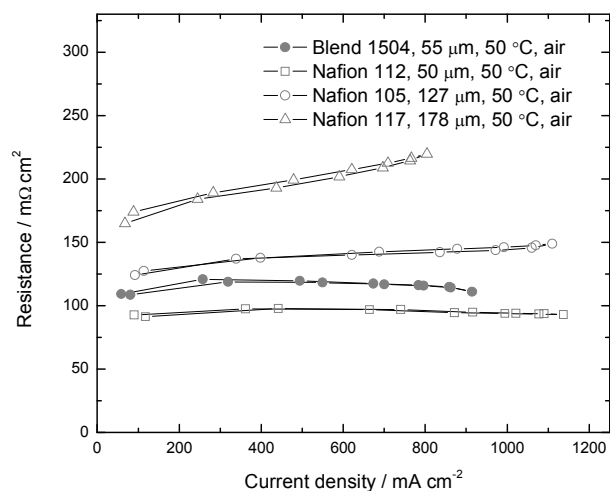## 8.3.2 Cross-linked sulfonimide membrane EW 1000

8.3.2.1 Ionic conductivities

The ionic conductivities of the Xlinked 1000 were also measured at BekkTech with a four point probe direct current (DC) method at different relative humidity (RH) at 80 °C

under atmospheric pressure in comparison with that of Nafion 112. The ionic conductivities vs. RH curves are shown in Figure 8.13. From the Figure, it is seen that Xlinked 1000 has slightly lower ionic conductivity than that of Nafion 112 at RH lower than 90%, but slightly higher than that of Nafion at RH higher than 90%.
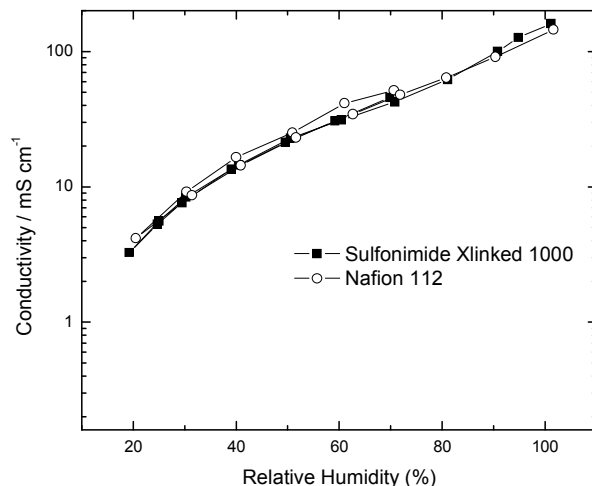
Figure 8.13 Ion conductivity of sulfonimide Xlinked 1000 in different humidity compared with Nafion 112, measured by BekkTek with four point probe DC method

8.3.2.2 H_2 cross over membranes by LSV

.The H_2 crossover of the Xlinked 1000 measured with LSV at 30 °C under atmospheric pressure is show in Figure 14 compared with H_2 crossover of Nafion 112, 105 and 117. In the measurement, all the other conditions are assumed as the same, the H_2 crossover difference was thought to be caused only by membrane itself. From Figure 8.14, Nafion 112 has highest H_2 crossover rate, Nafion 117 has lowest crossover rate (because it is the thickest membrane used in the measurement), although Xlinked 1000 has close thickness to that of Nafion 112, its H_2 crossover rate is lower that that of Nafion 112. This finding

may indicate cross-linking help strengthen the membrane. The H_2 crossover rate of Xlinked 1000 by LSV is calculated out according to Equation 8.1 and listed on Table 8.3.
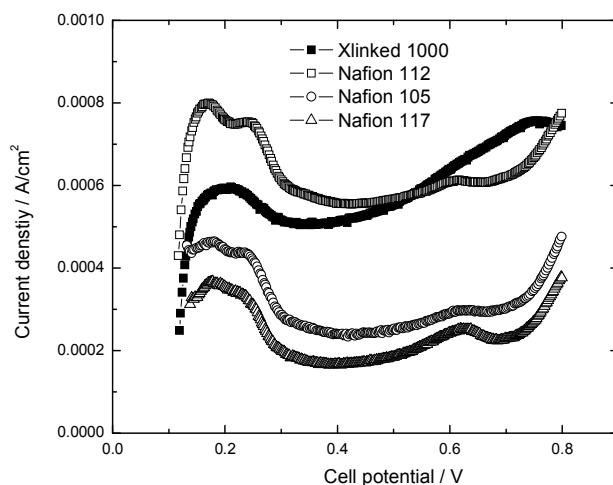
Figure 8.14 H_2 crossover of Xlinked 1000 membrane with Nafion 112, 105 and 117 by LSV at 30 °C cell temperatures, fully humidified.

Table 8.3 H_2 crossover rate of different membranes by LSV

Membranes	Xlinked 1000	Nafion 112	Nafion 105	Nafion 117
N_{H2} / mole s^{-1} cm^{-2}	2.6 E-9	2.9E-9	1.2E-9	8.6E-10

8.3.2.3 Single-cell testing performance of Xlinked 1000

The single cell testing performance of Xlinked 1000 under H_2/O_2 or H_2/air at 80 °C and 50 °C (cell temperatures) are shown in Figure 15 to 18 in comparison with Nafion 112, 105 and 117. Form Figure 15 and 16, Xlinked 1000 shows higher performance than that of all Nafion 112, 105 and 117 under H_2/O_2 condition both at 80 °C and 50 °C. The higher cell performance of Xlinked 1000 may bring about from sulfonimide acid nature in the polymer combined with low EW and thin thickness of the membrane.

Figure 8.15 Polarization curves of Xlinked 1000 compared with Nafion 112, 105 and 117 at 80 °C, H$_2$/O$_2$

Figure 8.16 Polarization curves of Xlinked sulfonimide 1000 compared with Nafion 112, 105 and 117 at 50 °C, H$_2$/O$_2$

The cell performance of Xlinked 1000 with all Nafion membranes, Nafion 112, 105 and 117 under H$_2$/air condition are all much lower than those at H$_2$/O$_2$ both at 80 °C and 50 °C (compare Figure 8.15, 8.16 with Figure 8.17 and 8.18). For Xlinked 1000 under H$_2$/air condition, its performance is slightly higher than that of Nafion 112, but higher

than that of all other membranes tested at 80 °C; while its performance is slightly lower

than that of both Nafion 112 and 105, but higher than that of Nafion 117 at 50 °C.

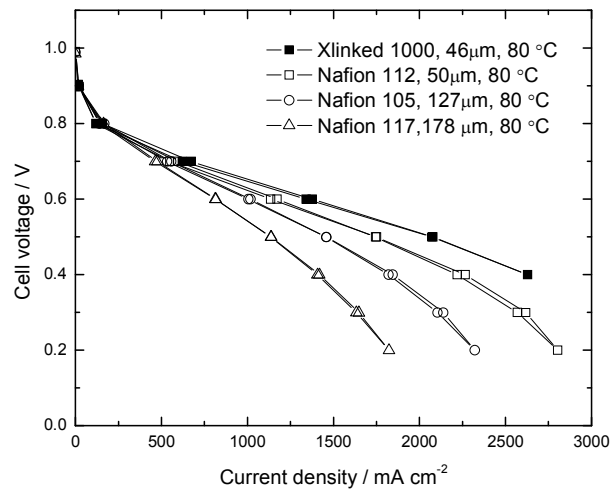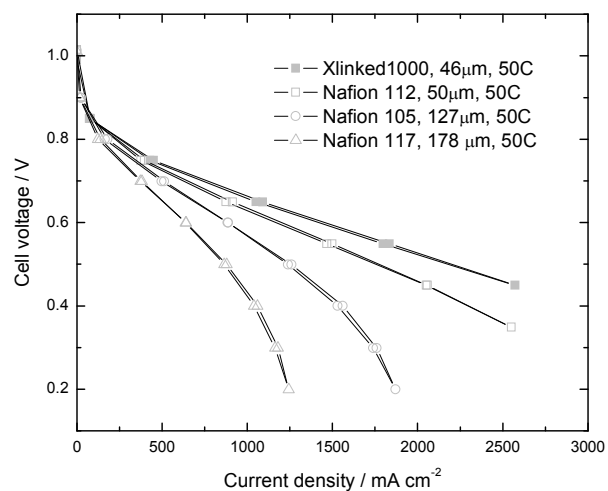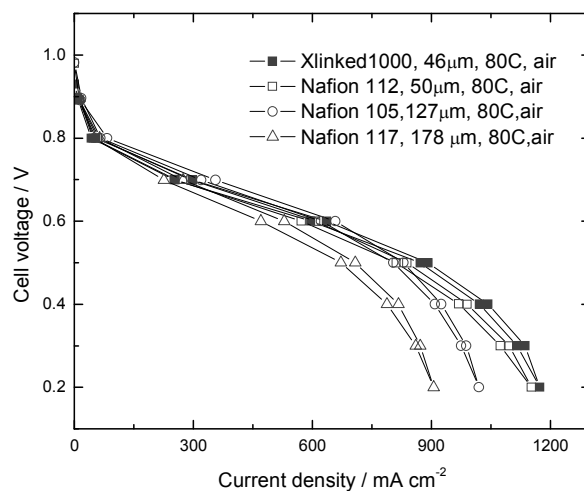Figure 8.17 Polarization curves of Xlinked 1000 compared with Nafion 112, 105 and 117 at 80°C, H_2/air
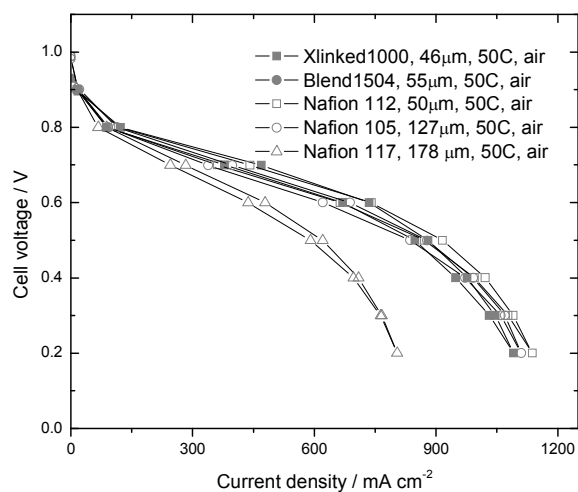
Figure 8.18 Polarization curves of Xlinked 1000 compared with Nafion 112, 105 and 117 at 50 °C, H_2/air

The areal resistance of the Xlinked 1000 operating at both H_2/O_2 and H_2/air at either 80

°C or 50 °C is shown in Figures 8.19 to 8.22 also in comparison with that of Nafion 111,

105 and 117. From these figures, the Xlinked 1000 displayed nearly the same areal resistance trend: areal resistance of Xlinked 1000 at the whole current density range measured is the smallest, next is Nafion 112; the final twos are Nafion 105 and 117. Nafion 117 is the thickest membrane with highest resistance. It can also be seen from these figures, due to higher performance at H_2/O_2 conditions, more water was produced in cathodes; therefore it might bring about flooding in the cathode and dryness in anode due to the electro-osmosis drag, the areal resistance increases as the current density increases. While for H_2/air, these membranes performance is much lower, the membrane resistance was almost not changed with the current density change especially for thinner membranes (Xlinked 1000, and Nafion 112).

The HFR resistance of these membranes monitored shows the similar trend as discussed above, but with higher areal resistance values (the figures are not shown).
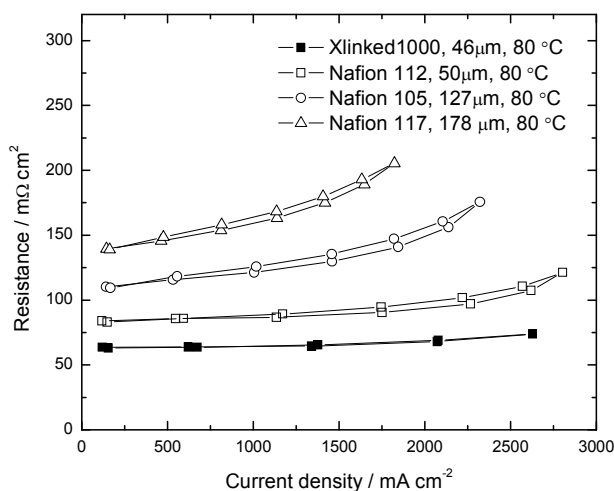
Figure 8.19 Areal resistance (by CI) curves of different membranes, Xlinked 1000, Nafion 112, 105 and 117 H_2/O_2 at 80 °C
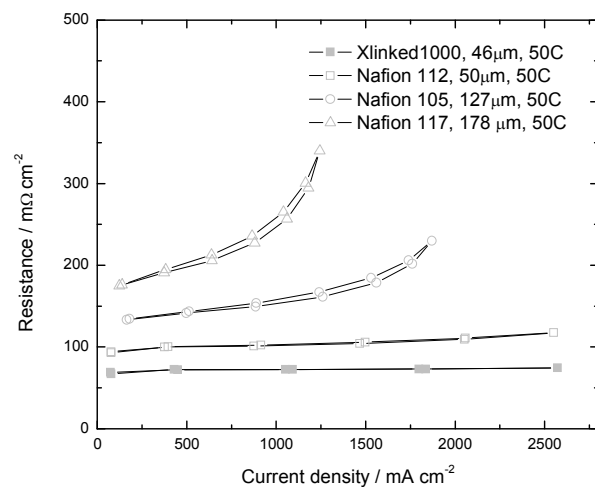
Figure 8.20 Areal resistance (by CI) curves of different membranes, Xlinked 1000, blend 1504, Nafion 112, 105 and 117 H_2/O_2 at 50 °C
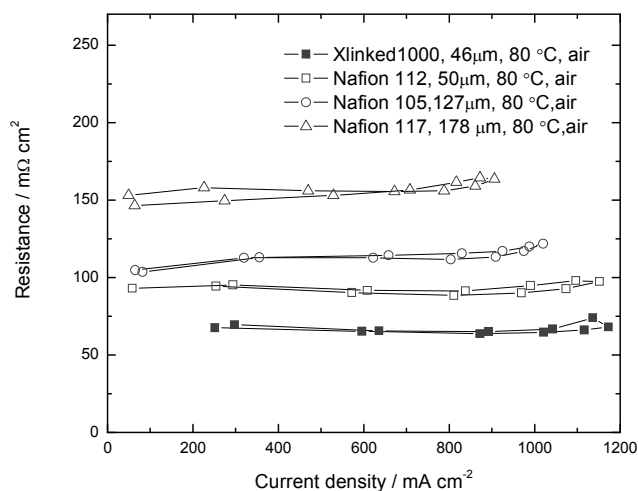
Figure 8.21 Areal resistance (by CI) curves of different membranes, Xlinked 1000, Nafion 112, 105 and 117 H_2/air at 80 °C
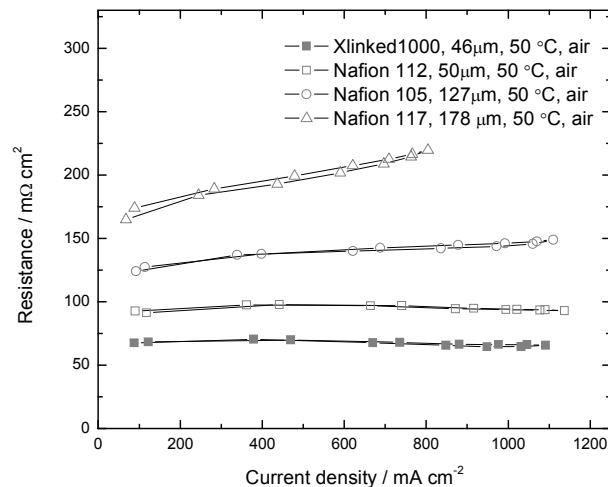
Figure 8.22 Areal resistance (by CI) curves of different membranes, Xlinked 1000, Nafion 112, 105 and 117 H$_2$/air at 50 °C

It is interesting to deduce membrane's conductivity from the resistance curves monitored by either CI or HFR assuming that the measured resistance is only from membrane resistance when current approaches zero. Table 8.4 shows the analysis results from the deduction for all membranes tested at H$_2$/O$_2$ at 80 °C, nearly 100% RH. As is seen from Table 8.4, for thin membranes (Blend 1504, Xlinked 1000, Nafion 112), the conductivity obtained from resistance curves are lower than measured by *ex-situ* DC methods, while for thick membranes(Nafion 105, 117), the conductivity of Nafion is close to the reported 0.1 S cm^{-1}. These difference was thought to be caused by the contact resistance (or plus resistance in the catalyst layer) in cells. Thin membrane has lower membrane resistance, so contact resistance takes more parts in the CI-monitored resistance. For thick membrane, contact resistance takes fewer parts. It is also seen that the membrane (cell) performance correlates with the conductance of the membranes. The conductance at 80 °C(H$_2$/O$_2$, 100%RH) shows the increasing order of Nafion 117,105,

182

blend 1504, Nafion112 and Xlinkded 1000, and the cell performance shows the nearly the same order(see Figures 8.5 and 8.15). Both conductivity and thickness decides the membrane performance.

Table 8.4 Membrane conductivity at 80 °C 100% RH deduced from resistance curves measured by CI

Membrane	Thickness	Resistance	Conductance	Conductivity 80C[a]	Conductivity[b]
	μm	$m\Omega\ cm^2$	S	$mS\ cm^{-1}$	$mS\ cm^{-1}$
Blend 1504	55	97.995	2.0	56.1	88.7
Xlinked 1000	46	63.15	3.2	72.8	154.4
Nafion 112	50	82.97	2.4	60.3	136.2
Nafion 105	127	110.75	1.8	114.7	
Nafion 117	178	138.99	1.4	128.1	

[a] conductivity calculated from resistance(extrapolated to current density to zero) monitored by CI method, assuming active membrane area of 5 cm^2, [b] conductivity measured by BekkTech with 4 point probe DC method at 80 °C 100% RH.

8.4   Conclusions

The Xlinked 1000 and Blend 1540 sulfonimide membranes were characterized in comparison with Nafion 112, 105 and 117 in respect to proton conductivity, H_2 crossover rate, areal resistance and single cell testing performance. Xlinked 1000 has very close ionic conductivity to that of Nafion 112, which has highest conductivity among all tested Nafion membranes (Nafion 112, 105 and 117). While Blend 1504 has lowest conductivity among all membranes tested perhaps due to it higher EW value (1504). Thinner membrane usually has higher H_2 crossover rate. Either through strengthening of membrane structure with cross-linking agent, or due to higher TFE component in the

membrane with higher EW/blending, the H_2 crossover rate of Xlinked 1000, and Blend 1504 is decreased comparison to that of Nafion 112, although they are in close thickness. The cell performance of Xlinked 1000 under H_2/O_2 both at 80 and 50 °C are better than all other membranes tested in experiments. The cell performance of Xlinked 1000 under H_2/air at 80 C is slightly higher than that of Nafion 112, but is slightly lower than that of Nafion 112 or 105. It is interesting that blend 1504 performed better at 50 °C both under H_2/O_2 or H_2/air conditions, but in total, Blend 1504 always performed lower than that of Nafion 112. Considering high EW nature of the Blend 1504, its performance is exceptionally high. In order to confirm this high blending effect, further work of blending of high EW and low EW sulfonimide polymers with resultant low EW blends is in progress.

8.5   Reference

1.   B. Smitha, S. Sridhar and A. A. Khan, *Journal of Membrane Science*, 2005, **259**, 10-26.

2.   S. J. Hamrock and M. A. Yandrasits, *Polymer Reviews*, 2006, **46**, 219 - 244.

3.   D. D. DesMarteau, *Journal of Fluorine Chemistry*, 1995, **72**, 203-208.

4.   J. J. Sumner, S. E. Creager, J. J. Ma and D. D. DesMarteau, *Journal of the Electrochemical Society*, 1998, **145**, 107-110.

5.   S. E. Creager, J. J. Sumner, R. D. Bailey, J. J. Ma, W. T. Pennington and D. D. DesMarteau, *Electrochemical and Solid-State Letters*, 1999, **2**, 434-436.

6.   S. C. Savett, J. R. Atkins, C. R. Sides, J. L. Harris, B. H. Thomas, S. E. Creager, W. T. Pennington and D. D. DesMarteau, *Journal of the Electrochemical Society*, 2002, **149**, 1527-1532.

7.   J. R. Atkins, C. R. Sides, S. E. Creager, J. L. Harris, W. T. Pennington, B. H. Thomas and D. D. DesMarteau, *Journal of New Materials for Electrochemical Systems*, 2003, **6**, 9-15.

8. H. Mei, Dissertation, 2006.

9. A. Mokrini and M. A. Huneault, *Journal of Power Sources*, 2006, **154**, 51-58.

10. R. Wycisk, J. Chisholm, J. Lee, J. Lin and P. N. Pintauro, *Journal of Power Sources*, 2006, **163**, 9-17.

11. M. N. A. M. Norddin, A. F. Ismail, D. Rana, T. Matsuura, A. Mustafa and A. Tabe-Mohammadi, *Journal of Membrane Science*, 2008, **323**, 404-413.

12. S. D. Mikhailenko, G. P. Robertson, M. D. Guiver and S. Kaliaguine, *Journal of Membrane Science*, 2006, **285**, 306-316.

13. F. C. Ding, S. J. Wang, M. Xiao and Y. Z. Meng, *Journal of Power Sources*, 2007, **164**, 488-495.

14. C. Zhang, X. Guo, J. Fang, H. Xu, M. Yuan and B. Chen, *Journal of Power Sources*, 2007, **170**, 42-45.

15. M. S. Wilson, J. A. Valerio and S. Gottesfeld, *Electrochimica Acta*, 1995, **40**, 355-363.

16. M. S. Wilson and S. Gottesfeld, *Journal of Applied Electrochemistry*, 1992, **22**, 1-7.

17. K. R. Cooper and M. Smith, *Journal of Power Sources*, 2006, **160**, 1088-1095.

18. S. K. Shyam, J. D. Yang and S. Y. Jung, *AIChE Journal*, 2006, **52**, 1916-1925.

19. K. R. Cooper, V. Ramani, J. M. Fenton and H. R. Kunz, *Experimental methods and data analyses for polymer electrolyte fuel cells*, 1.5 edn., Scribner Associates, Inc., 2007.

CHAPTER 9

SUMMARY AND CONCLUSION

9.1   Mesoporous carbons as catalyst supports in PEMFC

Mesoporous carbons such as carbon xerogel (CX) and silica-templated carbon (MC) were synthesized and investigated as catalyst supports for PEMFCs in comparison with the most commonly used carbon support (e. g. carbon black Vulcan XC-72R). *Ex-situ* characterization and in-cell testing results show that carbon xerogel as Pt catalyst support has close to or better performance than that of Vulcan XC-72R, but silica-templated mesoporous carbon has inferior performance to that of Vulcan XC-72R (on commercial Pt/XC-72R). Although MC has high specific surface area, large pore size, high pore volume, these textural advantages didn't transfer to a higher cell performance as expected. Why? Because fair comparison of different supports in fuel cell electrodes is complicated by many factors, with two significant ones listed as follows.

1) The Pt catalyst deposition onto carbon:

It is well known that the surface chemistry, surface area, pore structure and other properties of the carbon support affect the Pt particle size, the size distribution and Pt dispersion on the support, therefore the catalyst performance in the electrodes, which is also confirmed from current work. The common impregnation-reduction method of deposition Pt catalyst works well with commercial XC-72R support and the synthesized CX supports. The Pt particle size on XC-72R (synthesized Pt/XC-72R) and CX was close to that of Pt on XC-72R of commercial Pt/XC-72R catalyst, while Pt particle size on MC is larger and more clustered, and the Pt size distribution on MC is also broader. So the

inferior cell performance of MC was partially caused by this effect. In order for fair comparison, further work of development of a new method to deposit Pt catalyst onto MC is needed.

2) The electrode fabrication method:

It is understandable that the electrode performance is also directly affected by the electrode fabrication method. The thin film decal transfer method (with usual ink formulation) of fabricating electrode for PEMFC worked well for the commercial Pt/XC-72R, synthesized Pt/XC-72R and Pt/CX catalysts in experiments, but it failed with synthesized Pt/MC catalyst. Significant increase of Nafion content in the ink of Pt/MC catalyst helps form a smooth thin film on the PTFE template and will help electrode fabrication of Pt/MC catalyst by the decal transfer method. But, the excess addition of Nafion in the ink would change the electrode structure accordingly and therefore the cell performance of the electrode. For fair comparison of different carbon supports in application of PEMFCs, except for that the similar Pt catalyst on different supports is needed to be synthesized; optimization of ink formulation for different carbon supported Pt catalysts is also needed.

It is inferred that electrode performance, stability, durability are a combination of different properties of catalyst, carbon support and electrolyte in the electrode

9.2   Grafting of monofunctional or polymeric electrolyte on mesoporous carbons

A monofunctional aryl fluorosulfonimide electrolyte was grafted electrochemically on GC electrode via the relevant diazonium salt, the formed electrolyte layer was confirmed by XPS, EDS, the grafted layer on the GC was tested vial ferricyanide and hexamine

ruthenium probes, and its stability was also investigated in regard to high temperature, superacid environment, which simulates a PEMFC operation environment.

However, the electrochemical grafting was not practical for powdery carbon materials usually used to make electrode in PEMFCs, and also the scale-up is problematic. In order to graft the same monofunctional aryl fluorosulfonimide, chemical grafting of sulfonimide electrolyte via relevant diazonium salt was performed onto mesoporous carbons (such as XC-72, carbon xerogel). The electrolyte content was quantified by acid-base back titration method. For the well-known three-phase zone (or three-phase boundary) model in PEMFC, grafting electrolyte onto carbon supports, and then depositing Pt catalyst on them will increase three phase zone area in the electrodes, therefore the performance. However our testing didn't obtain expected results. After grafting electrolyte onto the carbon support, the Pt catalyst particle was larger and clustered on the carbon black samples with the common impregnation-reduction Pt deposition method. Similar to the situation in using mesoporous carbons as catalyst supports in PEMFCs, evaluation of grafting electrolyte on carbon support for PEMFC application was also complicated by many other factors such as catalyst deposition, electrode fabrication. Further work to develop better catalyst synthesis on electrolyte-grafted carbon supports is needed. Because after grafting, some electrolyte is already in the support, less binder (Nafion in electrode both as a binder and a proton conductor in the decal transfer electrode fabrication method) may be needed in electrode to obtain optimal performance, this in turn may present a challenge to the electrode fabrication of

the grafted carbon supports, especially for large pore volume carbon supported catalyst as explained in section 9.1.

The chemical grafting of polymer electrolyte (sulfonated poly (arylene ether sulfone)) on mesoporous carbon, carbon black is not effective as indicated by the acid-base titration results on the polymer-electrolyte-grafted carbon. The reasons for the low efficient grafting of polymer electrolyte onto carbon may be caused by two aspects: (1) the grafting chemistry, (2) the pore structure of the support.

There is little report about grafting polymer electrolyte onto carbon support for PEMFC application. Further study on the grafting is needed, especially development of analytical methods to verify every step in the polymerization grafting. So the work is not just to do the 'blind' synthesis and to test the grafted carbon in final fuel cell format.

Carbon black's aggregate and agglomerate structure might not be helpful to the polymer electrolyte grafting. Large pore volume, high surface area and large pore carbon material such as the silica-templated carbon was intended to used as the polymer electrolyte grafting substrate, but the above-motioned electrode fabrication problem of Pt/MC catalyst prevented the idea's execution. Further work in this direction may be worth to do.

9.3 Blended and cross-linked sulfonimide membranes as membrane materials in PEMFC

The new strategy of blending the same sulfonimide polymer with different EWs to make membranes seems to work well from the in-cell testing results of blend 1504 (see Chapter 8), and the cross-linking of low EW polymer to cast membrane (see testing of

190

cross-linked 1000) also looks successful, otherwise a large membrane piece (e.g. 3" x 3", good for MEA testing) from low EW sulfonimide polymer is difficult to cast. But, in order to confirm these finding, further work is recommended:

For blending strategy, (1) synthesis of low EW (e.g. EW 1100 or 1000) blend sulfonimide membranes, (2) fuel cell testing comparison of blended membrane with un-blended plain sulfonimide membranes of both low and high EW are needed.

For cross-linking strategy of low EW sulfonimide polymer, a comparison of cross-linked sulfonimide with plain (un-crosslinked) membrane with the same EW is needed.

For both blending and cross-linking strategies, other characterization methods such as SEM, TEM or EDX than the in-cell testing could be used to probe the blended or cross-linked membrane structure to understand the structure property relationship including these blending or cross-linking effects.

APPENDIX

List of publications

1. **Bing Liu** and Steve Creager, Silica-sol-templated mesoporous carbon as catalyst support for PEM fuel cell application. *Electrochimica Acta,* in review

2. **Bing Liu**, Hua Mei, Darryl DesMarteau and Steve Creager, Chemical grafting of an aryl fluorosulfonimide electrolyte onto carbon xerogel and carbon black. *Journal of Materials Chemistry*, submitted

3. **Bing Liu** and Steve Creager, Carbon xerogels as Pt catalyst supports for PEM fuel cell applications. *Journal of Power Sources*, in press

4. Creager, S. E.; **Liu, B**.; Mei, H.; DesMarteau, D., Electrochemical grafting of an aryl fluorosulfonimide electrolyte onto glassy carbon. *Langmuir*, 2006, 22 (25), 10747-10753

Conference proceedings

1. **Bing Liu**, Hua Mei, Stephen E Creager and Darryl DesMarteau, Grafting aryl fluorosulfonimide electrolyte onto carbon substrates, 212 ECS, October, 2007, Washington, DC

2. **Bing Liu** and Stephen Creager, Grafting electrolyte for fuel cell electrode application, SERMACS, October 2007, Greenville, SC

3. **Bing Liu**, Charles Milliken, Harold May, Steve Creager, Microbial fuel cells using general ion exchange and microporous membranes, MRS, April 2007, Clemson, SC

4. Mei, H.; **Liu, B**.; Creager, S. E.; DesMarteau, D. D., Novel diazonium zwitterions.231 ACS, March 2006, Atlanta, GA

5. Creager, S. E.; Mei, H.; **Liu, B**.; DesMarteau, D. D.; Smith, D. W.; Perpall, M. W., Fluorinated sulfonimide electrolytes grafted onto carbon: A potential route to high-performance PEM fuel cell electrodes. 228 ACS, August 2004, Philadelphia, PA